Self-Assembly and Selective Swelling in Lamellar Block Copolymer Photonic Gels

by

Yin Fan

B.E. Polymer Materials and Engineering,
Tsinghua University, 2007

Submitted to the Department of Chemical Engineering
in Partial Fulfillment of the Requirements for the Degree of

DOCTOR OF PHILOSOPHY IN POLYMER SCIENCE AND TECHNOLOGY
at the
MASSACHUSETTS INSTITUTE OF TECHNOLOGY

February 2014

Signature of Author: _____
Department of Chemical Engineering
January 28, 2014

Certified by: _____
Edwin L. Thomas
William and Stephanie Sick Dean of Engineering, Rice University
Thesis Supervisor

Certified by: _____
Bradley D. Olsen
Paul M. Cook Career Development Assistant Professor of Chemical Engineering
Thesis Co-Supervisor

Accepted by: _____
Patrick S. Doyle
Singapore Research Professor of Chemical Engineering
Chairman, Department Committee for Graduate Students

Self-Assembly and Selective Swelling in Lamellar Block Copolymer Photonic Gels

by

Yin Fan

B.E. Polymer Materials and Engineering
Tsinghua University, 2007

Submitted to the Department of Chemical Engineering
on January 28th, 2014, in Partial Fulfillment of the
Requirements for the Degree of
Doctor of Philosophy in Polymer Science and Technology

Abstract

Materials with responsive structural color have broad applications ranging from sensing to smart coating. Nature provides inspirations for the design of such materials. Mimicking the structure of the skin elements responsible for cephalopod's fast camouflage, we made photonic gels using lamellar block copolymer (BCP) films. Diblock copolymer poly(styrene-*b*-2-vinylpyridine) (PS-P2VP) of symmetric composition self-assembles into alternating PS and P2VP layers parallel to the substrate after solvent vapor annealing. In solvents that are selective to P2VP, the P2VP layers swell while the PS layers remain glassy. The glassy PS layers restrict the lateral expansion of the P2VP layers, and therefore the swelling of P2VP layers occurs only along the direction normal to the layer surface. The 1D swelling turns the lamellar BCP film into a Bragg stack comprised of alternating gel and glass layers, which reflects light in the visible regime. The BCP gels display responsive structural color to a variety of stimuli triggered by the swelling/deswelling of the gel layers, and can be used to indicate changes in the solution properties of the gel block in the selective solvent.

The thesis first looks into developing temperature-responsive or thermochromic photonic gels. The first example is a PS-P2VP/acetic acid photonic gel. P2VP has a temperature-dependent basicity and its swelling ratios in acetic acid solutions vary with temperature as degrees of protonation change. The PS-P2VP/acetic acid photonic gels showed blue-shifts in the reflection color at high temperatures which can be tuned by acid concentration, valency and counterion species. The second example of temperature-responsive photonic gels is PS-P2VP/cyclohexane. The PS – cyclohexane pair has an upper critical solution temperature (UCST) and the photonic gel's structural color red-shifts at high temperature. The temperature dependence can be tuned by the molecular weight of the PS-P2VP.

Next we show that the PS-P2VP photonic gels are also responsive to the composition of alcohol-water co-solvents. A model based on Flory-Huggins mixing and line defect network strain energy quantitatively relates the photonic gel's reflectivity to the Flory-Huggins

interaction parameter χ between P2VP and the co-solvent and the average defect density. The results indicate that the edge and screw dislocation line defects in lamellar self-assembly serve to create an interconnected network of glassy PS layers that restrict the selective swelling and hence the photonic response. The co-solvent quality responsive photonic gels provide a method to measure the Flory-Huggins χ parameter and the defect density in the lamellar BCP film.

Proteins can form ionic complexation with polyelectrolytes. The P2VP block in the lamellar PS-P2VP is converted into a polycation QP2VP by quaternization reactions. The ionic complexation between proteins and QP2VP triggers the swelling/deswelling of the QP2VP gel block, which changes the structural color of the lamellar PS-QP2VP photonic gels. We demonstrate that counterion coacervation as a novel mechanism to trigger the photonic responses of the BCP gels. Exposure to aqueous solutions of proteins alters the swelling ratios of the QP2VP gel layers in the PS-QP2VP gels due to the ionic interactions between proteins and the polyelectrolyte block. The real-time photonic responses of the PS-QP2VP gels are characterized by the reflective spectra recorded as a function of time and are related to the dynamic swelling behaviors of the QP2VP gel layers in protein solutions. The results suggest that the BCP gels and their associated structural colors provide a fast and visually interpretable method to differentiate different proteins due to their differences in size and charge.

Thesis Supervisor: Edwin L. Thomas
Title: William and Stephanie Sick Dean of Engineering, Rice University

Thesis Co-Supervisor: Bradley D. Olsen
Title: Paul M. Cook Career Development Assistant Professor of Chemical Engineering

Acknowledgements

First of all, I would like to thank my advisor Prof. Ned Thomas. It is my honor to be able to work with Ned for the past six years. Ned is knowledgeable, inspiring, and supportive as an advisor. His insights and perspectives were helpful to my research and also influenced my way of thinking. I am grateful for the freedom in research that Ned offers his group, which was a unique but great opportunity for me to think independently about both science and future career. I especially appreciate his continuing financial and intellectual support after his move to Rice University, without which I would have to give up playing with the materials that I love.

I owe a lot to Prof. Brad Olsen, who "adopted" me after Ned's move. Brad made my last years at MIT more productive and pleasant by allowing me to join his research group. I appreciate Brad's generosity in offering me his precious time and lab space as well as the financial support for the last year. Brad is a very organized person and working with him effectively suppresses procrastination.

I appreciate the help from Prof. Alfredo Alexander-Katz and Prof. Paula Hammond for serving on my thesis committee. Alfredo also offered additional help besides the duty in the committee and it was delightful to have research discussions with him. His insights as a theorist were very helpful to the modeling part of my research.

I would like to thank Dr. Joe Walish and Mr. Shengchang Tang, the co-authors of my first-author papers for their valuable input and help to my research. Joe showed me how to make the block copolymer photonic gels and was always patient with my questions and crazy ideas. Shengchang's amazingly abundant knowledge in chemistry and biology was a priceless resource for me in the late stage of my projects. Both Joe and Shengchang are personal friends as well, and I thank them for being great listeners all the time.

I thank all the past and present members in the Thomas group for research discussion and friendship: (most are doctors now and I omit the titles for brevity) Sisi Ni, Jon Singer, Lin Jia, Daniel Alcazar, Henry Koh, Rafal Mickiewicz, Ho Sun Lim, Markus Retsch, Jae-Hwang Lee, Woo Soo Kim, and Ji-Hyun Jang. Group alumni Prof. Chinedum Osuji, Dr. Chaitanya Ullal, and Prof. Jongseung Yoon were also kind to give me many good suggestions when I had the chance to meet them in conferences.

I also thank the past and present members in the Olsen group for their help during everyday lab work, group meetings, and group social activities in the last two years: Mitchell Wang, Matt Glassman, Carla Thomas, Chris Lam, Charlotte Stewart-Sloan, Dongsook Chang, Michelle Sing, Yan Xia, Minkyu Kim, Manos Gkikas, Guokui Qin, and Mingjiang Zhong. It was fun to work and make friends back in my home department at the end of graduate school.

I am lucky to have worked with many other great people at MIT. Dr. Steve Kooi and Mr. Bill DiNatale in the ISN helped me with electron microscopy, optical measurements and many other experimental issues. Prof. Rubner in DMSE and CMSE offered help with lab space and research discussions.

I could not imagine myself surviving graduate school without my friends at MIT and in the Boston area. I thank Jane Wang, Hyeongho Shin, Adam Zeiger, and Alex Scott in my PPST class for working through the classes and qualifying exams together; Qing Han, Jingjing Xu, Jie Chen, Ying Diao, Ying Yang, Jessie Wong, Chia-Hua Lee, Xianwen Mao for the company in everyday life; Yuan Xiong, Charles Sing, and Shireen Goh as my art/music buddies for sharing many concert and museum trips; my college friends, Wen Zhou and Yanyan Lu in Harvard and BU for their constant care and friendship. It was their friendship and company that made my life as a foreign graduate student enjoyable, and I take them dear to my heart at all times.

Last but not least, I thank my family for their unconditional love and support. My parents provided me the best within their abilities in my entire life, which often means sacrifices on their side. I feel sorry for leaving them to study abroad as their only child, and I thank them for their courage and understanding to send me away so that I had the chance to outgrow who I was. I am truly blessed to have the best parents that I could imagine, who were not only the financial source to me for 20 years but also great friends that I can always talk to. I am also deeply indebted to my boyfriend Dr. Jialue Fan, whose kindness, patience, and wisdom led my way through the last stage in graduate school.

Table of Contents

List of Figures

List of Tables

Thesis Overview

Chapter 1 "Introduction" includes the background information on block copolymers, photonic crystals, and the lamellar PS-P2VP photonic gels.

Chapter 2 "Methods" describes in detail the methods to prepare, characterize, and model the PS-P2VP photonic gels, the homopolymer gel synthesis, and characterization of the protein solutions.

Chapter 3 "Temperature Responsive PS-P2VP Photonic Gels" presents two types of temperature responsive photonic gels based on lamellar PS-P2VP.

Chapter 4 "Co-Solvent Quality Responsive PS-P2VP Photonic Gels" explores the photonic responses of the lamellar PS-P2VP gels in alcohol-water co-solvents.

Chapter 5 "Protein Responsive PS-QP2VP Photonic Gels" demonstrates protein-polyelectrolyte coacervation as a novel mechanism to trigger the photonic responses of the quaternized PS-P2VP gels.

Chapter 6 "Summary and Future Work" summaries the key results in the thesis and suggests directions for the future research.

The Appendix "Transfer Matrix Method (TMM) code" includes the MATLAB code used to calculate the reflectivity of the photonic gels.

1. Introduction

Nature provides lots of fascinating examples of dynamic camouflage, some of which can adjust within milliseconds. Such features are useful for stimuli sensing, smart coatings for buildings, and switchable battlefield uniforms. Block copolymers (BCP) self-assemble into periodic structures and can be used as a synthetic mimic for the structural colors seen in animals. Polymer gels are well known for their sensitive responses to changes in their surrounding solution environment. By selectively swelling one block in the self-assembled lamellar BCP, 1D photonic gels with fast responses to a wide variety of stimuli can be made.

This chapter starts with the natural camouflage examples that inspired the design of the photonic gels (Section 1.1), and then briefly introduces photonic crystals (Section 1.2) and block copolymers (Section 1.3), followed by examples of block copolymer photonic crystals (Section 1.4). Responsive photonic gels made from the lamellar diblock copolymer poly(styrene-*b*-2-vinylpyridine) (PS-P2VP) are then discussed in Section 1.5. Polymer solution properties and the swelling/deswelling of the gel block are the mechanism of the BCP gels' photonic responses and are discussed in Section 1.6. Defects in BCP self-assembly affect the dynamic and equilibrium swelling of the BCP gels and their photonic properties and are discussed in Section 1.7. The interactions between proteins and polyelectrolyte gels can trigger the photonic responses of the BCP gels and are discussed in Section 1.8.

1.1. *Multilayer reflectors in nature*

Camouflage is an important feature that some animals use to adapt to their living environment. The functions of camouflage include defense against predators, communication

with other members of their species, and protection from the environment.[1] Common types of camouflage include background matching, deceptive resemblance, disruptive coloration, and countershading.

Cephalopods have the most versatile camouflage in nature. They use all the aforementioned camouflage techniques, and more amazingly, are able to switch to the camouflaged state in a very short time.[2] Prof. Roger Hanlon at the Marine Biological Laboratory in Woods Hole, MA carries out detailed studies on the skin structure and neural biology of cephalopods. His group discovered that in addition to the pigment-containing sacs termed "chromatophores", the "iridophores" containing a number of plates and "leucophores" containing a random group of spherical assemblages are also responsible for the rapid adaptive coloration (see Figure 1.1).[3]

Chromatophores contribute to the coloration by the absorption of light from the dyes they contain. The iridophores and leucophores reflect or scatter light with the parallel plates or spheres respectively. Color change occurs when the chromatophores expand due to the stretching of the surrounding muscles or when the spacings of the microstructures in irodophores are altered. The optical effects caused by iridophores and leucophores can be explained by photonic crystal theory (see Section 1.2).

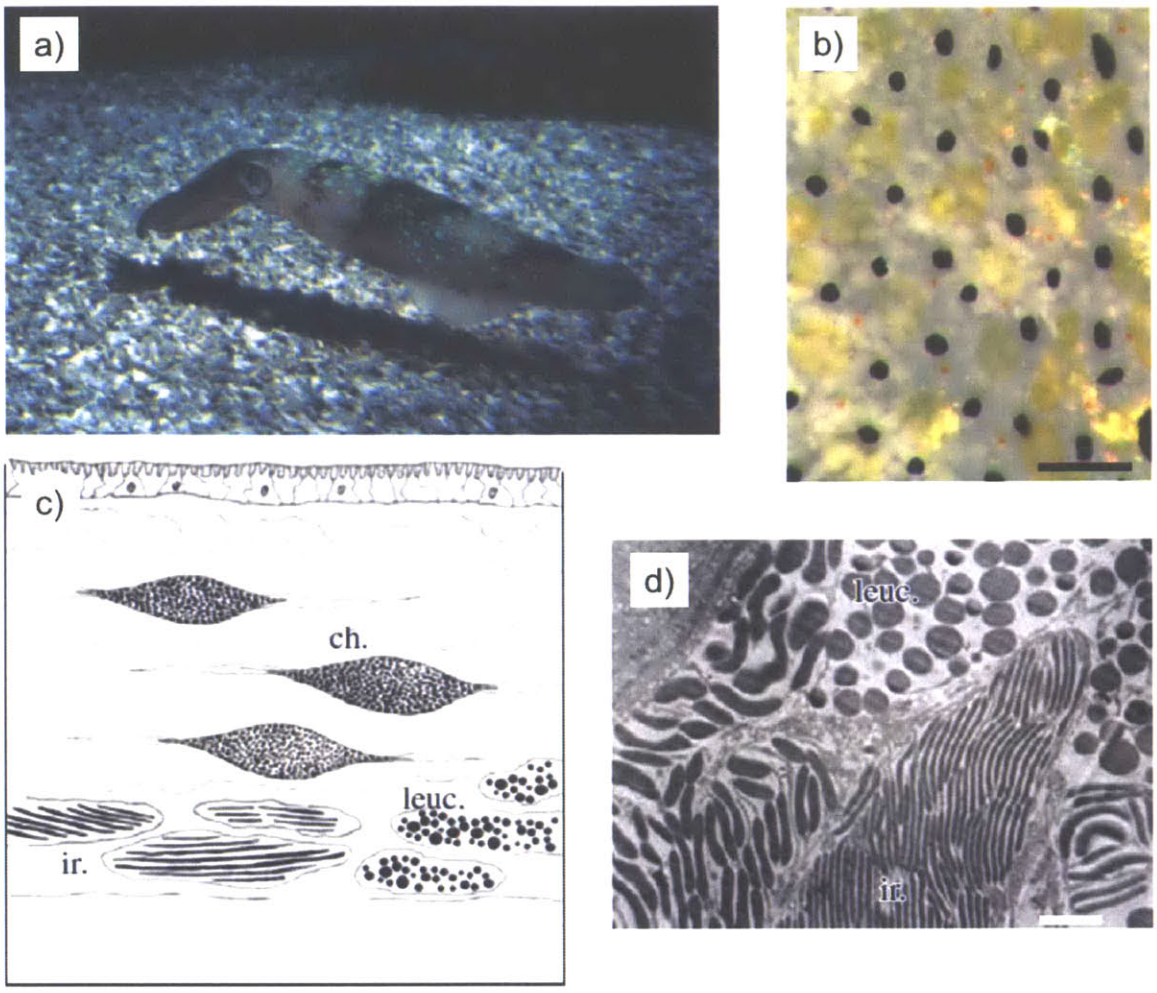

Figure 1.1. Images of the skin colors and the responsible structure elements of cephalopods.[3] a) Photo of the squid *Loligo pealeii*. b) Close-up view of the cuttlefish skin (*Sepia officinalis*) showing chromatophores (including laterally expanded cells as the yellow regions, partially retracted cells as the dark brown regions, and completely retracted cells as the orange regions) and leucophores (the white regions). Scale bar: 1 mm. c) Schematic of the skin in cross section showing chromatophores (ch., the cells with densely packed pigments), iridophores (ir., the cells with parallel platelets), and leucophores (leuc., the cells with randomly sized and distributed spheres). d) Cross-sectional electron micrograph of the cuttlefish skin (*S. officinalis*) with leucophores and iridophores. Scale bar: 1 μm.

1.2. *Photonic crystals*

Photonic crystals are periodic structures that affect the propagation of electromagnetic waves including visible light. The first studies on photonic crystals dates back to the study of Bragg stacks in the 19th century,[4] 100 years before the concept was coined in 1987.[5, 6] Bragg stacks are multilayers composed of materials with different layer refractive indices and thicknesses, like the parallel protein platelets comprising the iridophores in the cephalopod skin shown in Figure 1.1.

The optical property of a Bragg stack can be computed by the transfer matrix method (TMM).[7, 8] The equations are based on the Maxwell equations and the continuity of the wave functions of the propagating electromagnetic waves at the interfaces of materials in the Bragg stack. Reflection from a Bragg stack depends on the thicknesses and refractive indices of both types of layers, the wavelength, polarization and direction of the incident light and can be tuned via these parameters. The details of TMM calculations can be found in Chapter 2 of this thesis.

The fabrication of photonic crystals of the proper symmetry and periodicity is challenging. The reported methods include both top-down (e.g. lithography)[9, 10] and bottom-up (e.g. self-assembly of colloidal crystals)[11] approaches. Block copolymer self-assembly is another bottom-up approach and will be introduced in details in Section 1.3.

1.3. *Block copolymers*

Block copolymers (BCP) are polymers comprised of blocks of two or more different monomers. Due to the connectivity by the covalent bonds between the blocks, BCPs with incompatible blocks cannot macroscopically phase separate like polymer blends. Microphase separation occurs instead if the blocks of the BCP are incompatible and long enough, forming

periodic micro- or nano-structures. Examples of diblock copolymer microdomain structures are shown in Figure 1.2.

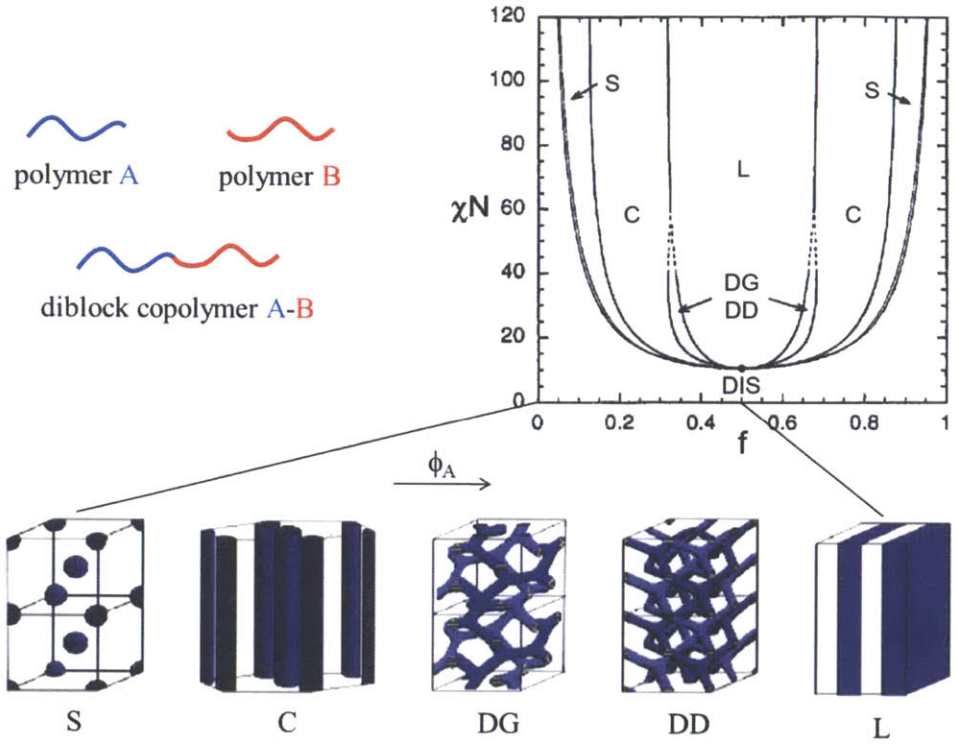

Figure 1.2. Schematic of a diblock copolymer, its phase diagram[12] and the morphologies of different geometries, including sphere (S), cylinder (C), double gyroid (DG), double diamond (DD), and lamellae (L).[13]

The variables in the diblock copolymer phase diagram are the segregation strength between the two blocks and the volume fraction or composition. The segregation strength depends on χ the interaction parameter between the two blocks and N the total number of monomers in the BCP. The lamellar phase has a broad window around the middle ($\phi = 0.5$) of the composition axis in the phase diagram. In the strong segregation limit ($\chi N > 100$), the lamellar spacing scales with the BCP's number of monomers or molecular weight as $d \sim N^{2/3}\chi^{1/6}$.[12] The junctions of the

blocks are aligned on the interfaces between the block layers in the lamellar diblock copolymer, and the polymer chains have configurations like tethered brushes (see Figure 1.3).

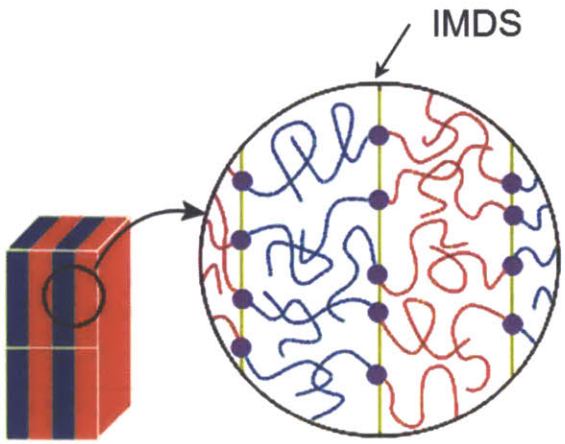

Figure 1.3. A zoom-in view on a lamellar diblock copolymer showing the tethered brush configuration. The purple circles represent the covalent bonds between the blocks which are located at the inter-material dividing surface (IMDS) between the different chemical domains.

1.4. *Block copolymer photonic crystals*

BCP microphase separation[12, 13] provides a facile bottom-up method to fabricate photonic crystals. The various 1D, 2D, and 3D periodic structures that BCPs form provide a variety of structural symmetries for the photonic crystals. Dielectric contrast between the BCP domains can be achieved by selecting the proper block chemistry. The periodicity needs be controlled by the molecular weight of the BCP or by blending with additives in order to reach the frequencies or wavelengths of interest.[14] Sufficient long range order and domain orientation are necessary as well.

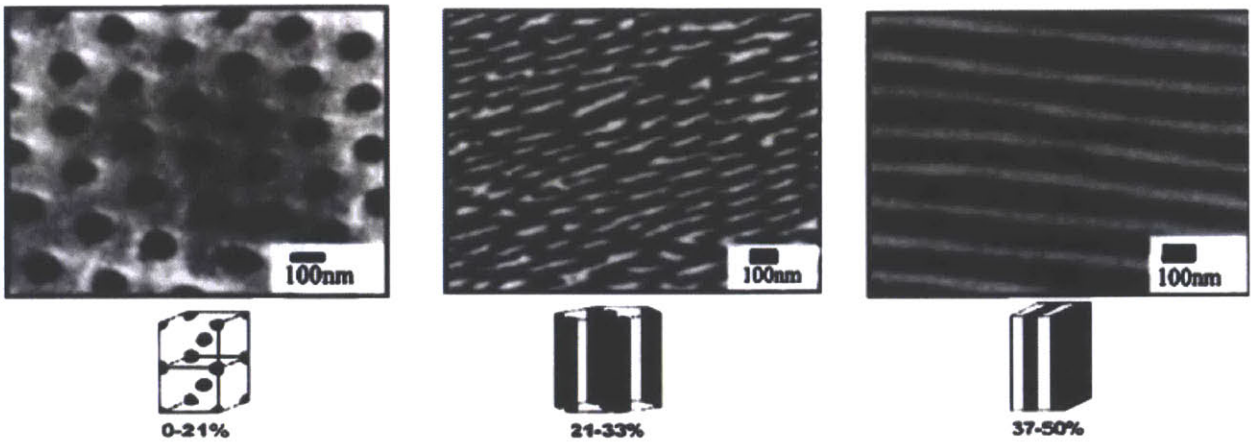

Figure 1.4. Images and associated schematics of block copolymer based photonic crystals.[15] Left: scanning electron microscope (SEM) image of poly(styrene-*b*-isoprene) (PS-PI) 194/197 kg/mol copolymer swollen with PS homopolymer; middle: atomic force microscope (AFM) image of a roll-cast PS-PI 320/680 kg/mol copolymer; right: transmission electron microscope (TEM) image of lamellar structures by PS-PI 194/197 kg/mol swollen with PS and PI homopolymers.

BCPs of roughly symmetric block composition self-assemble into a lamellar morphology. With the proper choice of block chemistry and molecular weights, long-range ordered lamellar BCPs on a flat substrate reflect light and display colors across the visible spectral regime.[15, 16] Fabrication of BCP photonic crystals with photonic band gaps in the visible regime remains challenging as the both synthesis and processing become more difficult with high molecular weights BCPs.

1.5. *Responsive PS-P2VP photonic gels*

As an alternative to using high molecular weight BCPs that are hard to synthesize and process, a selective solvent can be employed to swell one block in the BCP lamellae and to

increase both the domain spacing and the refractive index contrast, thus creating color from the originally colorless material.[17] The 1D photonic crystal made by selectively swelling the BCP is called a photonic gel. The diblock copolymer used for the photonic gels in this thesis is poly(styrene-*b*-2-vinylpyridine) (PS-P2VP). In the first work on PS-P2VP gels, the P2VP block of a 190k/190k PS-P2VP was quarternized and water or salt solutions (ammonium chloride NH_4Cl) were used as the selective solvent (see Figure 1.5).

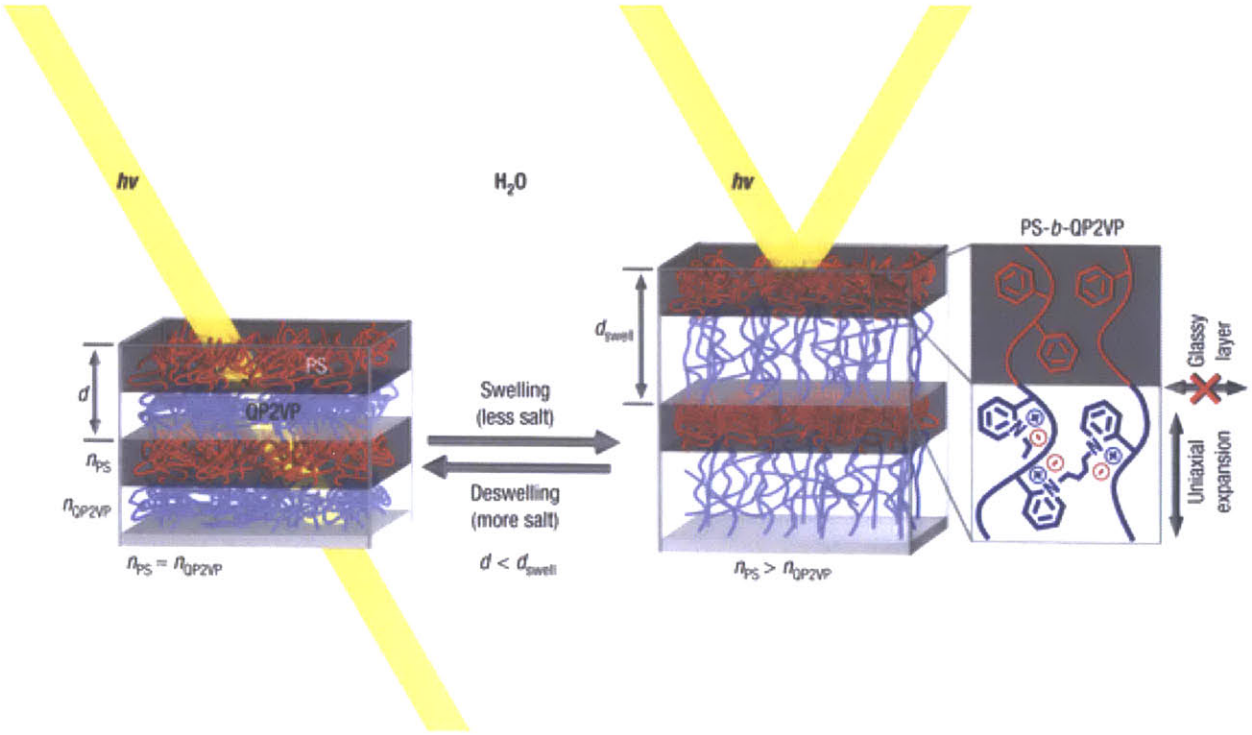

Figure 1.5. Schematic of the photonic gel film structure and the tuning mechanism.[17] The hydrophobic and glassy PS layers (red) limit the expansion of the quaternized P2VP gel layers (blue) to the direction along the layer normal only. The photonic responses were triggered by the concentration of the salt NH_4Cl in the solution. The swelling ratio of the quaternized P2VP layers decreases with increased salt concentration, and therefore, the reflectivity of the photonic gel blue-shifts in more concentrated salt solutions.

In addition to selectively swelling one block in the BCP, broadband dynamic tunability of the reflective color can also be achieved in BCP photonic gels by swelling both blocks with a neutral solvent.[18] The rapid solvent transport and corresponding large volume changes in the gel layers of the lamellar BCP gels contribute to the sensitive and reversible photonic responses on the sub-second time scale to stimuli such as pH, salt concentration, temperature, and mechanical strain.[17, 19-22]

1.6. *Polymer solutions and gels*

The photonic responses of the PS-P2VP gels result from the swelling/deswelling of the P2VP block layers triggered by the changes in the solution environment. The behavior of the gel block in a lamellar BCP – selective solvent system can be inferred from the solution properties of the corresponding homopolymer in the same solvent. Thus, homopolymer solution thermodynamics is essential to the understanding and control of the BCP gels' photonic responses.

Polymer-solvent pairs with no specific interactions can be treated using the Flory-Huggins theory.[23] The theory assumes that both the segments of the polymer and the solvents are equal in size and distributed on a lattice. The pair-wise interactions between the lattice points only depend on the interacting species but not the direction, and are therefore only enthalpic. The free energy of mixing is composed of an entropic term of the arrangements of the polymer and solvent on the lattice and an enthalpic term accounting for the pair-wise interactions. The free energy of mixing ΔF_{mix} for a solution system of n_1 solvent molecules and n_2 polymer molecules is:

$$\Delta F_{mix} = kT\left(n_1 \ln \phi_1 + n_2 \ln \phi_2 + \chi n_1 \phi_2\right) \tag{1.1}$$

In Equation (1.1), ϕ_1 and ϕ_2 are the volume fractions of the solvent and the polymer in the solution, respectively, and $\phi_1 + \phi_2 = 1$. χ is the segmental interaction parameter of the polymer and solvent pair. The number of solvent molecules is usually much larger than the number of polymers in a polymer solution, so the second term in Equation (1.1) can be neglected.

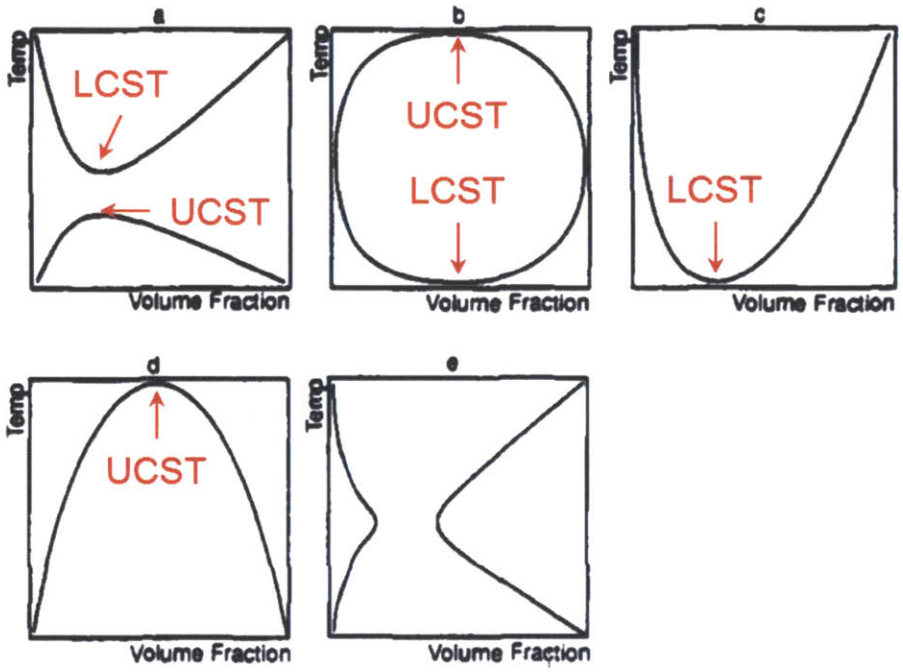

Figure 1.6. Possible phase diagrams of temperature vs. concentration for a binary polymer solution.[24] a) high LCST and low UCST; b) high UCST and low LCST; c) LCST; d) UCST; e) hourglass shape given by coalesced UCST and LCST boundaries.

Although not necessarily predicted or explained by the Flory-Huggins theory, critical solution behaviors exist in polymer-solvent systems (see Figure 1.6). Both upper and lower critical solution temperatures (UCST/LCST) are observed and in some cases a single system can show both types of behaviors.[24] At temperatures below the UCST or above the LCST, polymer solutions with compositions in certain range phase separate and the two new phases are in

thermodynamic equilibrium. UCST type phase behavior originates from the increasing entropy term in the free energy at elevated temperature, and the interaction between polymer and solvent is usually weak or does not vary with temperature, e.g. polystyrene and cyclohexane.[25] LCST systems often have hydrogen bonding or other strong interactions that have entropic contribution to the χ parameters. A famous LCST example is poly(*N*-isopropylacrylamide) in water.[26] Sharp changes in solubility occur as the system crosses the binodal in the phase diagram, which can be used to create sensitive color changes in the photonic gels as the volumes of the gel layers change abruptly.

Crosslinked polymers swell in good solvents but cannot dissolve due to the crosslinking. The swollen polymer networks form highly swollen 3D gels. The stretched subchains have fewer possible configurations and therefore their entropy decreases due to rubber elasticity, which competes with the favorable free energy of mixing. The thermodynamic equilibrium of swelling is given by the Flory-Rehner theory as shown in Equation (1.2).[27]

$$\ln\left(1-\frac{1}{\alpha}\right)+\frac{1}{\alpha}+\frac{\chi}{\alpha^2}+\frac{\rho_2 V_1}{M_c}\left(\frac{1}{\alpha^{1/3}}-\frac{1}{2\alpha}\right)=0 \qquad (1.2)$$

α is the swelling ratio of the gel by volume, $\alpha = V_{gel}/V_{dry}$; ρ_2 is the density of the dry polymer; V_1 is the molar volume of the solvent; M_c is the molecular weight between crosslinks. In a good solvent, $\alpha > 1$ and $\chi < 1/2$; α decreases with decreasing M_c, suggesting that the polymer network of higher crosslink density swells less in the same solvent.

Importantly, the Flory-Rehner theory provides a method to measure the effective χ parameter of a polymer-solvent pair, which quantifies the interaction between the polymer and the solvent

and is key to understanding the photonic responses of the lamellar BCP gels as will be shown in Chapter 4.

1.7. *Defects in block copolymer self-assembly*

Various types of defects have been observed in BCP self-assembly and the possible causes include polydispersity of the BCP, kinetic constraints or insufficient mobility toward the most stable equilibrium configurations, etc. Defects play important roles in both the dynamic and the equilibrium photonic properties of the lamellar BCP gels. Vertical pores exist in samples processed by solvent vapor annealing probably due to solvent condensation onto the BCP film and subsequent film dissolution.[17] Line defects, both screw and edge dislocations have also been observed in lamellar BCPs.[28-30] The screw dislocations (see Figure 1.7) especially serve as fast solvent transport pathways because they serve to interconnect the P2VP layers along the direction normal to the layers during swelling and contribute to the rapid responses (on a sub-second time scale) of the photonic gels.

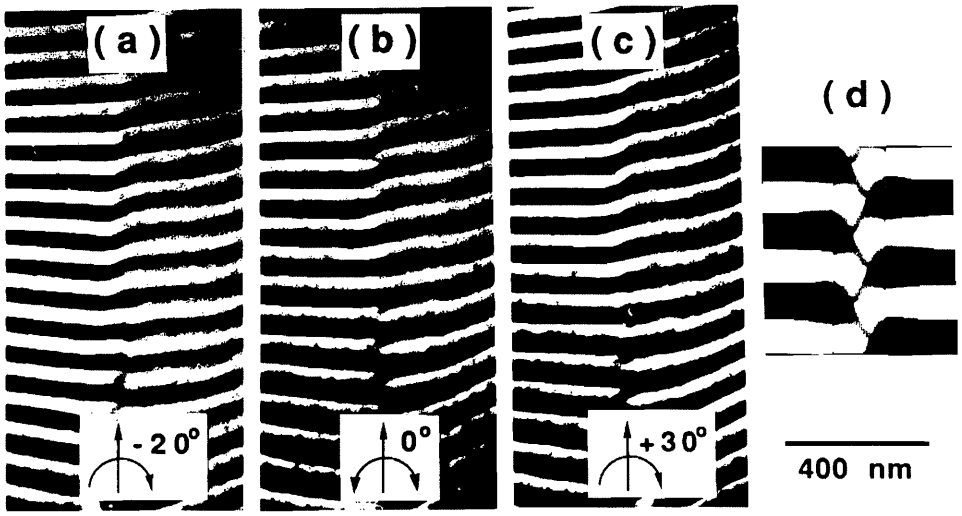

Figure 1.7. A screw dislocation observed in TEM images (a ~ c) and computer simulation (d) of a poly(styrene-*b*-butadiene) (PS-PB) BCP blended with homopolymers PS and PB.[28]

Both screw and edge dislocations also affect the equilibrium swelling ratios of the PS-P2VP gels. The PS layers form an interconnected network of sheets due to the connectivity of the dislocation cores, and the layers of the lamellar PS-P2VP are pinned by these defects. The swelling of the P2VP layers imposes a mechanical strain on the glassy PS layer network, which is the counterforce to the swelling of the lamellar PS-P2VP much like the crosslinked subchains limiting the swelling of a homopolymer gel. Without the defects, the PS-P2VP lamellae may unbind in a selective solvent. Unbinding was observed in a low molecular weight PS-P2VP BCP but not in the ones used for the photonic gels.[30] The low molecular weight BCP may have fewer defects in the self-assembly because of the faster kinetics and easier access to the equilibrium microstructure, and therefore not enough counterforce to layer unbinding.

There are few studies reported on screw or edge dislocations in aligned lamellar BCP films. Studies on liquid crystals shed light because of the similarity of the liquid crystal's smectic phase and the BCP lamellae. Y. Bouligand's schematics of the screw and edge dislocations in smectic liquid crystals[31] (see Figure 1.8) can be adapted to describe the defect networks present in the lamellar PS-P2VP used as the photonic gels in this thesis. The network of dislocations lines depicted in Figure 1.8c play an important role in the quantitative model of BCP swelling, which will be covered in detail in Chapter 4.

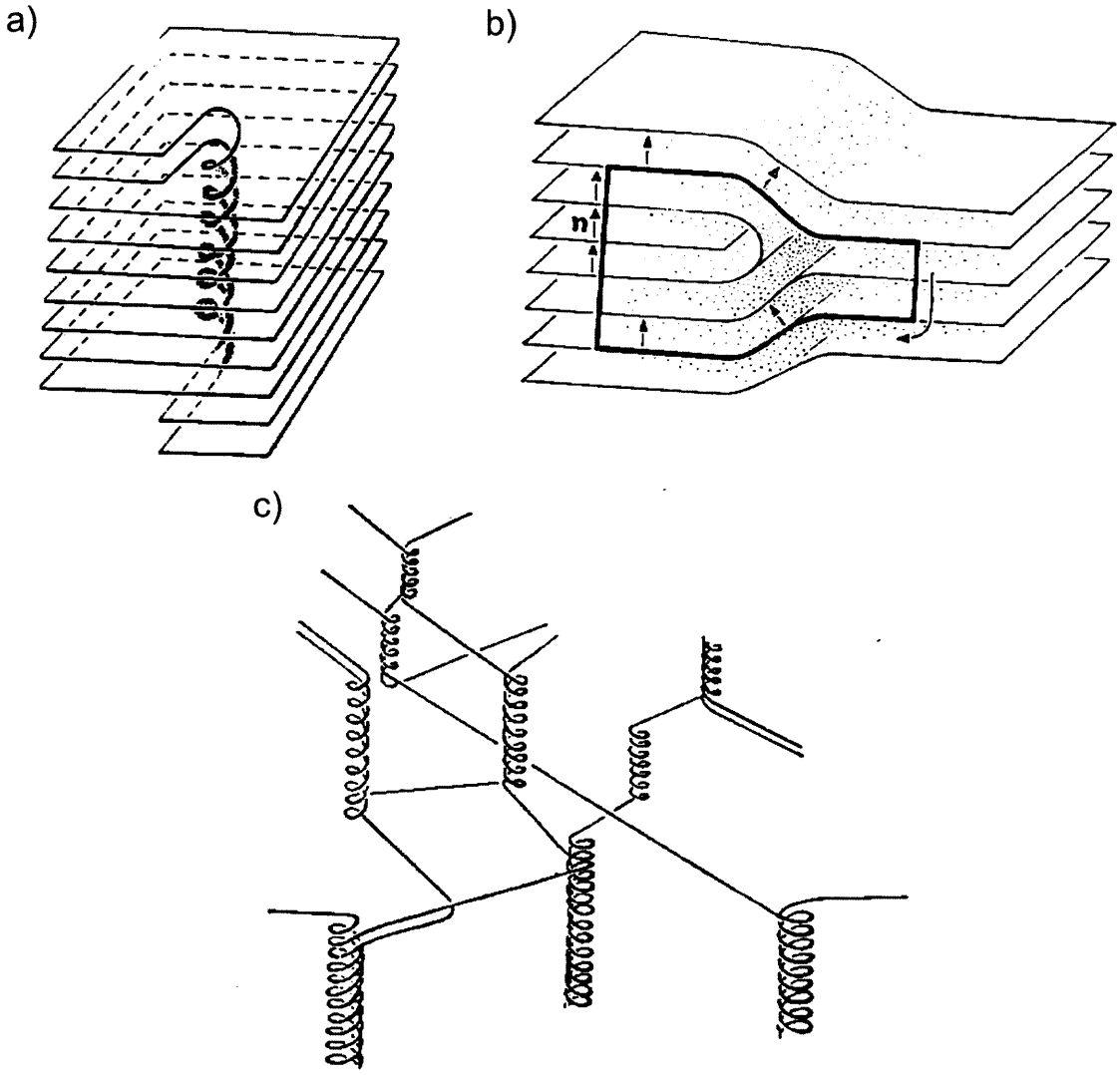

Figure 1.8. Schematics of the line defects in a smectic liquid crystal.[31] a) A screw dislocation; b) an edge dislocation; c) the dislocation network comprising of several screw (helices) and edge (lines) dislocations.

The defect structures in the self-assembly need be controlled in order to obtain consistent performance of the photonic gels. The number of defects in a BCP system at thermodynamic equilibrium can be calculated;[32] however, the PS-P2VP films of the photonic gels may not be at the equilibrium state due to the high molecular weights and the solvent vapor annealing

processing. Structural analysis on BCP films processed at different conditions is needed to establish the relationship between defect structures and processing conditions, which is beyond the scope of this thesis and will be discussed as future work in Chapter 6.

1.8. *Biomolecule – polyelectrolyte interactions*

Biomolecules such as proteins, DNAs and RNAs have attracted a lot of attention for their biological functionalities and crucial roles in living organisms. Proteins can be structural components to construct and support cells, catalysts for *in vivo* reactions, or carriers of small molecules. DNA and RNA carry the genetic information and are necessary to the reproduction and continuity of the species. These biomolecules can be treated as charged chains or particles when their physical properties in solutions are considered. Experimental techniques for the characterization of biomolecules include dynamic and static light scattering, zeta potential, ultraviolet-visible spectrometry, and circular dichroism.

Synthetic polyelectrolytes are charged synthetic macromolecules and have been demonstrated as a facile building block for functional materials via methods like alternating layer-by-layer deposition of polycation/polyanion molecules.[33-35] The size and charge density of the polyelectrolyte can be controlled by synthesis. Like small molecules, polyelectrolytes undergo dissociation/association reactions in solutions and the equilibrium constants of such reactions are quantitative measures for the strength of the polyelectrolytes.

Biomolecules and synthetic polyelectrolytes form ionic complexes due to electrostatic interactions in aqueous solutions.[36] Applications of the study on biomolecule-polyelectrolyte interactions include ionic hydrogels for protein delivery and entrapment, enzyme immobilization, protein separations, and microencapsulation using protein-polyelectrolyte coacervates.[36] The

formation and structures of such complexes are related to the hydrophobicity, chain stiffness, and charge sequence of the polyelectrolyte (Figure 1.9) as well as the charge anisotropy of the proteins (Figure 1.10).[37, 38]

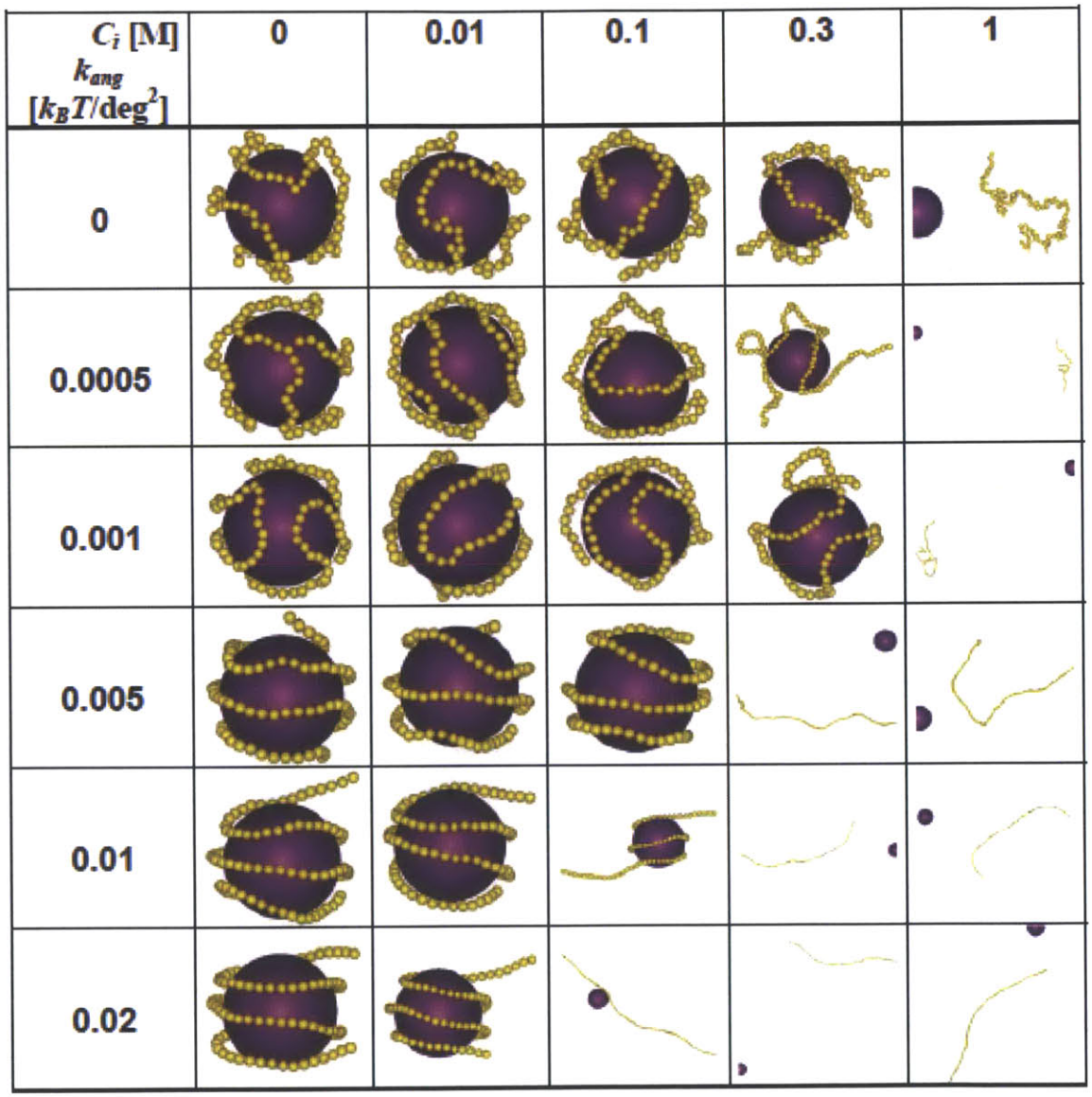

Figure 1.9. Monte Carlo simulated equilibrated conformations of semiflexible polyelectrolyte-particle complexes as a function of salt concentration and chain flexibility.[37]

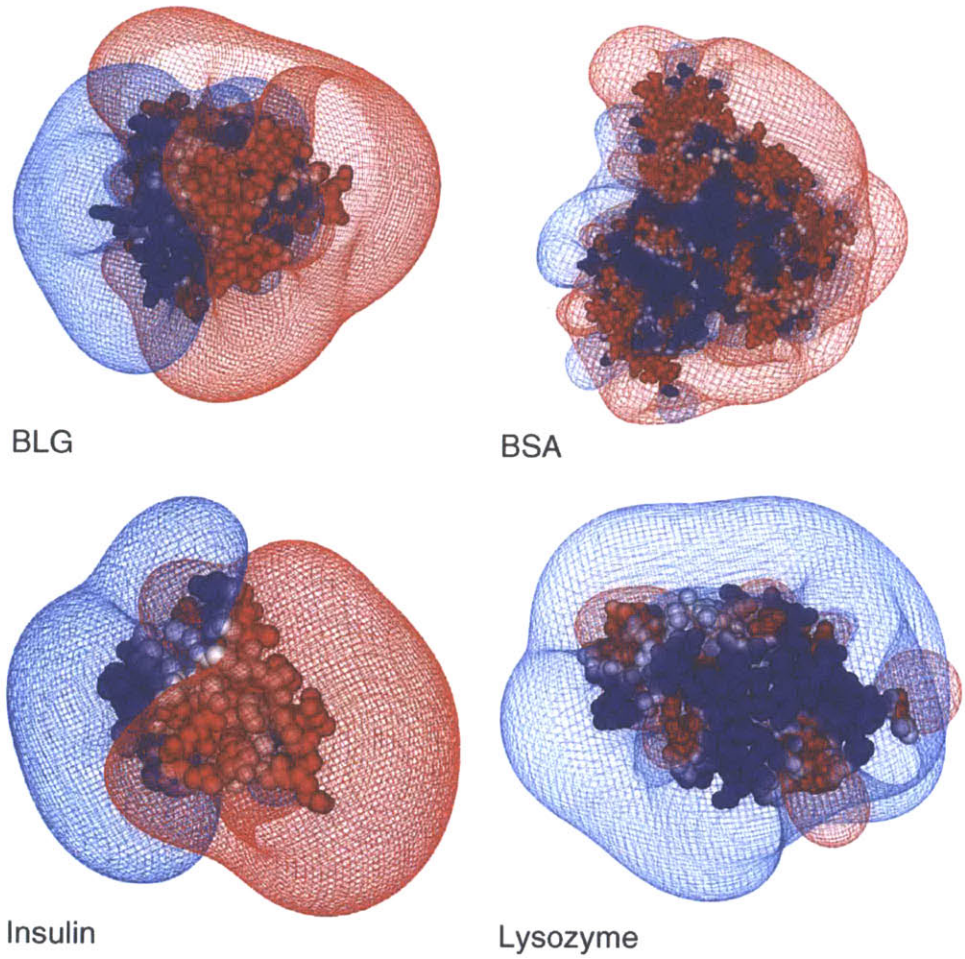

Figure 1.10. Delphi representations of electrostatic potentials for β-lactoglobulin (BLG), bovine serum albumin (BSA), insulin, and lysozyme at pH 7.[38] The red and blue colors represent the - 0.1 and 0.1 kT/e potential surfaces around the different proteins.

The ionic interactions between biomolecules and polyelectrolyte gels lead to swelling/deswelling of the polyelectrolyte gels, which can be used as a new stimulus to induce photonic responses in the lamellar BCP gels. The photonic responses to the biomolecule solutions indicate the ionic interactions between the biomolecule and the polyelectrolyte gel block. All the aforementioned parameters influencing such interactions can be used as tuning variables for the photonic responses. In PS-P2VP based systems, the charge density, chain

stiffness, and hydrophobicity of the polyelectrolyte can be adjusted via the pyridine quaternization reaction that converts the neutral P2VP chains into polycations. The size and charges of the biomolecules affect both the transport into the lamellar BCP gels and the steady-state swelling ratios and resultant colors of the photonic gels. Therefore, the BCP photonic gels have a novel potential utility as a fast and visually interpretable method to differentiate different proteins.

References

1. Hanlon, R. T. Camouflage & Adaptive Coloration. *http://hermes.mbl.edu/mrc/hanlon/coloration.html.*

2. Hanlon, R. *Curr. Biol.* **2007**, *11*, 400-404.

3. Mathger, L. M.; Denton, E. J.; Marshall, N. J.; Hanlon, R. T. *J. R. S. Interface* **2009**, S149-S163.

4. Rayleigh, J. W. S. *Phil. Mag.* **1888**, 256-265.

5. Yablonovitch, E. *Phys. Rev. Lett.* **1987**, *20*, 2059-2062.

6. John, S. *Phys. Rev. Lett.* **1987**, *23*, 2486-2489.

7. Born, M.; Wolf, E. *Principles of optics: electromagnetic theory of propagation, interference and diffraction of light;* ; New York ; Cambridge University Press: Cambridge, UK, 1997.

8. Yeh, P. *Optical waves in layered media;* Wiley: New York, 1988.

9. Qi, M.; Lidorikis, E.; Rakich, P.; Johnson, S.; Joannopoulos, J.; Ippen, E.; Smith, H. *Nature* **2004**, *6991,* 538-542.

10. Ullal, C.; Maldovan, M.; Thomas, E.; Chen, G.; Han, Y.; Yang, S. *Appl. Phys. Lett.* **2004**, *26,* 5434-5436.

11. Wijnhoven, J.; Vos, W. *Science* **1998**, *5378,* 802-804.

12. Bates, F.; Fredrickson, G. *Phys. Today* **1999**, *2,* 32-38.

13. Park, C.; Yoon, J.; Thomas, E. *Polymer* **2003**, *22,* 6725-6760.

14. Urbas, A.; Sharp, R.; Fink, Y.; Thomas, E. L.; Xenidou, M.; Fetters, L. J. *Adv. Mater.* **2000**, *11,* 812-814.

15. Edrington, A. C.; Urbas, A. M.; DeRege, P.; Chen, C. X.; Swager, T. M.; Hadjichristidis, N.; Xenidou, M.; Fetters, L. J.; Joannopoulos, J. D.; Fink, Y.; Thomas, E. L. *Adv. Mater.* **2001**, *6,* 421-425.

16. Yoon, J.; Mathers, R.; Coates, G.; Thomas, E. *Macromolecules* **2006**, *5,* 1913-1919.

17. Kang, Y.; Walish, J. J.; Gorishnyy, T.; Thomas, E. L. *Nat. Mater.* **2007**, *12,* 957-960.

18. Lee, W.; Yoon, J.; Thomas, E. L.; Lee, H. *Macromolecules* **2013**, *17,* 6021-6024.

19. Lim, H. S.; Lee, J.; Walish, J. J.; Thomas, E. L. *ACS Nano* **2012**, *10,* 8933-8939.

20. Walish, J. J.; Fan, Y.; Centrone, A.; Thomas, E. L. *Macromol. Rapid Commun.* **2012**, *18,* 1504-1509.

21. Chan, E. P.; Walish, J. J.; Thomas, E. L.; Stafford, C. M. *Adv. Mater.* **2011**, *40,* 4702-4706.

22. Chan, E. P.; Walish, J. J.; Urbas, A. M.; Thomas, E. L. *Adv Mater* **2013**, *29,* 3934-3947.

23. Flory, P. J. *Principles of polymer chemistry;* Cornell University Press: Ithaca, 1953.

24. Qian, C.; Mumby, S. J.; Eichinger, B. E. *Macromolecules* **1991**, *7,* 1655-1661.

25. Saeki, S.; Kuwahara, N.; Konno, S.; Kaneko, M. *Macromolecules* **1973**, *2,* 246-250.

26. Hirotsu, S.; Hirokawa, Y.; Tanaka, T. *J. Chem. Phys.* **1987**, *2,* 1392-1395.

27. Flory, P. J.; Rehner, J. *J. Chem. Phys.* **1943**, *11,* 521-526.

28. Gido, S. P. Constant mean curvature and minimal surface grain boundary morphologies in diblock copolymers : characterization and modeling, Massachusetts Institute of Technology, Dept. of Chemical Engineering, 1993.

29. Gido, S.; Gunther, J.; Thomas, E.; Hoffman, D. *Macromolecules* **1993**, *17,* 4506-4520.

30. Fan, Y.; Walish, J. J.; Tang, S.; Olsen, B. D.; Thomas, E. L. *Macromolecules*, Article ASAP.

31. Bouligand, Y. *Journal De Physique* **1972**, *5-6,* 525-547.

32. Mishra, V.; Fredrickson, G. H.; Kramer, E. J. *ACS Nano* **2012**, *3,* 2629-2641.

33. Decher, G. *Science* **1997**, *5330,* 1232-1237.

34. Tang, Z.; Wang, Y.; Podsiadlo, P.; Kotov, N. A. *Adv Mater* **2006**, *24,* 3203-3224.

35. Wang, Y.; Angelatos, A. S.; Caruso, F. *Chemistry of Materials* **2008**, *3,* 848-858.

36. Cooper, C. L.; Dubin, P. L.; Kayitmazer, A. B.; Turksen, S. *Current Opinion in Colloid & Interface Science* **2005**, *1–2,* 52-78.

37. Wallin, T.; Linse, P. *Langmuir* **1996**, *2,* 305-314.

38. Seyrek, E.; Dubin, P.; Tribet, C.; Gamble, E. *Biomacromolecules* **2003**, *2,* 273-282.

2. Methods

This chapter describes in detail the methods to prepare, characterize, and model the photonic gels, the homopolymer gel synthesis, and characterization of the protein solutions.

2.1. *BCP film preparation*

2.1.1. Polymers and film casting

Diblock copolymers poly(styrene-*b*-2-vinylpyridine) (PS-P2VP) of roughly symmetric block compositions were purchased from Polymer Source, Inc. The various polymers used in this thesis are summarized in Table 2.1. The molecular weight and polydispersity data were from the supplier, and the polymers were used for film casting without further purification or treatment.

Table 2.1. Summary of PS-P2VP polymer samples used in the thesis.

#	M_n(PS) kg/mol	M_n(P2VP) kg/mol	polydispersity	ϕ(PS)	chapter(s)
1	57	57	1.08	0.50	3
2	102	97	1.12	0.51	3, 4, 5
3	190	190	1.10	0.50	3

PS-P2VP films were cast from propylene glycol monomethyl ether acetate (PGMEA, Alfa Aesar) solutions. The types of substrates were selected based on the purpose of the samples: silicon wafers for film thickness measurements with ellipsometry; glass slides photonic response characterization with UV-Vis or optical fiber spectrometer; quartz spectrometer cuvettes for UV-Vis spectrometry with temperature control.

All substrates were cleaned using the following procedure:

1) Sonicate in 2% Hellmanex II Cell Cleaning Concentrate solution for 15 minutes;
2) Rinse with Milli-Q water (deionized water purified by the Millipore Milli-Q water purification station with a resistivity at 18.2 MΩ·cm at 25 °C) for 15 times;
3) Repeat 1) and 2) once;
4) Sonicate in ethanol for 2 minutes;
5) Replace ethanol and repeat 4) once;
6) Blow dry with nitrogen;
7) For substrates that were not immediately used, soak in ethanol for storage.

The substrates were then treated with silane to increase the affinity and selectivity to the P2VP block. The process of silane treatment was:

1) Put 1 mL iodotrimethylsilane in a 20 mL glass vial;
2) Put cleaned and dried substrates and the silane vial in a desiccator;
3) Apply vacuum for 5 minutes;
4) Turn off vacuum and let the substrates sit in the closed desiccator for 10 minutes;
5) Use the substrates within 15 minutes.

5 % by weight PS-P2VP solutions in PGMEA were used for film casting. Samples on glass slides or silicon wafers were cast by spin coating using a Specialty Coating Systems (SCS) G3P-8 spin coater. The BCP solution was spread onto the slide/wafer with a glass Pasteur pipette and spun coat at 500 rpm with a 5-second ramp for 90 seconds. For 102k/97k PS-P2VP, this method yielded uniform films of thicknesses around 600 nm. The films cast from the 57k/57k PS-P2VP

were not smooth enough for ellipsometry measurements, and those from the 190k/190k were not uniform and the thickness ranges from 800 to 1200 nm.

Samples on the inner wall of quartz cuvettes were cast from the same 5 % PS-P2VP/PGMEA solution. 15 μL solution was spread onto the optical wall of the cuvette from the inside using a pipette, and the film was then dried slowly in a loosely covered 70x50 mm glass crystallization dish. The films cast in this way were around 1 μm thick.

2.1.2. **Solvent vapor annealing**

The as-cast PS-P2VP films were then annealed in chloroform (Mallinckrodt) vapor to align the lamellae parallel to the substrate surface. The annealing conditions needed be adjusted to fit BCPs of different molecular weights and on different types of substrates. The setups and parameters described below worked best for the 102k-97k PS-P2VP, which was the primary BCP used for the majority of work in this thesis.

Samples on wafers or glass slides were annealed in the setup shown in Figure 2.1. The solvent annealing chamber was composed of two glass crystallization dishes. The samples were held above the solvent surface by a group of glass test tubes. 5 mL chloroform was added to the chamber which sat on a hot plate set at 50 °C. A glass heating plate with conductive coating was placed on top of the cover dish to prevent solvent condensation. The glass plate was connected to a digital controller and the temperature was set at 60 °C, higher than the hot plate and chloroform vapor temperature so that chloroform condensation on the inner surface of the cover dish was prevented. The setup was wrapped in aluminum foil. Annealing was completed after the solvent dried out in approximately 12 hours.

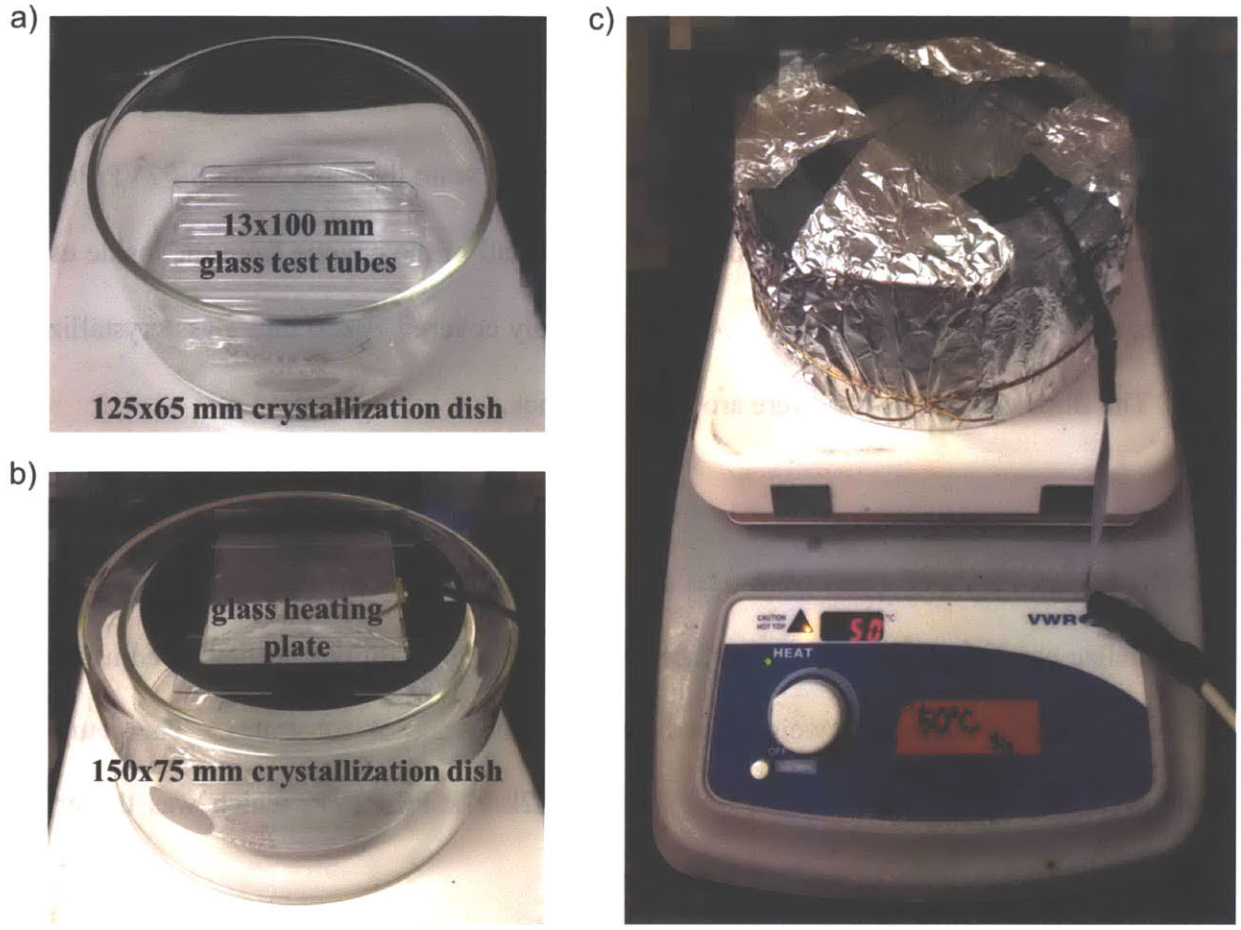

Figure 2.1. The solvent vapor annealing setup for samples on glass slides or silicon wafers. a) The bottom crystallization dish and the glass test tubes; b) the cover crystallization dish and the glass heating plate on top; c) the finished setup wrapped in aluminum foil and placed on a 50 ˚C hot plate. The setup anneals up to three 3x1" glass slides per batch.

Samples in cuvettes were annealed in the setup shown in Figure 2.2. The solvent annealing chamber was a glass crystallization dish. The cuvette samples were placed on the bottom of the dish along with a 10 mL glass beaker filled with chloroform. The dish was covered with a piece of aluminum foil with holes to prevent solvent condensation inside the cuvette if the vapor

pressure was too high. The setup was placed on a hot plate set at 50 °C. A full beaker of solvent (10 mL) dried out overnight when annealing was completed.

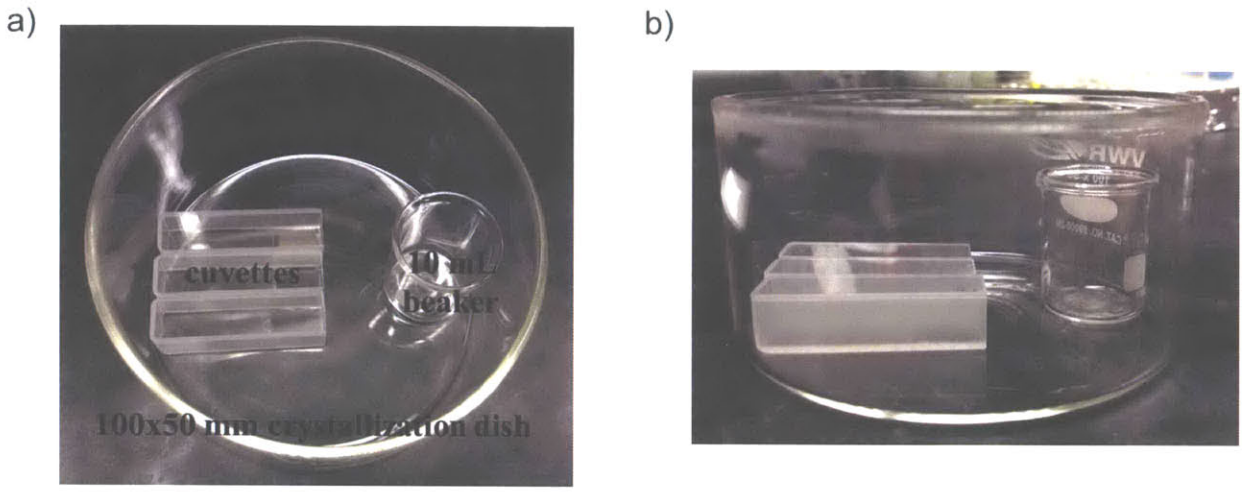

Figure 2.2. The solvent vapor annealing setup for samples in cuvettes. a) Top view and b) side view. The aluminum foil and hot plate are omitted.

As annealing proceeded, it was helpful to know the degree of long-range lamellar order in the BCP film. A quick method to test the alignment was to add ethanol onto the film surface and to watch for the reflection colors. A film that did not show color in ethanol did not have enough long-range order and needed more annealing. For films that showed color, the colors offered a rough estimation of the degree of domain alignment, as the tilted domains and an abundance of defects tended to blue-shift the reflectivity. For the 57k-57k and 102k-97k PS-P2VP samples, purple and green reflection colors in ethanol indicated sufficient annealing. The ethanol swelling method was a quick and non-destructive way to test the annealing progress because the film's chemistry and morphology in the dry state remained unaltered after the ethanol evaporated.

2.1.3. **Quaternization reactions**

The annealed PS-P2VP films swelled and showed color in alcohols but did not swell enough to show color in water. The work in Chapter 5 with protein solutions requires photonic gel samples that swell and show reflective color in aqueous solutions. To enable aqueous swelling at neutral pH, we converted the P2VP block into a polyelectrolyte block. The pyridine groups in the P2VP block reacted with bromides to form pyridinium. The charge density of the polyelectrolyte can be controlled by the extent of conversion of the reaction. The quaternized PS-P2VP films swelled in water and showed reflective color.

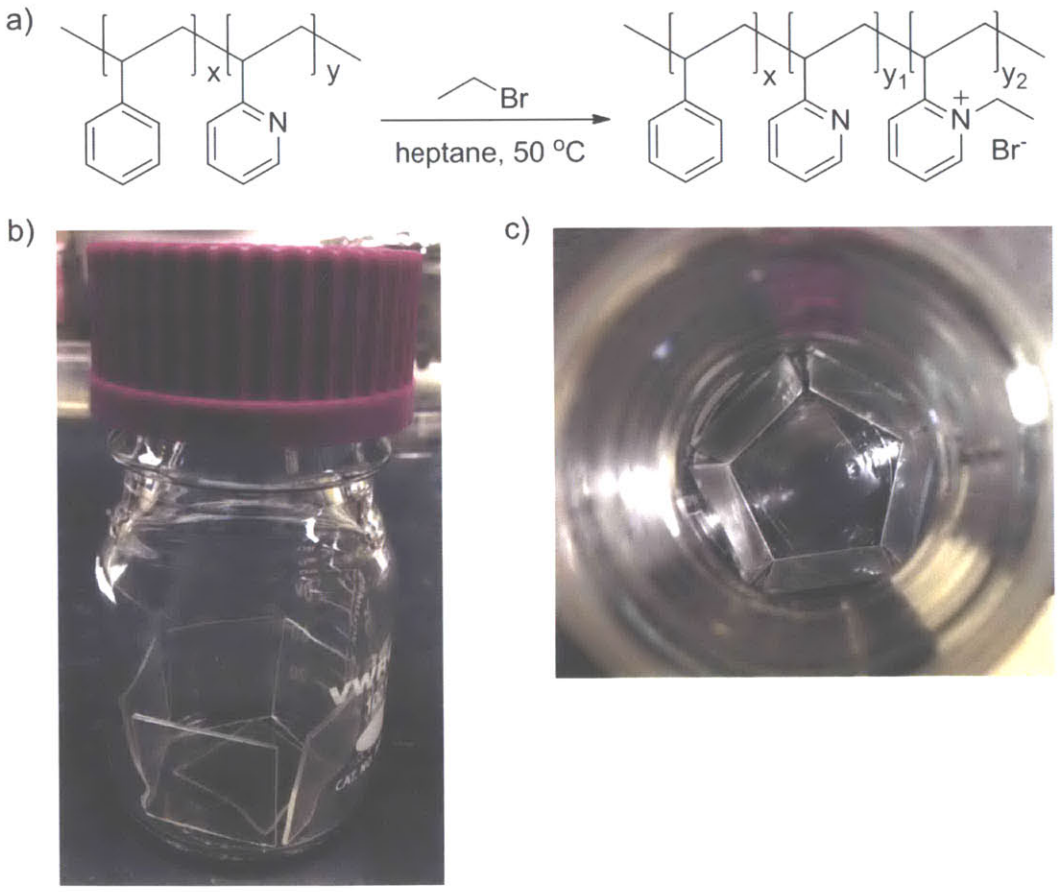

Figure 2.3. The quaternization reaction and experimental setup for the quaternization of annealed PS-P2VP films. a) The quaternization reaction between PS-P2VP and

bromoethane; b) side view of the 100 mL glass jar containing six 1x1" BCP film samples; c) top view of the arrangement of the six slides: five on the wall with the film sides facing inward and one on the bottom with the film side facing up. The reaction mixture is omitted.

Table 2.2. Summary of quaternization reagents or reaction conditions for samples used in Chapter 5.

variable	base	mole %	additive	mole %	reaction time
conversion	bromoethane	100	N/A	N/A	1 day
					2 days
					3 days
					4 days
hydrophobicity	bromoethane	100	1-bromopropane	0	3 days
		99		1	3 days
		95		5	3 days
		90		10	3 days
crosslink density	bromoethane	100	1,6-dibromohexane	0	3 days
		99.5		0.5	3 days
		99		1	3 days
		98		2	3 days

The quaternization reaction setup for the samples used in Chapter 5 is shown in Figure 2.3. The annealed samples were cut into 1x1" squares and placed into a 100 mL glass jar filled with 50 mL reaction mixture. The liquid-phase reaction mixture was a heptane solution containing 10 % by volume bromide. The bromide reagents were bromoethane or mixtures of bromoethane

with 1-bromopropane or 1,6-dibromohexane. The conditions of the quaternization reactions were summarized in Table 2.2.

After the reaction ends, the samples were taken out of the jar and soaked in ethanol to remove the reagents. Glass slide staining dishes were used to hold the samples. Ethanol is replaced every 30 minutes twice. The washed samples were blown dry with nitrogen and cut into 1/3x1" pieces for spectrometry.

2.2. *BCP film characterization*

2.2.1. **Ellipsometry**

The thickness of the dry BCP films was measured by a J.A. Woollam XLS-100 spectroscopic ellipsometer. A silicon wafer was used as the substrate. A single incidence angle at 70 ° was used and data from 200 to 1000 nm were used for the fitting. A blank substrate was measured first to calibrate the thickness of the silicon dioxide layer on the Si wafer. The model was based on 1 mm Si and unknown SiO_2 thickness for fitting. The usual calculated SiO_2 thickness was 1.5 μm. Then the P2VP samples were cast on the same substrates and measured and modeled as a Cauchy layer with a refractive index of 1.6, assumed constant at all wavelengths. Due to the surface roughness and non-uniformity of the films, the exact shapes of the peaks in the spectra cannot always be matched in the fitting. Fitting is satisfactory as long as most peak positions were matched. An example of the ellipsometry data and model fitting for a 102k/97k PS-P2VP film is shown in Figure 2.4. The film thickness obtained from this fitting was 592 nm.

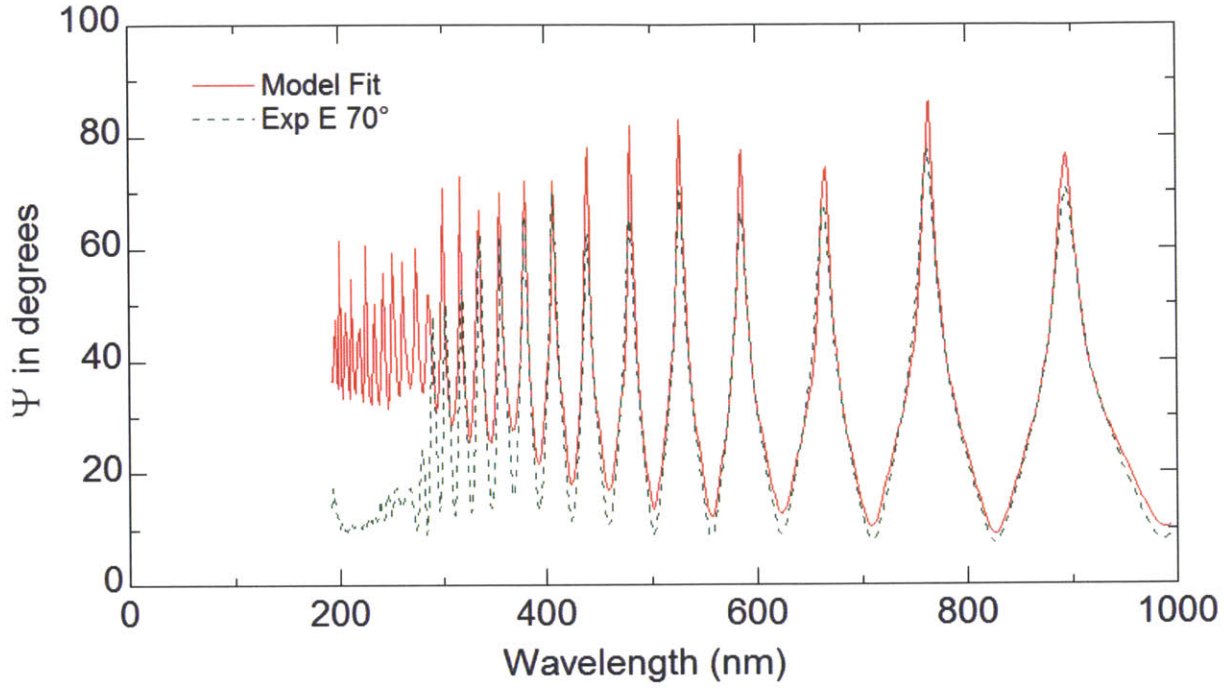

Figure 2.4. Ellipsometry data and model fitting for a 102k/97k PS-P2VP film spun cast on a Si wafer using a 5 % BCP solution in PGMEA at 500 rpm. The thickness of the film calculated from the fitting was 592 nm.

2.2.2. **Cross-sectional TEM**

Transmission electron microscope (TEM) was used to image the cross-section of the PS-P2VP films to measure the domain spacing in the dry state, estimate the degree of lamellar ordering, and identify the types of (dislocation) defects present in the films.

A JEOL JEM-9320FIB single-beam focused ion beam system (FIB) was used to cross-section the annealed BCP films on silicon wafers. To protect the sample from radiation damage, the sample was first coated with a carbon layer by applying the permanent marker ink, and then sputtered with gold for 60 seconds. The typical gold thickness was approximately 10 nm. The

slice was taken out by glass probes under a microscope and placed on 400 square mesh copper grids with carbon films (EMS CF-400-Cu).

The cross-section slices were then stained in iodine vapor. Approximately 0.1 g I_2 was placed in a 50 mL glass jar and sublimed into a vapor at room temperature. Samples were put into the jar for staining at room temperature overnight. The P2VP block appeared dark in TEM after staining due to the I_2 interaction with the pyridine groups. A JEOL JEM 2000FX TEM was used with the acceleration voltage at 120 kV to take the bright-field TEM images shown in this thesis.

2.3. *Photonic properties*

2.3.1. **UV-Vis spectrometer**

We used a Varian Cary 6000i UV-Vis-NIR spectrophotometer to measure the steady-state transmission spectra of the swollen photonic gels. Films cast inside cuvettes were used and the spectra from 200 to 800 nm with a spectral resolution of 2 nm were collected. Due to BCP absorption, reflection spectra below 300 nm did not provide useful information.

A temperature controlled sample holder was needed for the temperature response study in Chapter 3. A cuvette with an annealed PS-P2VP film on one inner optical wall filled with water at room temperature was used for baseline. Cuvettes with annealed polymer films were filled with acid solutions at room temperature, cooled to 0 °C, and then heated up to 95 °C with spectra collected every 5 °C. An equilibration time of 10 min was allowed after each temperature change. The temperature series at each acid concentration was collected from the same film sample and different samples were used for acid solutions of different concentrations.

In Chapter 4, the reflection spectra of the PS-P2VP photonic gels swelling in alcohol-water co-solvents were collected. BCP films cast in quartz cuvettes were used as the photonic gels. A blank cuvette was used as baseline. A cuvette with an annealed film was filled with alcohol-water co-solvents, starting from pure alcohol to roughly 30 % by volume alcohol when the reflection peak moved below 300 nm, with spectrum taken every 10 % change in the alcohol concentration. An equilibration time of 3 min was used at each sampling point to ensure steady-state swelling. All UV-Vis data presented in Chapter 4 were collected on the same PS-P2VP film, which was blown dry with nitrogen before swelling again.

2.3.2. **Fiber spectrometer**

Time-dependent reflection spectra were measured with an Ocean Optics HR4000CG-UV-NIR high-resolution spectrometer in transmission mode (Figure 2.4).

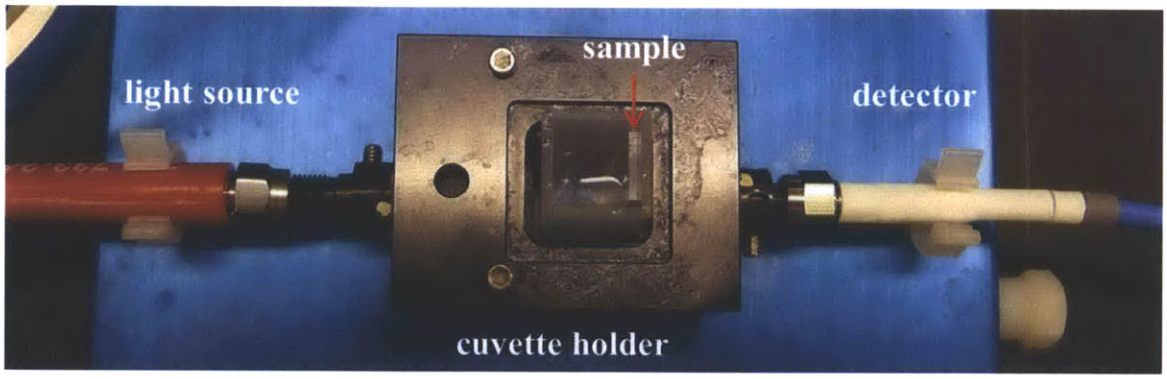

Figure 2.5. The Ocean Optics optical fiber spectrometer setup for time-dependent reflectivity measurements.

The fiber spectrometer can be used to collect both successive and single spectra. For successive spectra, the high-speed acquisition mode was selected with 5 ms integration time and 10 scans to average, thus an interval of 50 ms between the successive spectra. The single spectra

were saved with 5 ms integration time and 100 scans to average. The successive spectra were collected at the beginning of the swelling process of the PS-P2VP gels to capture the short-time responses, and the single spectra were collected in the later stage with intervals longer than 3 min between the time points.

Annealed and quaternized samples on glass slides were cut into 1/3x1" pieces for the time-dependent spectra measurements. A quartz cuvette was filled with the buffer or protein solution and the sample was slid in along the optical wall with the film side facing the solution. A blank glass slide immersed in the solution was used as baseline. The dry sample was soaked in the buffer solution for 10 min. The spectra over the first minute was recorded as a reference for the solvent transport and defect density, and a single spectrum was saved at the end of the 10 min equilibration period as the t = 0 point. The swollen sample was immediately transferred into a separate cuvette containing the protein solution. The spectra over the first 5 min were recorded. Single spectra were taken at t = 7, 10, 15, 30 min and then at the end of each hour. For each sample, the buffer solution and the protein solution had the same pH and buffer composition so that the data could be used to analyze the role of proteins on the photonic responses.

Figure 2.5 shows a typical set of data collected on one photonic gel sample. The two color maps were the first minute and the first five minutes of the photonic gel swelling in the buffer and protein solutions, respectively. The spectra at selected time points were plotted in the overlay plot. The noise in the spectra has been filtered by using the MATLAB command "smooth". The reflectivity peak wavelengths were obtained from the spectra by picking the maximum in reflectance in the range of the first-order peaks using the MATLAB command "max".

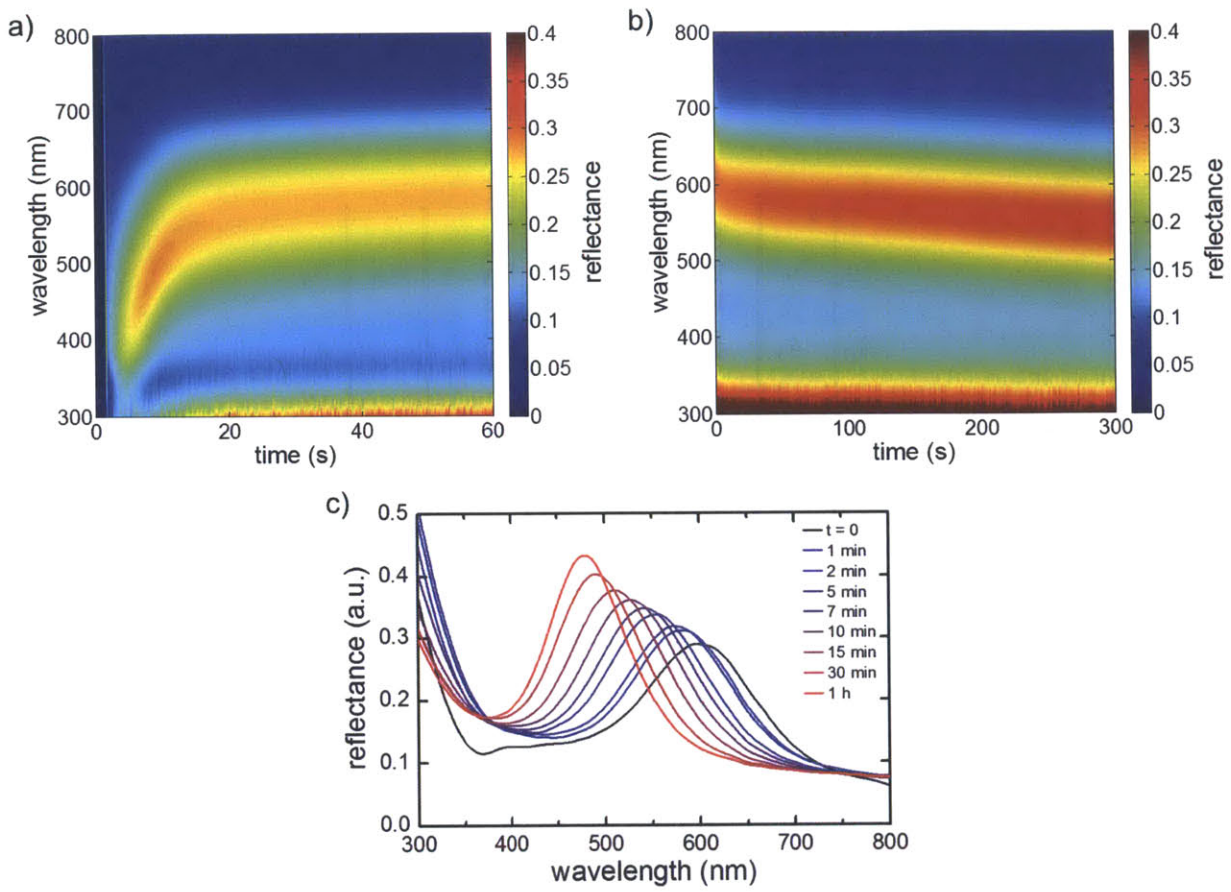

Figure 2.6. Real-time reflection spectra of a bromoethane quaternized PS-P2VP photonic gel in 1 % BSA solution in 10 mM pH 8 tris buffer. a) Color map of the reflection spectra in the first minute of the dry BCP film swelling in the buffer solution; b) color map of the reflection spectra in the first 5 minutes of the BCP gel swelling in the protein solution; c) the photonic gel's reflection spectra after being transferred into the protein solution for various times.

2.4. *Transfer matrix method (TMM)*

The reflectivity of the BCP photonic gels can be calculated by using the transfer matrix method (TMM) for isotropic layered media.[1, 2] The reflection and transmission of

electromagnetic radiation through a multilayer dielectric medium (see Figure 2.6) can be solved by using a 2x2 matrix method.

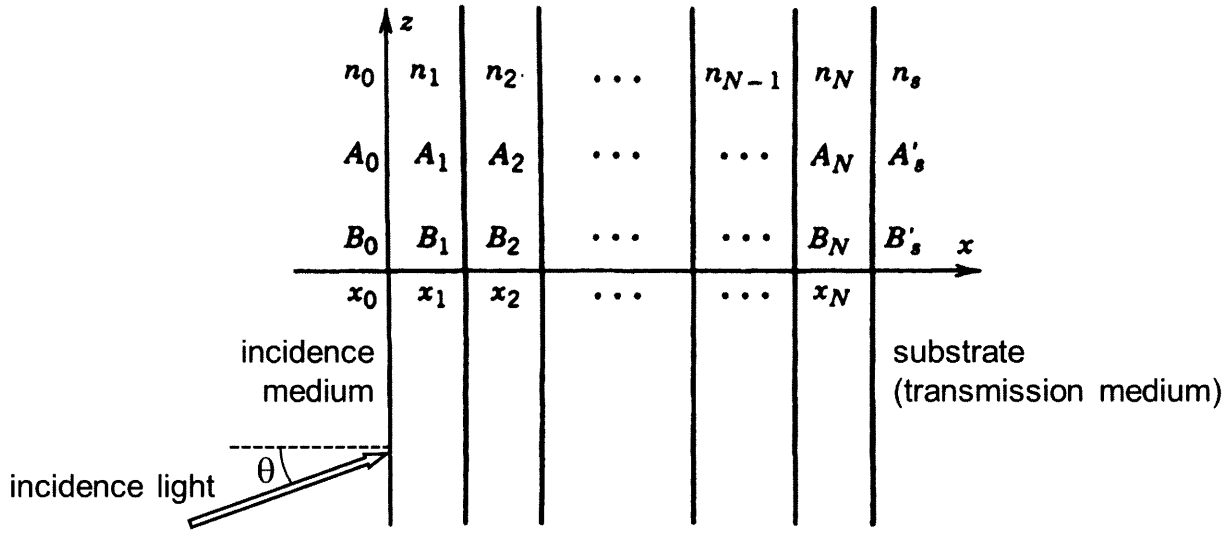

Figure 2.7. Schematic of a multilayer dielectric medium and an incidence light.[1] N was the number of layers; A_0 and B_0 were the amplitudes of the plane waves in medium at the incidence interface, and A'_s and B'_s were the amplitudes of the plane waves in the medium at the substrate interface.

The TMM simulation in this thesis assumed that each layer in the multilayer medium was homogeneous and isotropic. We also neglected the imaginary part of the complex refractive index n^*, which was related to the relative permittivity ε_r by Equation (2.1):

$$n^{*2} = (n + i\kappa)^2 = \varepsilon_r \tag{2.1}$$

with $\kappa = 0$. We also neglected dispersion and assumed that the real part of the refractive index was independent of the frequency or the wavelength of the incidence wave.

The dielectric structure is described by the refractive indices and the thicknesses of the layers in Equations (2.2) and (2.3):

$$n_l = \begin{cases} n_0, & l = 0, \text{ incidence medium} \\ n_1, & l = 1,3,5..., \text{ odd layers, medium 1} \\ n_2, & l = 2,4,6..., \text{ even layers, medium 2} \\ n_s, & l = s, \text{ substrate} \end{cases} \tag{2.2}$$

$$d_l = \begin{cases} d_1, & l = 1,3,5..., \text{ odd layers, medium 1} \\ d_2, & l = 2,4,6..., \text{ even layers, medium 2} \end{cases} \tag{2.3}$$

The electric field of a general plane-wave solution that satisfies Maxwell's equations can be written as:

$$E = E(x)e^{i(\omega t - \beta z)} \tag{2.4}$$

where x is the position along the direction normal to the layers, ω is the angular frequency of the plane wave, t is the propagation time, β is the z component of the wave vector, and z is the position in the direction parallel to the layers. The electric field distribution $E(x)$ in Equation (2.4) can be written as:

$$E(x) = \begin{cases} A_0 e^{-ik_{0x}(x-x_0)} + B_0 e^{ik_{0x}(x-x_0)}, & x < x_0 \\ A_l e^{-ik_{lx}(x-x_l)} + B_l e^{ik_{lx}(x-x_l)}, & x_{l-1} < x < x_l \\ A_s' e^{-ik_{sx}(x-x_N)} + B_s' e^{ik_{sx}(x-x_N)}, & x > x_N \end{cases} \tag{2.5}$$

k_{lx} in Equation (2.5) is the x component of the wave vectors and is related to the ray angle θ_l by:

$$k_{lx} = \sqrt{\left(n_l \frac{\omega}{c}\right)^2 - \beta^2}, \quad k_{lx} = n_l \frac{\omega}{c} \cos\theta_l, \quad l = 0,1,2,...,N,s \tag{2.6}$$

A_l and B_l in Equation (2.5) and Figure 2.6 represent the amplitude of the right-traveling and left-traveling plane waves at interface $x = x_l$, respectively.

The two modes of the plane wave need be considered separately in the calculation. Waves of the transverse electric (TE) mode has no electric field and only a magnetic field along the direction of propagation, while the waves of the transverse magnetic (TM) mode has no magnetic field and only an electric field along the direction of propagation. Using the condition that *E(x)* for the TE wave is a continuous function of x, the column vectors of A_l and B_l in the multilayer were related by:

$$\begin{pmatrix} A_0 \\ B_0 \end{pmatrix} = D_0^{-1} D_1 \begin{pmatrix} A_1 \\ B_1 \end{pmatrix}; \quad \begin{pmatrix} A_l \\ B_l \end{pmatrix} = P_l D_l^{-1} D_{l+1} \begin{pmatrix} A_{l+1} \\ B_{l+1} \end{pmatrix}, \quad l = 1,2,...,N \tag{2.7}$$

where D_l are the transmission matrices that link the amplitudes of the waves upon the two sides of the interfaces and are given by:

$$\begin{aligned} D_l &= \begin{pmatrix} 1 & 1 \\ n_l \cos\theta_l & -n_l \cos\theta_l \end{pmatrix} \quad \text{for TE wave} \\ D_l &= \begin{pmatrix} \cos\theta_l & \cos\theta_l \\ n_l & -n_l \end{pmatrix} \quad \text{for TM wave} \end{aligned} \tag{2.8}$$

and P_l the propagation matrix that accounts for propagation through the bulk of the layer:

$$P_l = \begin{pmatrix} e^{i\phi_l} & 0 \\ 0 & e^{-i\phi_l} \end{pmatrix} \quad \text{with} \quad \phi_l = k_{lx} d_l \tag{2.9}$$

Therefore, the relation between A_0, B_0 representing the incidence wave and A'_s, B'_s representing the transmission wave can be written as:

$$\begin{pmatrix} A_0 \\ B_0 \end{pmatrix} = M \begin{pmatrix} A'_s \\ B'_s \end{pmatrix} \quad \text{with} \quad M = D_0^{-1} \left[\prod_{l=1}^{N} D_l P_l D_l^{-1} \right] D_s \tag{2.10}$$

The 2x2 matrix M in Equation (2.10) is called the transfer matrix of the multilayer problem.

The reflectance and transmittance coefficients for an incidence light from medium 0 were defined as:

$$r = \left(\frac{B_0}{A_0} \right)_{B_s = 0} \tag{2.11}$$

and can be expressed by the elements in the transfer matrix:

$$r = \frac{M_{21}}{M_{11}} \tag{2.12}$$

Provided that the incidence medium is lossless, the reflectance is given by:

$$R = |r|^2 = \left| \frac{M_{21}}{M_{11}} \right|^2 \tag{2.13}$$

The reflectance from a photonic gel for the incidence light of a certain wavelength can thus be calculated by using Equation (2.13). Assuming that swelling only occurs in the P2VP layers along the direction normal to the lamellae, we obtain the parameters of the multilayer as:

$$n_l = \begin{cases} 1, & l = 0, \text{ incidence from air} \\ n_{PS} = 1.6, & l = 1,3,5..., \text{ odd layers, medium 1} \\ n_{P2VP\ gel} = n_e, & l = 2,4,6..., \text{ even layers, medium 2} \\ 1.5, & l = s, \text{ silica substrate} \end{cases}$$

$$d_l = \begin{cases} d_{PS} = \dfrac{d_0}{2}, & l = 1,3,5..., \text{ odd layers, medium 1} \\ d_{P2VP\ gel} = \dfrac{\alpha d_0}{2}, & l = 2,4,6..., \text{ even layers, medium 2} \end{cases} \tag{2.14}$$

where n_e is the effective refractive index of the P2VP gel layers given by:[3]

$$\phi_s \frac{n_s^2 - n_e^2}{n_s^2 + 2n_e^2} + \phi_{P2VP} \frac{n_{P2VP}^2 - n_e^2}{n_{P2VP}^2 + 2n_e^2} = 0 \tag{2.15}$$

where ϕ_s and ϕ_{P2VP} were the volume fractions of the solvent and P2VP in the gel layers, and n_s and n_{P2VP} the refractive indices of the solvent and dry P2VP (1.6), respectively.

The layer thicknesses in Equation (2.14) were given in reference to d_0 the lamellar spacing of the dry PS-P2VP films and α the swelling ratio of the P2VP layers.

If all the layers and the bounding media of the Bragg stack were pure dielectrics with real n, the conservation of energy requires that the reflectance and transmittance satisfy:

$$R + T = 1 \tag{2.16}$$

In this thesis, all spectral data were taken in transmission mode and converted to reflection by using Equation (2.16).

2.5. *Homopolymer gel synthesis and characterization*

The homopolymer gel refers to the chemically crosslinked P2VP gels used to measure the χ parameter in Chapter 4. The gels were random copolymers that contained 98 % 2VP and 2 % divinylbenzene (DVB) by molar fractions. The "homopolymer" term is used to differentiate these gels from the lamellar PS-P2VP BCP gels.

2VP monomer (Aldrich) was distilled under vacuum before use. 2 % by mole DVB (Aldrich, purified by passing through a neutral alumina column) was added to the 2VP as crosslinker and the mixture was dissolved at a concentration of 40 % by volume in 1:1 ethanol-water. 225 μL ammonium persulfate (AMPS, Mallinckrodt) aqueous solution (10 weight %) and 10 μL *N,N,N',N'*-tetramethylethylenediamine (TEMED, IBI Scientific) were added per 30 mL reaction mixture to initiate the polymerization at room temperature. The reaction mixture was then poured into a mold with two glass plates and a 5 mm thick silicone rubber spacer (see Figure 2.8). A clear gel formed overnight. After 24 hours, the gel was taken out from the mold and soaked in pure ethanol. The solvent as changed every 12 hours for 6 times to extract unreacted monomers and low molecular weight oligomers, after which the gel had reached swelling equilibrium in ethanol.

Uniaxial compression experiments were performed on a Zwick/Roell Z2.5/TS1S materials testing machine and TestXpert V10.1 master softwwere (Ulm, Germany) with a 20 N load cell. All tests were performed at room temperature. A cylindrical gel (25 mm in diameter and approximately 8 mm in thickness) was cut out by a custom made cutter. A preload of 0.01 N was applied to the specimen and the compression was performed at a nominal strain rate of 10 %

sec^{-1} to 10 % nominal strain. The compression modulus was calculated from the linear region between 5 % and 10 % nominal strain. The shear modulus was 1/3 of the compression modulus.

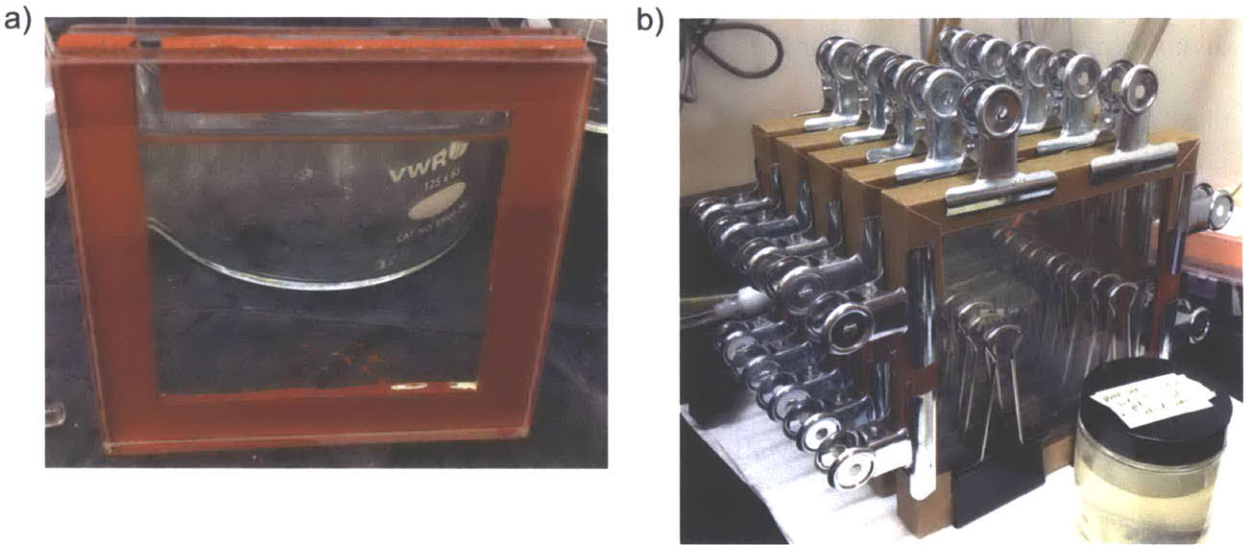

Figure 2.8. The gel casting mold for the synthesis of the homopolymer P2VP gels. a) The mold with two glass plates and a rubber spacer; b) the sealed molds filled with the reaction mixture. The reaction took place at room temperature overnight.

Gel pieces ~ 2 g were dried in hood and then in a vacuum oven, both at room temperature. The dried gel pieces were soaked in an alcohol-water mixture for 3 days. The mass swelling ratios were taken as the ratio of the swollen gel weight and the dry P2VP network weight.

2.6. *Protein solutions and characterization*

Tris buffer solutions were used to make the protein solutions employed in Chapter 5. The buffer strength was 10 mM. 2-amino-2-(hydroxymethyl)-1,3-propanediol (Tris) was dissolved in MilliQ water. The solution was then titrated to the desired pH (7, 8, or 9) using a 1 M hydrochloric acid (HCl) solution. The solution pH was measured by a Mettler Toledo S20

SevenEasy™ pH meter. The tris solution with the desired pH is then diluted to the desired concentration (10 mM).

Proteins in the lyophilized powder form were purchased from Aldrich and used without further purification. 1 % by weight proteins were dissolved in the Tris buffers and the solutions were used directly for photonic gel measurements. 0.1 % by weight solutions were filtered with 0.2 μm cellulose acetate filters used for dynamic light scattering or ζ potential tests. If not immediately used for tests, the solutions were stored in a 4 °C cold room before use. All solutions were less than 1 day old when used for tests.

The sizes of the proteins were measured by dynamic light scattering (DLS) using a Wyatt DynaPro NanoStar Light Scatterer. The test temperature was 25 °C and the model for globular protein was selected in the software for the size calculation. 0.1 % by weight protein solutions were filtered and used for DLS.

The charges of the proteins in solution were characterized by a Brookhaven Zeta Phase Analysis Light Scattering (PALS) ζ potential analyzer. 0.1 % by weight protein solutions were filtered and used in the ζ potential analyzer with disposable polystyrene cuvettes.

References

1. Yeh, P. *Optical waves in layered media;* Wiley: New York, 1988.

2. Born, M.; Wolf, E. *Principles of optics: electromagnetic theory of propagation, interference and diffraction of light;* ; New York ; Cambridge University Press: Cambridge, UK, 1997.

3. Ho, P.; Thomas, D.; Friend, R.; Tessler, N. *Science* **1999**, *5425,* 233-236.

3. Temperature Responsive PS-P2VP Photonic Gels

This chapter presents two types of temperature responsive photonic gels based on lamellar PS-P2VP. The PS-P2VP/acetic acid gels show blue-shifts in structural color at increased temperatures and the temperature dependence can be tuned via the acid concentration. The PS-P2VP/cyclohexane gels are transparent at room temperature and show structural colors that red-shift at increased temperatures. The temperature responsive photonic gels have applications in sensors and display units.

3.1. *Motivation and the two designs*

Materials that can change their color in response to temperature changes are thermochromic and can be applied as sensors and smart coatings in the fields such as fashion and toys.[1] Thermochromic photonic crystals based on colloidal crystals or liquid crystals have been reported.[2-6] Block copolymer photonic crystals have been used to demonstrate highly tunable thermochromic behaviors.[7-9] Photonic gels made by selectively swelling lamellar PS-P2VP films change their structural colors in response to a variety of stimuli such as salt concentration, electric field, and mechanical compression.[10-12] In this chapter, we use the lamellar PS-P2VP and solvents that are preferentially selective to the PS or to the P2VP block respectively and their strong temperature-dependent solubility to make temperature responsive photonic gels that can either blue- or red-shift in color.

The first design employs a PS-P2VP photonic gel via swelling of the P2VP block in aqueous solutions of acetic acid.[13] The pyridine in the P2VP block is a weak base and can be protonated in acid solutions. The acid dissociation constant of the pyridinium (K_a) is temperature-

dependent[14-16] and the change of K_a with temperature drives the swelling/deswelling of the P2VP block and changes the structural color of the PS-P2VP photonic gels. The K_a values show that the basicity of the pyridine decreases with increasing temperature and correspondingly the solubility and swelling ratios of P2VP in acetic acid solutions decreases with temperature. Therefore, the structural color should blue-shift at increased temperatures (Figure 3.1a).

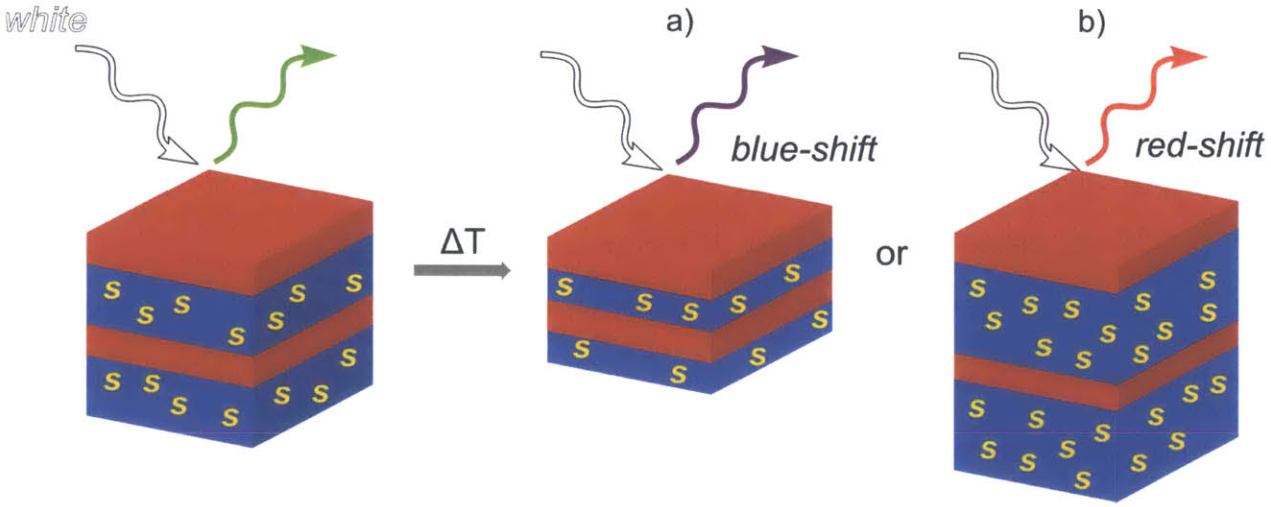

Figure 3.1. Schematics of the two designs for temperature-responsive photonic gels that show a) blue-shift and b) red-shift in reflectivity at increased temperatures. "S" indicates the solvents.

The second design utilizes the PS-P2VP – cyclohexane system. The upper critical solution temperature (UCST) behavior of PS in cyclohexane has been reported (see Figure 3.2)[17, 18] and the transition temperatures are around room temperature. The P2VP block can be quaternized or crosslinked into a linear or network polycation and with such reduced P2VP solubility, at high temperatures cyclohexane becomes a selective solvent to the PS block. Thus, the lamellar PS-P2VP/cyclohexane system shows structural color when heated due to the swelling of the PS layers. As the temperature increases, the photonic gel's reflectivity undergoes further red-shifts.

If the lamellar spacing of the BCP is large enough, the photonic gels may show reflectivity peaks above 800 nm in the near infra-red (NIR) regime. Materials that can switch from no reflection at room temperature to NIR reflection at a high temperature find practical applications such as smart windows or building coatings, etc.

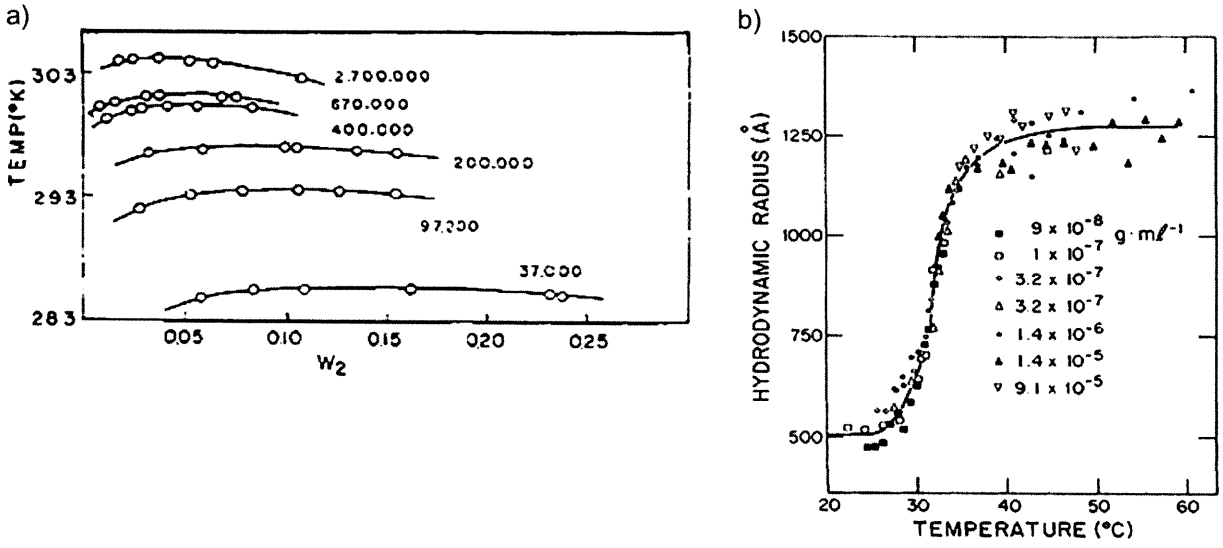

Figure 3.2. UCST phase diagram of PS of various molecular weights in cyclohexane;[17] b) hydrodynamic radii of PS M_w 2.7x10^7 g/mol in cyclohexane solutions of various concentrations showing a collapse at 32 °C.[18]

3.2. *PS-P2VP/acetic acid photonic gels*

PS-P2VP with a number average molecular weight of 57 kg/mol (PS) and 57 kg/mol (P2VP) was cast on the inner wall of a quartz cuvette, annealed in chloroform vapor, and immersed in acetic acid-water solutions before being cooled just above the solution's freezing point. Acetic acid-water solutions from 0.01 to 1 mol/L were extremely preferential to the P2VP block. The acid solutions selectively swelled the P2VP block, changing the P2VP block's layer spacing and

effective refractive index to give rise to a lamellar structure with large enough periodicity that could reflect visible light (see Figure 3.3).

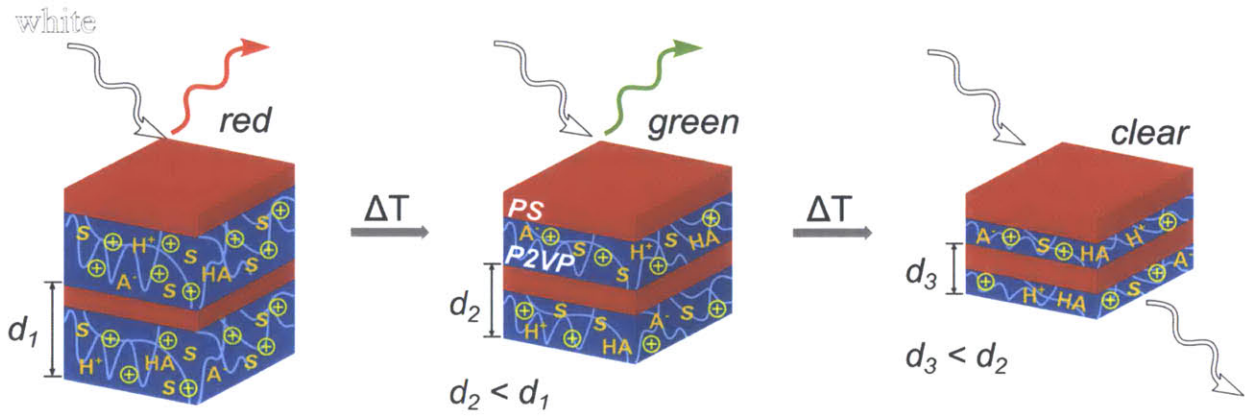

Figure 3.3. Schematic of the temperature-dependent swelling behavior and the corresponding reflectivity of PS-P2VP/acetic acid photonic gels.

The temperature responses of the PS-P2VP gels were measured from 0 °C to 95 °C with 5 °C increments. The temperature range was determined by the freezing and boiling points of water and the glass transition of the PS block (~ 100 °C). The experiments showed that the reflectivity of the PS-P2VP photonic gels in low concentration acetic acid-water solutions (from 0.01 to 0.1 mol/L, pH 3.38 to 2.88) blue-shifted for over 100 nm at increased temperatures (Figure 3.4a), while the samples in more concentrated acid solutions (0.5 and 1 mol/L, pH 2.53 to 2.38) displayed little to no peak shift with temperature (Figure 3.4b).

Temperature affected several parameters of the photonic gel. The optics of a quarter-wave stack as a special case of Bragg stacks was solely determined by the product of the refractive index n_i and the layer spacing d_i of the two media $n_i d_i$. The photonic gels as a general case of the Bragg stacks required a full optical simulation using TMM but the behavior of parameter

$n_i(T)d_i(T)$ was sufficient for qualitative estimation. The layer spacing and the refractive index of the glassy PS layers would change due to thermal expansion. Due to the restriction of the PS layers and the silica glass substrates, the photonic gel could only undergo shape changes in the direction along the lamellae normal. Since *d* was inversely proportional and *n* was roughly proportional to the density, and the product *nd* for the PS layers was approximately constant. The temperature-dependent properties of the P2VP/acetic acid-water layers were more complicated. The density of water was weakly temperature-dependent (0.9998 g/cm^3 at 0 °C to 0.9584 g/cm^3 at 100 °C). Since the major component of the P2VP gel layers was water, the thermal expansion of the gel layers could be estimated by the thermal expansion of water, which was small comparing to the P2VP swelling ratio change due to the change in temperature. Therefore, the effect of thermal expansion was small relative to the thermodynamic changes in the P2VP/ acetic acid-water layer and could be neglected.

The remaining variable of the photonic gels that changed with temperature was the swelling ratio of the P2VP caused by the change in acid/base dissociation/association equilibrium. There were two variables related to P2VP protonation: the dissociation constants of acetic acid and P2VP. The pK_a ($-\log_{10}K_a$) of acetic acid shifted from 4.78 at 5 °C to 4.75 at 20 °C,[19] indicating that the acetic acid solution was more acidic when heated. The effect of temperature on the acetic acid's dissociation thus led to red-shifts of the reflectivity peak of PS-P2VP photonic gels at increased temperatures, which *contradicted* the experimental observation.

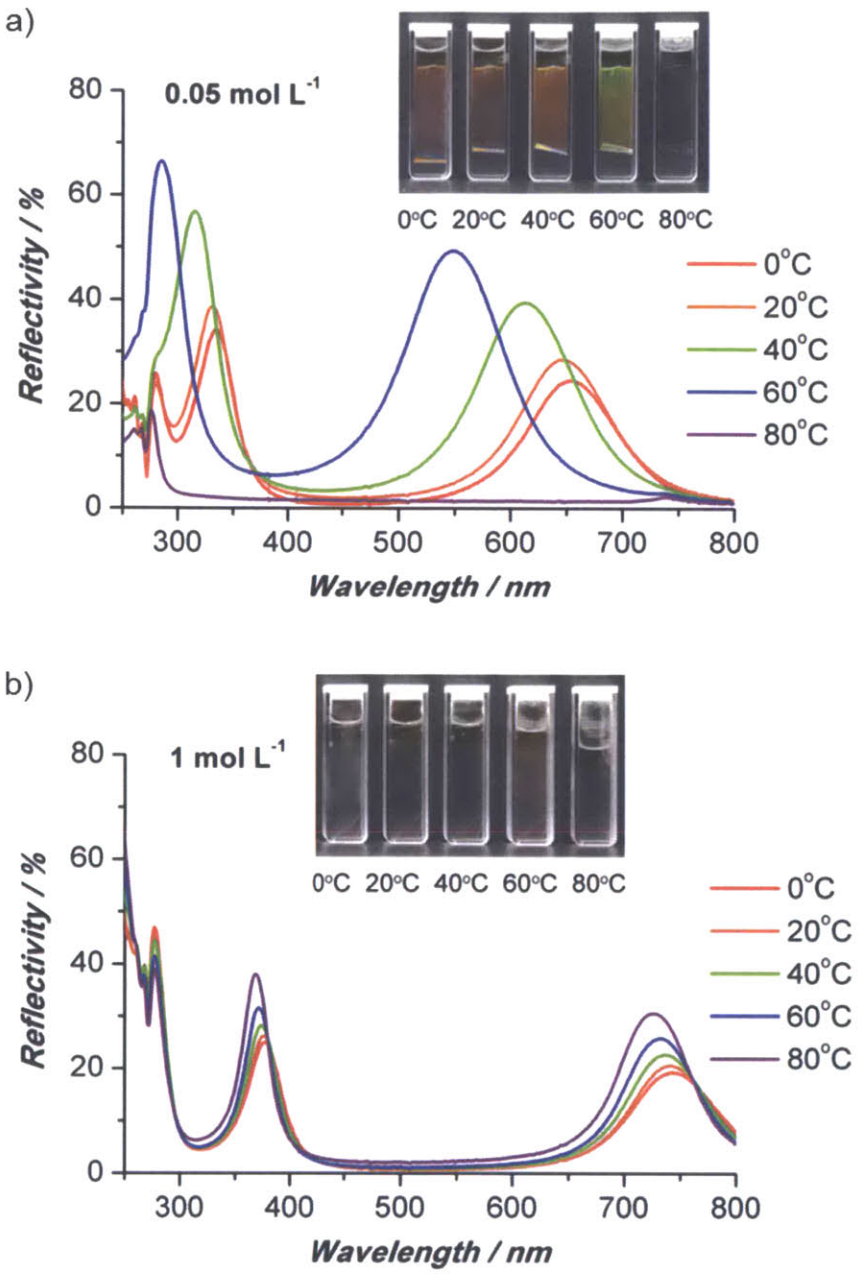

Figure 3.4. The reflection spectra and photos of PS-P2VP films immersed in a) 0.05 and b) 1 mol/L acetic acid solutions at various temperatures showing strong and weak temperature dependence of the reflectivity peaks respectively. The multiple peaks in the same spectrum are the (0 0 1) and (0 0 2) peaks located at λ and λ/2 (see 1 mol/L at 0 ˚C for example, the two peaks are at ~ 750 nm and ~ 375 nm).

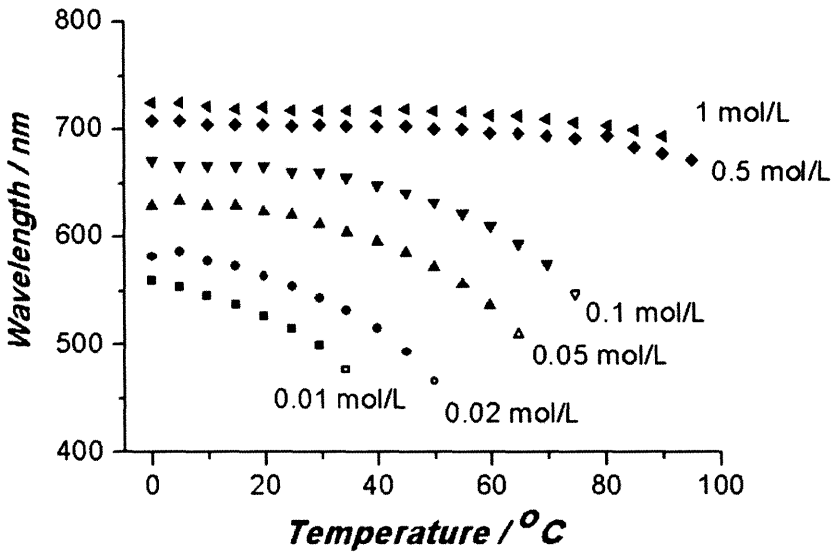

Figure 3.5. PS-P2VP reflectivity peak position as a function of temperature in different acetic acid-water solutions. Data points with hollow markers indicate the last temperature that the film shows color before transitioning to a colorless state upon further heating.

This suggested that the P2VP dissociation constant was the key variable responsible for the photonic gels' temperature responses. Data on the temperature dependence of the dissociation constant of the protonated P2VP (P2VP's conjugated acid) could not be found in the literature but reports suggested a decrease in the pK_a of organic bases upon heating.[14-16] For example, the pK_a of pyridine in a 50 % methanol-water solution decreased from 4.14 at 20 °C to 3.81 at 50 °C,[16] and the change of the pyridine pK_a with temperature in aqueous solutions was found to be approximately -0.011 $^{\circ}C^{-1}$.[15] Thus, the decrease of pK_a with temperature of the pyridium groups in the P2VP block was likely the cause of the blue-shifts of the reflectivity peaks of the photonic gels at increased temperatures.

At a constant temperature, the P2VP solubility and swelling ratios in acetic acid solutions depended on the pH or concentration of the acid solution. In less concentrated acid solutions, the

fraction of protonated pyridine groups decreased, leading to decreased swelling of the P2VP layers and a blue-shift of the reflectivity peak (Figure 3.6).

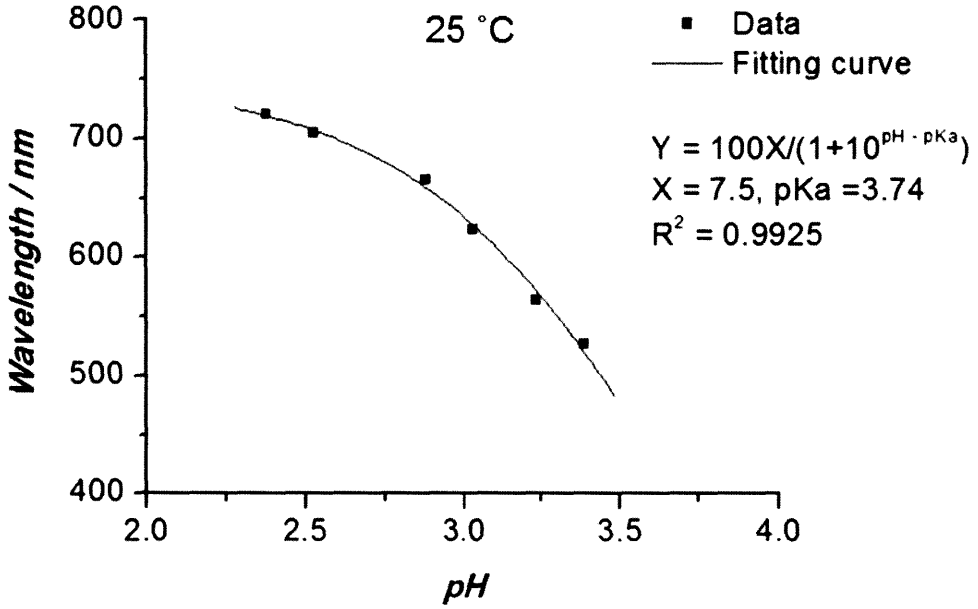

Figure 3.6. The reflectivity peak wavelengths of the PS-P2VP photonic gels in acetic acid solutions at 25 °C plotted as a function of the solution pH. The pK_a of P2VP at 25 °C can be estimated by fitting the two-parameter model assuming proportionality between the P2VP degree of protonation and the reflectivity peak wavelength. The best fit gives a pK_a value of 3.67 ± 0.1.

The photonic gel's reflectivity peak shift at a fixed temperature could be used to estimate the pK_a of the P2VP block. We assumed that the reflectivity peak wavelength (Y) was proportional to the degree of protonation on the P2VP block (Z) by a coefficient of $100X$.

$$Y = 100X \cdot Z \tag{3.1}$$

The acid dissociation constant of protonated P2VP was defined as:

$$K_a = \frac{[H^+][P2VP]}{[P2VP^+]} \tag{3.2}$$

The degree of protonation could be calculated from the pK_a and the solution pH by:

$$Z = \frac{[P2VP^+]}{[P2VP^+]+[P2VP]} = \frac{[H^+]}{[H^+]+K_a} = \frac{1}{1+10^{pH-pK_a}} \tag{3.3}$$

By fitting Equation (3.3) using the peak wavelengths vs. pH data in Figure 3.6, we estimated the pK_a of P2VP to be 3.67 ± 0.1 at 25 °C. The pK_a of P2VP has been reported to be 4.5 in a 0.5 mol L^{-1} potassium chloride water solution at room temperature (for an electro-polymerized P2VP)[20] and 3.45 in an ethanol/water solution containing 45 % ethanol by volume.[21] Our estimation of 3.67 was reasonable comparing to these literature data.

In summary, the PS-P2VP/acetic acid photonic gels showed temperature responses that were primarily driven by the temperature-dependent pK_a of P2VP. The photonic responses could be tuned by the acid concentrations as more concentrated acids led to decreased peak shifts with temperature. The sensitive responses to temperature in acetic acids of 0.01 to 0.1 mol/L could be used for sensing or smart display applications, while the insignificant temperature dependence of the photonic gels in 0.5 and 1 mol/L acetic acid might be used for applications such as the measurement of ion concentration over a range of temperatures where the robustness against temperature variation was favored.

3.3. *PS-P2VP/cyclohexane photonic gels*

IR and NIR radiation from the sunlight is an important heating component for buildings especially in the summer. An energy efficient method that helps control the indoor temperature is to use smart window coatings comprised of materials with temperature responsive reflectivity.

The materials transmit IR/NIR radiation in cold weather and reflect the radiation on hot days by creating reflectivity peaks in the IR/NIR regime. Such materials can be made by selectively swelling a lamellar BCP with an upper critical solution temperature (UCST) solvent. The PS/cyclohexane system shows a θ temperature at 34 °C[22-24] and a UCST around 24 °C,[17, 18, 25] so cyclohexane is a promising solvent candidate for the photonic gel. The solubility of P2VP in cyclohexane should be low enough to ensure that cyclohexane preferentially swells PS and the glassy P2VP layers restrict the lateral expansion of the PS gel layers and prevent the dissolution of the entire BCP film.

Temperature-dependent spectral tests demonstrated that immersing a lamellar PS-P2VP film in cyclohexane made a temperature responsive photonic gel. The transmission spectra of the PS-P2VP/cyclohexane gels were collected from 20 °C to 75 °C by a UV-Vis spectrometer and converted to reflection spectra by assuming zero absorption or scattering. The boiling point of cyclohexane was 80 °C which set the upper limit of the test temperatures. Figure 3.7 showed that at or below room temperature (20 °C) the gel exhibited no reflectivity in the UV-Vis regime. As the temperature increased and passed the θ temperature of the PS-cyclohexane system at 34 °C, a reflectivity peak appeared and red-shifted with temperature. BCPs of higher molecular weights showed larger peak wavelengths and peak shifts due to the increased lamellar spacing.

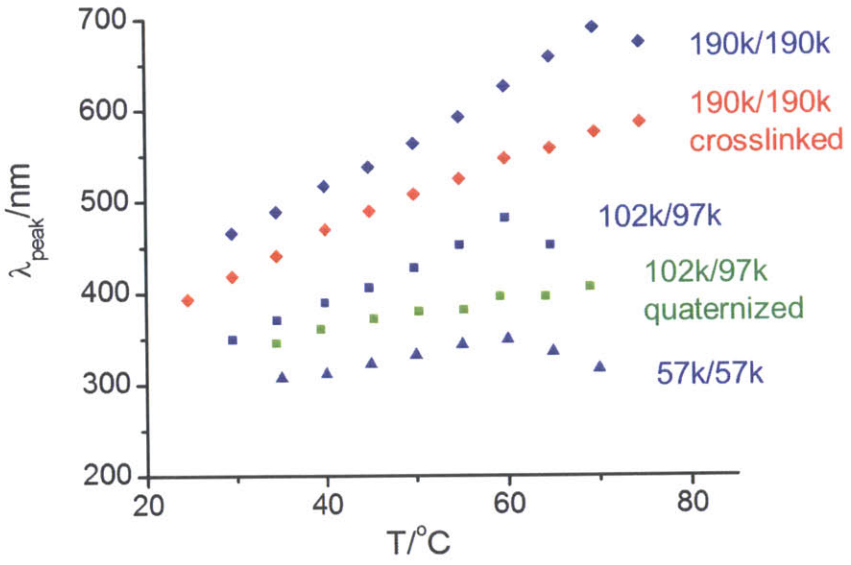

Figure 3.7. The reflection peak wavelengths of PS-P2VP/cyclohexane photonic gels at increasing temperatures. BCPs of three molecular weights are used. The blue series of data points are from the untreated PS-P2VP films; the green data series is PS-P2VP quaternized by bromoethane; the red data series is PS-P2VP quaternized and crosslinked by 1,6-dibromohexane.

The photonic gels made from untreated PS-P2VP films (see the data series in blue in Figure 3.7) showed a steady red-shift with increasing temperature but then a blue-shift at higher temperatures (above 65 °C for 57k/57k and 102k/97k, above 75 °C for 190k/190k). The BCP film surface appeared rougher after the swelling experiments, which suggested that the film had slightly dissolved in cyclohexane at high temperatures. The high-temperature phenomena were probably due to the swelling of P2VP in cyclohexane. To reduce the solubility and eliminate swelling of the P2VP block, the BCP films could be treated by quaternization reactions that converted the pyridine groups into pyridiniums. Monofunctional reagents such as bromoethane (EtBr) quaternized the P2VP and the polycation product had a lower solubility in cyclohexane

due to the increased polarity difference. Difunctional reagents like 1,6-dibromohexane (DBH) crosslinked the P2VP during quaternization and the crosslinking helped reduce the swelling ratio of the P2VP block in cyclohexane. The data series in green and red in Figure 3.7 suggested that both EtBr quaternization and DBH quaternization/crosslinking successfully suppressed the blue-shifts at high temperatures, although the entire $\lambda_{peak}(T)$ curves were also shifted to lower wavelengths.

3.4. *Summary and future work*

Photonic gels of two types of temperature responses are made from lamellar PS-P2VP films. The PS-P2VP/acetic acid photonic gels show blue-shifts in reflection color at increased temperatures and the PS-P2VP/cyclohexane photonic gels show red-shifts with temperature. The temperature responses of the PS-P2VP/acetic acid photonic gels can be tuned by the acid concentration and those of the PS-P2VP/cyclohexane photonic gels by the BCP molecular weights. The PS-P2VP/acetic acid photonic gels can be used for temperature sensing or as temperature independent display material. The PS-P2VP/cyclohexane photonic gels need further development for the smart IR/NIR reflection coating application.

Besides acetic acid, other acids can be used to make photonic gels with the lamellar PS-P2VP. Counterion species plays an important role to the photonic gel's properties.[26] Strong acids such as hydrochloric acid can be used to compare the effect of acidity and counterions. The valency of the counterions on the photonic responses can be studied by using multivalent acids such as sulfuric acid and phosphoric acid.

More experiments on the PS-P2VP/cyclohexane photonic gels are needed. The quaternization or crosslinking reactions need be optimized so that the P2VP swelling is

suppressed while the PS swelling is not restricted. High molecular weight BCPs are preferred in order to achieve reflections in the NIR regime.

Ionic liquids may be used to make temperature responsive photonic gels by selectively swelling lamellar PS-P2VP films. The phase behaviors of PS-P2VP diblock copolymers in ionic liquids have been studied.[27-31] Several ionic liquids show UCST type behavior for P2VP and low solubility for PS. Such ionic liquids are good solvent candidates to make photonic gels with red-shifts in reflectivity. BCP photonic gels have been made from PS-P2VP and ionic liquids[32] and the temperature responses are worth exploring.

BCPs such as poly(styrene-*b*-*N*-isopropylacrylamide) (PS-PNIPAM) and poly(styrene-*b*-methyl methacrylate) (PS-PMMA) may be interesting to explore as well. The gels of PS-PNIPAM swollen in water may show dramatic blue-shifts at increased temperatures because of the sharp LCST transitions of PNIPAM in water.[33] PMMA also has a UCST in methanol[34] so PS-PMMA/methanol gels may show red-shifts in reflectivity at increased temperatures.

References

1. White, M. A.; LeBlanc, M. *J. Chem. Educ.* **1999**, *9,* 1201-1205.

2. Weissman, J. M.; Sunkara, H. B.; Tse, A. S.; Asher, S. A. *Science* **1996**, *5289,* 959-960.

3. Matsubara, K.; Watanabe, M.; Takeoka, Y. *Angew. Chem. , Int. Ed.* **2007**, *10,* 1688-1692.

4. Ueno, K.; Matsubara, K.; Watanabe, M.; Takeoka, Y. *Adv Mater* **2007**, *19,* 2807-2812.

5. Debord, J. D.; Lyon, L. A. *J Phys Chem B* **2000**, *27,* 6327-6331.

6. Hu, Z. B.; Lu, X. H.; Gao, J. *Adv Mater* **2001**, *22,* 1708-1712.

7. Osuji, C.; Chao, C. Y.; Bita, I.; Ober, C. K.; Thomas, E. L. *Adv. Funct. Mater.* **2002**, *11-12,* 753-758.

8. Valkama, S.; Kosonen, H.; Ruokolainen, J.; Haatainen, T.; Torkkeli, M.; Serimaa, R.; Ten Brinke, G.; Ikkala, O. *Nat. Mater.* **2004**, *12,* 872-876.

9. Yoon, J.; Lee, W.; Thomas, E. L. *Macromolecules* **2008**, *13,* 4582-4584.

10. Kang, Y.; Walish, J. J.; Gorishnyy, T.; Thomas, E. L. *Nat. Mater.* **2007**, *12,* 957-960.

11. Walish, J. J.; Kang, Y.; Mickiewicz, R. A.; Thomas, E. L. *Adv. Mater.* **2009**, *30,* 3078-3081.

12. Chan, E. P.; Walish, J. J.; Thomas, E. L.; Stafford, C. M. *Adv. Mater.* **2011**, *40,* 4702-4706.

13. Walish, J. J.; Fan, Y.; Centrone, A.; Thomas, E. L. *Macromol. Rapid Commun.* **2012**, *18,* 1504-1509.

14. Hall, N. F.; Sprinkle, M. R. *J. Am. Chem. Soc.* **1932**, *9,* 3469-3485.

15. Perrin, D. D. *Aust. J. Chem.* **1964**, *4,* 484-488.

16. Castells, C. B.; Rafols, C.; Roses, M.; Bosch, E. *J. Chromatogr. A* **2003**, *1-2,* 41-53.

17. Saeki, S.; Kuwahara, N.; Konno, S.; Kaneko, M. *Macromolecules* **1973**, *2,* 246-250.

18. Swislow, G.; Sun, S.; Nishio, I.; Tanaka, T. *Phys. Rev. Lett.* **1980**, *12,* 796-798.

19. Calder, G. V.; Barton, T. J. *J. Chem. Educ.* **1971**, *5,* 338-340.

20. Tantavichet, N.; Pritzker, M. D.; Burns, C. M. *J Appl Polym Sci* **2001**, *6,* 1493-1497.

21. Ferruti, P.; Barbucci, R. *Adv. Polym. Sci.* **1984**, 55-92.

22. Krigbaum, W. R.; Flory, P. J. *J. Am. Chem. Soc.* **1953**, *8,* 1775-1784.

23. Krigbaum, W. R. *J. Am. Chem. Soc.* **1954**, *14,* 3758-3764.

24. Krigbaum, W.; Geymer, D. *J. Am. Chem. Soc.* **1959**, *8,* 1859-1868.

25. Sun, S.; Nishio, I.; Swislow, G.; Tanaka, T. *J. Chem. Phys.* **1980**, *12,* 5971-5975.

26. Lim, H. S.; Lee, J.; Walish, J. J.; Thomas, E. L. *ACS Nano* **2012**, *10,* 8933-8939.

27. He, Y.; Li, Z.; Simone, P.; Lodge, T. P. *J. Am. Chem. Soc.* **2006**, *8,* 2745-2750.

28. Lu, H.; Chen, W.; Russell, T. P. *Macromolecules* **2009**, *22,* 9111-9117.

29. Lu, H.; Lee, D. H.; Russell, T. P. *Langmuir* **2010**, *22,* 17126-17132.

30. Virgili, J. M.; Hexemer, A.; Pople, J. A.; Balsara, N. P.; Segalman, R. A. *Macromolecules* **2009**, *13,* 4604-4613.

31. Virgili, J. M.; Nedoma, A. J.; Segalman, R. A.; Balsara, N. P. *Macromolecules* **2010**, *8,* 3750-3756.

32. Noro, A.; Tomita, Y.; Shinohara, Y.; Sageshima, Y.; Walish, J. J.; Matsushita, Y.; Thomas, E. L. *ACS Nano* , Submitted.

33. Tanaka, T. *Sci. Am.* **1981**, *1,* 124-138.

34. Cowie, J. M. G.; McEwen, I. J.; Garay, M. T. *Polym. Commun.* **1986**, *5*, 122-124.

4. Co-Solvent Quality Responsive PS-P2VP Photonic Gels

This chapter explores the photonic responses of the lamellar PS-P2VP gels in alcohol-water co-solvents. The photonic responses are triggered by swelling/deswelling of the P2VP block in alcohol-water co-solvents of different compositions. The co-solvent quality for P2VP is characterized by the Flory-Huggins interaction parameter χ measured from crosslinked homopolymer P2VP gel swelling and the Flory-Rehner theory. Quantitative models are proposed to capture the swelling behaviors of the P2VP block in the lamellar BCP. Model fitting suggests that the BCP swelling is driven by the free energy of mixing between P2VP and the co-solvent and retarded by the mechanical deformation of the glassy PS layer network with defects. This work establishes the quantitative relationship between the reflective color of the photonic gel, the effective χ parameter of the swellable block and the solvent, and the defect density of the BCP film, and demonstrates the potential utility of these photonic materials as a quick means to measure solvent quality or defect density.

4.1. *Motivation and co-solvent selection*

The lamellar PS-P2VP photonic gels have been previously demonstrated to show tunable photonic responses to a large variety of stimuli such as ionic strength, electric field, mechanical compression, temperature, and counterion species.[1-5] The photonic responses result from the reflection of light waves by the periodic lamellar structure of the BCP gels and are triggered by swelling/deswelling of the P2VP block in the PS-P2VP gels. In this chapter, we attempt to establish a quantitative relationship between the photonic responses of the PS-P2VP gels, the lamellar microstructure of the BCP film, and polymer solution thermodynamics between P2VP and the selective solvent.

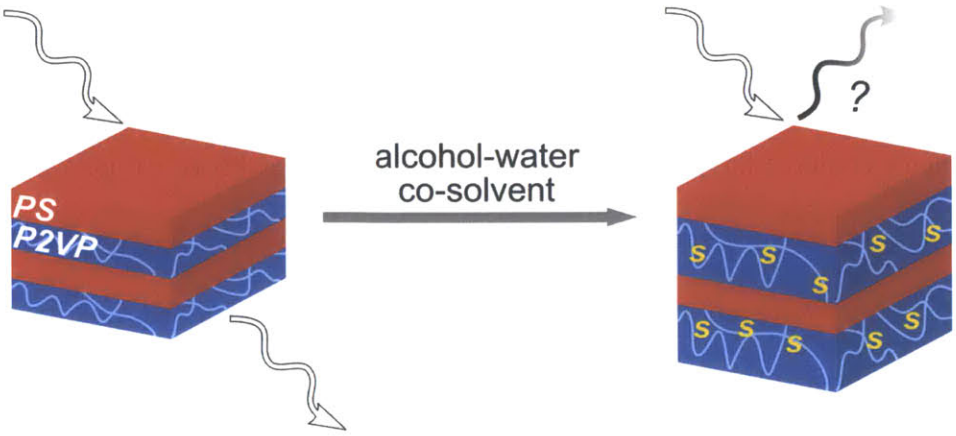

Figure 4.1. Schematic of the co-solvent quality responsive photonic gels made of lamellar PS-P2VP in binary mixtures of alcohol (methanol, ethanol, or 1-propanol) and water.

All aforementioned studies on PS-P2VP based photonic gels employed the polyelectrolyte form of the P2VP block, either by irreversible quaternization using bromoalkanes[1-3, 5] or by reversible quaternization using protons in acidic solutions.[4] The complexity of polyelectrolyte adds to the difficulty to model the selective swelling of the BCPs. Therefore, a charge-neutral solvent that does not induce quaterization of the pyridine groups in the P2VP is preferred for the study. In addition, the solvent should not dissolve or swell PS and should have a distinct refractive index from the polymers so that the swollen BCP can show visible color reflection as Bragg stacks. Water is a non-solvent for both PS and P2VP; alcohols such as methanol, ethanol, and 1-propanol are poor solvents for PS but good solvents for P2VP at room temperature. The binary mixtures of alcohol and water are non-solvents for PS but have tunable solubility for P2VP; all alcohols and water have refractive indices around 1.3 which provide enough contrast from the refractive indices of PS and P2VP at 1.6 (see Table 4.1 for the solubility parameters and refractive indices at 25 °C). In addition, the alcohol-water systems have been reported to show non-linear co-solvency for several polymers,[6-9] i.e. the solubility of the polymers in the co-solvent shows a minimum or maximum instead of following a monotonic relation between the

solubilities in the two pure solvents. A similar non-linear co-solvency effect of the alcohol-water mixtures for P2VP, if exists, can be captured by the photonic responses of the PS-P2VP gels to the co-solvent compositions, probably in the form of a non-monotonic dependence of the reflection peak wavelengths on the co-solvent compositions. Therefore, the as-annealed PS-P2VP without quaternization treatment and the binary mixtures of methanol, ethanol or 1-propanol with water were selected as the model system to understand the correlations between photonic band gap and polymer solution thermodynamics in BCP photonic gels.

Table 4.1. Solubility parameters at 25 °C and refractive indices at a wavelength of 589 nm at 20 °C.[10-16]

material	δ (MPa$^{1/2}$)	n
PS	17.5	1.60
P2VP	23.3	1.60
water	47.9	1.33
methanol	29.7	1.33
ethanol	26.0	1.36
1-propanol	24.3	1.38

4.2. *Photonic responses and BCP swelling ratios*

The quality of the alcohol-water co-solvents for P2VP can be changed at a fixed temperature by choice of the alcohol and by adjusting the volume fraction of alcohol $\phi_{alcohol}$ in the co-solvent because of the very different solubilities of P2VP in water and alcohol (see Table 4.1).

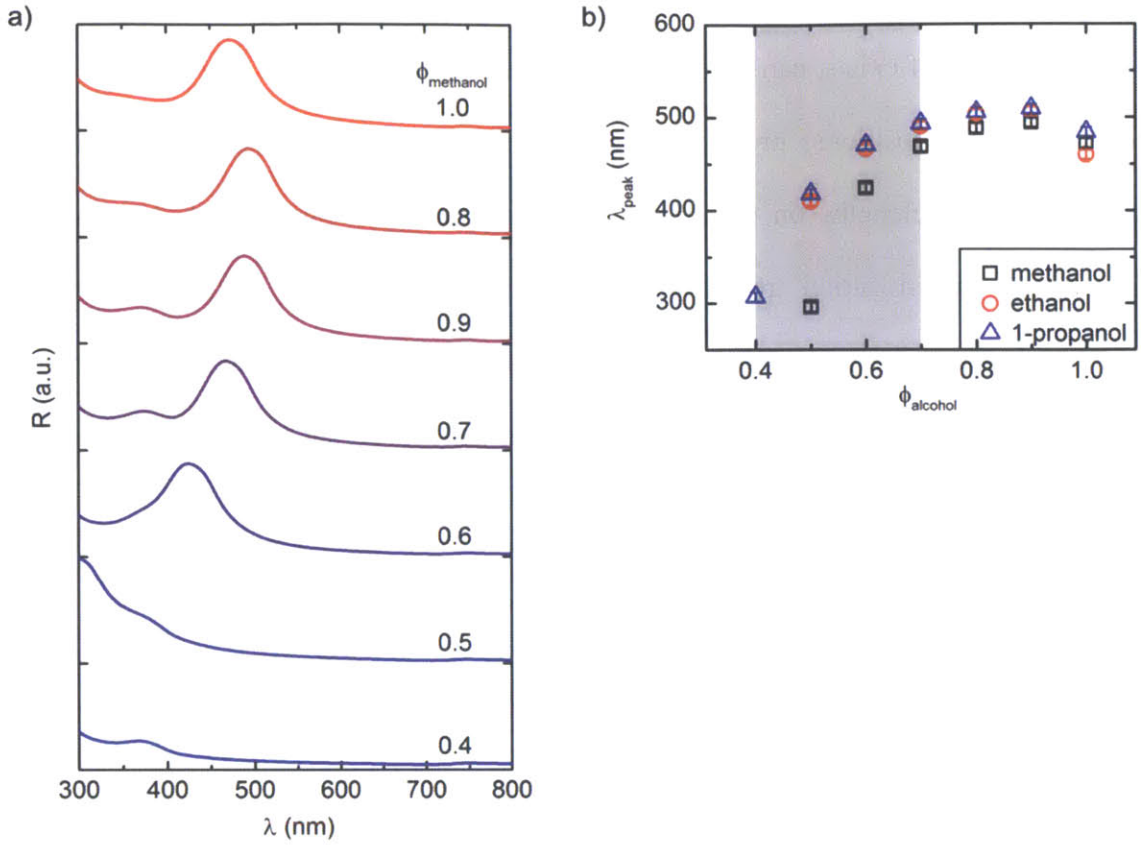

Figure 4.2. Reflection spectra of a PS-P2VP photonic gel in methanol-water co-solvents of varying methanol volume fraction $\phi_{methanol}$; b) reflectivity peak wavelengths of PS-P2VP photonic gels in three different alcohol-water co-solvents. As $\phi_{alcohol}$ decreases from pure alcohol, the reflectivity peak initially red-shifts and then blue-shifts towards lower $\phi_{alcohol}$ with a broad maximum at $\phi_{alcohol} \sim 0.9$ in all three co-solvents.

As expected, the reflection spectra of the PS-P2VP/alcohol-water photonic gels depend on co-solvent composition. Figure 4.2a shows the reflection spectra of the PS-P2VP gels in methanol-water and the wavelengths of the reflectivity peaks in the three alcohol-water co-solvents. Pure alcohols swell P2VP, and the photonic gels reflect visible light due to the increased P2VP layer thickness and the increased refractive index mismatch between the PS and the swollen P2VP layers. As a non-solvent, addition of water is expected to shrink the P2VP gel

layers and blue-shift the reflectivity of the photonic gel. The reflection spectra show blue-shifts with increasing water concentration for $\phi_{alcohol} < 0.9$ and the visual color of the photonic gels changed from green to blue to clear. The sensitive peak shifts between $\phi_{alcohol}$ 0.4 and 0.7 (highlighted in Figure 4.2b) suggest that the photonic gels may be used as co-solvent composition indicators in this range. Interestingly, the overall peak shift behaviors with co-solvent composition are in all cases non-monotonic with a broad maximum in the wavelength of the peak reflectivity at $\phi_{alcohol} \sim 0.9$.

The densities and refractive indices of the alcohol-water mixtures are needed to calculate the swelling ratios of the P2VP block in the BCP. The densities and refractive indices were interpolated using handbook data on the concentrative properties of aqueous solutions of methanol, ethanol, and 1-propanol.[13] Both densities and refractive indices data are at 20 °C, and the refractive indices are at a wavelength of 589 nm.

The co-solvent composition indicated by $\phi_{alcohol}$ is a mixture of alcohol and water with the original volumes by the ratio of $\phi_{alcohol}/(1-\phi_{alcohol})$. The weight fraction based handbook data are converted to volume fractions by Equation (4.1).

$$\phi_{alcohol} = \frac{w_{alcohol}/\rho_{alcohol}}{w_{alcohol}/\rho_{alcohol} + (1-w_{alcohol})/\rho_{water}} \tag{4.1}$$

$w_{alcohol}$ is the weight fraction of the alcohol. $\rho_{alcohol}$ and ρ_{water} are the densities of pure alcohol and pure water respectively.

The densities and refractive indices for the alcohol-water mixtures with $\phi_{alcohol}$ ranging from 0.4 to 1.0 used in the paper can be calculated by piecewise cubic Hermite interpolation.

The molecular volumes of the co-solvents can then be calculated by Equation (4.2).

$$V_s = \frac{\left[\rho_{alcohol}\phi_{alcohol} + \rho_{water}\left(1-\phi_{alcohol}\right)\right]/\rho_s}{\frac{\rho_{alcohol}\phi_{alcohol}}{M_{alcohol}} + \frac{\rho_{water}\left(1-\phi_{alcohol}\right)}{M_{water}}} \tag{4.2}$$

V_s is the molecular volume of the co-solvent. ρ_s is the density of the co-solvent, already calculated by interpolation; $M_{alcohol}$ and M_{water} are the molecular weights of the alcohol and water respectively.

The calculated refractive indices and molecular volumes are listed in Table 4.2.

Table 4.2. Calculated refractive indices and molecular volumes of alcohol-water co-solvents at 20 °C, 589 nm.

	methanol-water		**ethanol-water**		**1-propanol-water**	
$\phi_{alcohol}$	V_s ($cm^3\ mol^{-1}$)	n_s	V_s ($cm^3\ mol^{-1}$)	n_s	V_s ($cm^3\ mol^{-1}$)	n_s
1	40.42	1.329	58.28	1.361	74.68	1.385
0.9	35.33	1.336	46.82	1.365	56.30	1.383
0.8	31.47	1.340	39.22	1.366	45.18	1.380
0.7	28.45	1.342	33.79	1.365	37.76	1.376
0.6	26.03	1.343	29.70	1.363	32.45	1.371
0.5	24.07	1.343	26.55	1.360	28.45	1.366
0.4	22.46	1.342	24.08	1.356	25.35	1.361

The lamellar BCP gel's reflection spectrum can be simulated using the transfer matrix method (TMM).[17, 18] The variables for the reflectance are incidence angle, incident light wavelength, refractive indices and thickness of the two layer materials. In this paper, only normal incidence is considered. The reflection spectrum is composed of reflectance for a range of incident wavelengths. The glassy PS layers have fixed refractive index at 1.6 and thickness at

28 nm (half the dry lamellar periodicity d_0). The P2VP gel layer thickness can be calculated from the swelling ratio by Equation (4.3):

$$d_{gel} = \alpha d_{P2VP} = \frac{\alpha}{2} d_0 \tag{4.3}$$

The effective refractive index of the gel layers n_e can be calculated following Ho et al. by Equation (4.4):[19]

$$\phi_s \frac{n_s^2 - n_e^2}{n_s^2 + 2n_e^2} + \phi_{P2VP} \frac{n_{P2VP}^2 - n_e^2}{n_{P2VP}^2 + 2n_e^2} = 0 \tag{4.4}$$

ϕ_s and ϕ_{P2VP} are the volume fractions of the co-solvent and P2VP in the gel layers and $\phi_s + \phi_{P2VP} = 1$. n_s and n_{P2VP} are the refractive indices of the co-solvent and P2VP.

The dispersion (i.e. the wavelength dependence of the refractive index) is small ($dn/d\lambda$ are -0.040, -0.012, -0.031 μm^{-1} for water, methanol, and ethanol respectively)[14-16] and is therefore neglected in the calculations.

TMM modeling reveals that the peak shifts are mainly due to changes in P2VP block swelling ratios (see Figure 4.3). The refractive index of each alcohol-water co-solvent is nearly constant at all compositions because of the close refractive indices values of water and the alcohols (see Table 4.1). The P2VP layers cannot expand laterally so the swelling ratios are equal to the thickness ratios of swollen P2VP to dry P2VP layers. TMM modeling suggests a roughly linear relationship between the reflectivity peak wavelengths and the P2VP swelling ratios α_{P2VP} as a comprehensive result of changes in both thickness and effective refractive index of the swollen P2VP layers. The modeling captures the P2VP swelling ratio trends with a maximum between 0.8 and 0.9 $\phi_{alcohol}$ for all three alcohol-water co-solvents, consistent with the reflectivity peak shifts in Figure 4.2.

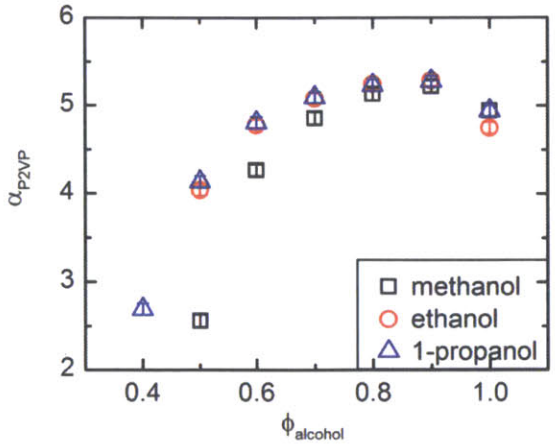

Figure 4.3. TMM calculated P2VP block swelling ratios α_{P2VP} in PS-P2VP/alcohol-water photonic gels of varying alcohol volume fraction $\phi_{alcohol}$.

Non-linear co-solvency has been reported for several polymers in alcohol-water co-solvents.[6-9] Although not reported in the prior literature, a similar maximum co-solvency effect of the alcohol-water mixtures to P2VP is likely the cause for the non-monotonic peak shifts in the photonic gels.

4.3. *Homopolymer gels*

In order to more quantitatively relate the solvent quality to the photonic response, the Flory-Huggins χ parameters between P2VP homopolymer and the co-solvents were measured by a gel swelling approach. Chemically crosslinked P2VP were synthesized by copolymerizing 2VP and DVB (2 mol %). Uniaxial compression tests were used to measure the crosslink density of the homopolymer P2VP gels.

The Young's modulus E of the crosslinked gel is taken as the slope of the linear region of the stress-strain curve (see Figure 4.4).

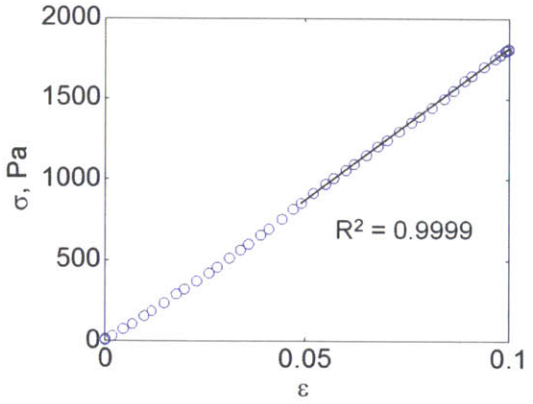

Figure 4.4. A representative engineering stress-strain curve from uniaxial compression. The slope of the marked linear region is the measured Young's modulus *E*, approximately 18.9 kPa.

By assuming the gel's Poisson's ratio as 0.5, the shear modulus *G* can be calculated by Equation (4.5):

$$G = \frac{E}{3} \tag{4.5}$$

G is approximately 6.3 kPa.

The molecular weight between crosslinks for a gel with a known swelling ratio can be estimated by Equation (4.6):

$$M_c = \frac{\varphi_{P2VP}\rho_{P2VP}RT}{G} = \frac{\rho_{P2VP}RT}{\alpha G} \tag{4.6}$$

φ_{P2VP} is the volume fraction of P2VP in the gel, ρ_{P2VP} is the bulk density of P2VP, and α is the swelling ratio by volume.

M_c is approximately 29.3 kg mol^{-1} for this gel.

The shear moduli, equilibrium swelling ratios, and molecular weights between crosslinks of the 5 gels cast in separate molds from a single batch of reaction mixture are listed in Table 4.3.

Table 4.3. Shear moduli, swelling ratios, and molecular weights between crosslinks of 5 replicates of crosslinked P2VP gels.

Sample	G (kPa)	α	M_c (kg mol^{-1})
1	6.7 ± 0.8	15.9 ± 0.9	26.4 ± 3.4
2	7.0 ± 0.3	14.7 ± 0.2	27.2 ± 1.3
3	7.2 ± 0.4	14.8 ± 0.5	26.4 ± 1.6
4	6.2 ± 0.3	15.6 ± 0.3	29.0 ± 1.7
5	6.2 ± 0.1	15.3 ± 0.3	29.3 ± 0.7

The average crosslink densities of the P2VP gels were measured to be ~ 27 kg mol^{-1}.

Neglecting the influence of crosslinkers as a different type of monomer, the effective Flory-Huggins parameters of P2VP in alcohol-water co-solvents χ_{eff} can be calculated from Flory-Rehner theory in Equation (4.7):

$$\ln\left(1-\frac{1}{\alpha}\right)+\frac{1}{\alpha}+\frac{\chi_{eff}}{\alpha^2}+\frac{\rho_{P2VP}V_s}{M_c}\left(\frac{1}{\alpha^{1/3}}-\frac{1}{2\alpha}\right)=0 \qquad (4.7)$$

α is the volume swelling ratio of the gel and ρ_{P2VP} is the density of dry P2VP, 1.15 g cm^{-3}.[20] V_s is the molar volume of the co-solvent and can be calculated from the molecular weight and density of the co-solvent using handbook data (see Supporting Information). M_c is the molecular weight between crosslinks measured by compression tests of surface lubricated gel discs.

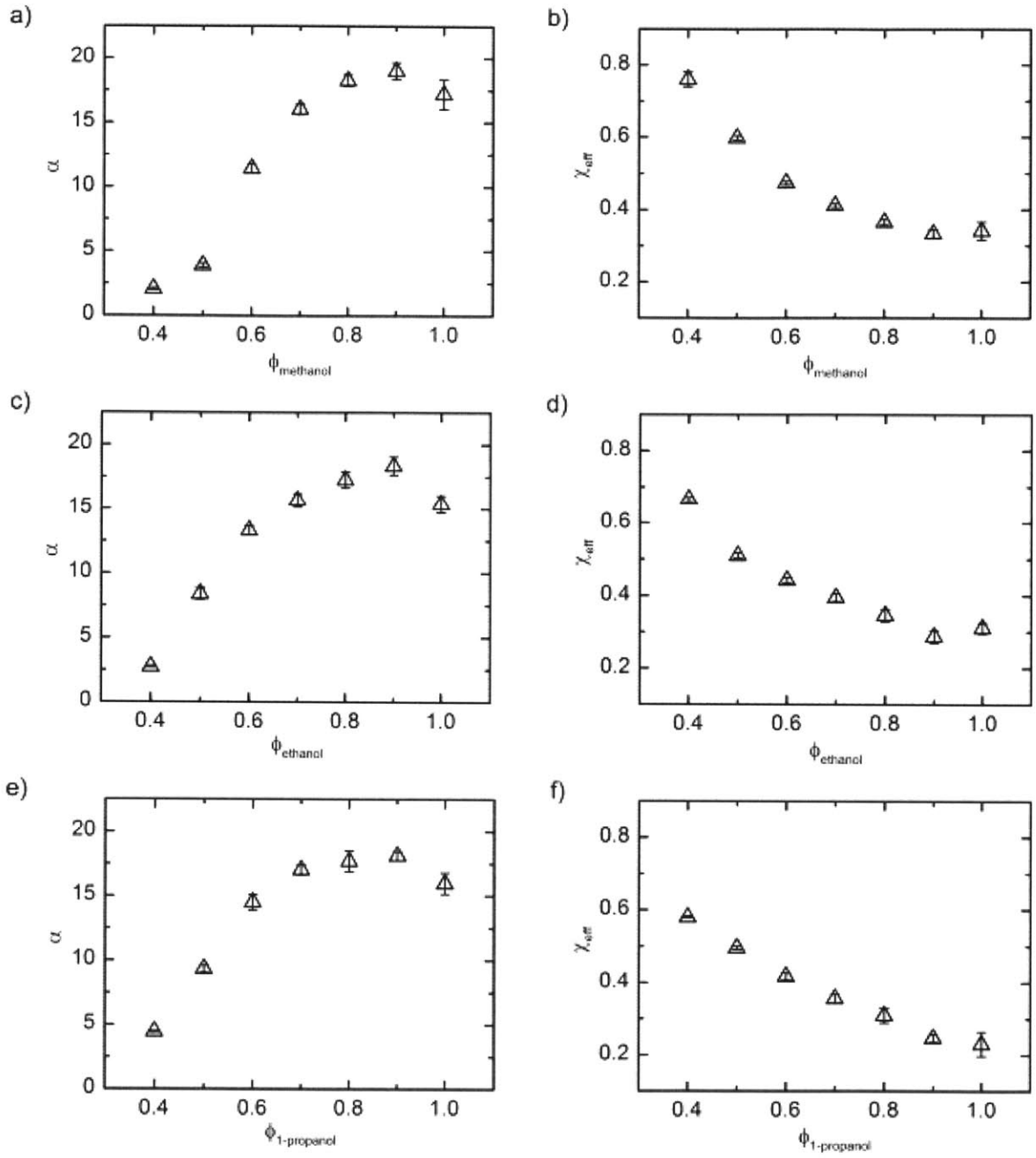

Figure 4.5. The swelling ratios of crosslinked P2VP homopolymer gels in a) methanol, c) ethanol, and e) 1-propanol – water co-solvents and the effective Flory-Huggins interaction parameters χ_{eff} calculated by the Flory-Rehner theory between P2VP and b) methanol, d) ethanol, and f) 1-propanol – water co-solvents.

The χ_{eff} values measured from homopolymer P2VP gel swelling experiments vary non-monotonically with the co-solvent composition. As shown in Figure 4.5, the swelling ratios of the P2VP homopolymer gel in alcohol-water co-solvents vary with co-solvent composition in a similar way with those of the PS-P2VP BCPs in Figure 4.3 arising from the non-monotonic co-solvency of alcohol-water mixtures for P2VP. Figure 4.5 demonstrates a clear similarity of all three alcohol-water co-solvents to swell the P2VP homopolymer network. The χ_{eff} values indicate a slight decrease in co-solvent quality for P2VP in the order of 1-propanol, ethanol, and methanol. This observation is in accord to the relative solubility parameters with the 1-propanol – water co-solvents having the closest solubility parameter values to P2VP and therefore the lowest χ_{eff}. We also confirmed the aforementioned non-monotonic solubility trend of the P2VP blocks in the BCP/alcohol-water co-solvent systems with the swelling ratios of crosslinked P2VP homopolymer gels in Figure 4.5.

4.4. *BCP Swelling models*

Swelling of the gel layers within a lamellar BCP (Figure 4.3) is qualitatively similar with but quantitatively different from swelling of crosslinked homopolymer gels (Figure 4.5). Swelling in crosslinked gels is isotropic, driven by the free energy of mixing and hindered by the entropy decrease due to subchain network stretching as described by the Flory-Rehner theory.[21] In lamellar BCPs, the chains are tethered at a fixed junction density to the interfaces and since one block is glassy, the selective swelling is only along the layer normal. BCPs with perfect lamellar morphology are expected to swell infinitely in a good solvent due to the entropy-driven unbinding of bilayers into planar micelles. Indeed, annealed BCP films of a low molecular weight (M_n 7.8/10.0 kg mol^{-1} for PS/P2VP) dissolved in methanol, a selective solvent for P2VP, demonstrating layer unbinding. Dissolution or unbinding in selective solvents was not observed

with a much higher molecular weight BCP (M_n 102/97 kg mol^{-1} for PS/P2VP) used in this chapter. The difference likely results from the unbinding kinetics and especially the degree of perfection in the lamellar order.

Four BCP swelling models have been proposed (see Table 4.4).

Table 4.4. Summary of the four BCP swelling models.

#	**driving force**	**retarding force**	**fitting variable**
1	excluded volume of P2VP blobs in co-solvent	elasticity of P2VP brushes	N/A
2	Flory-Huggins mixing of P2VP and co-solvent	clasticity of P2VP "network"	effective P2VP crosslink density
3		elastic strain energy of PS defect core deformation	average distance between PS defect cores
4		strain energy of dislocation network	average distance between dislocation lines

4.4.1. **Model 1: P2VP brush swelling**

The P2VP chains in the aligned lamellar diblock copolymer films are tethered on the interfaces with PS layers due to the connectivity between the two blocks. The expansion of the P2VP chains in selective solvents (like the alcohol-water mixtures used in this chapter) can only occur in the direction normal to the lamellae due to the confinement imposed by the glassy PS layers. The swelling ratios of the P2VP chains can be estimated by using a tethered brush swelling model introduced by S. Alexander and reviewed by S. Milner.[22, 23]

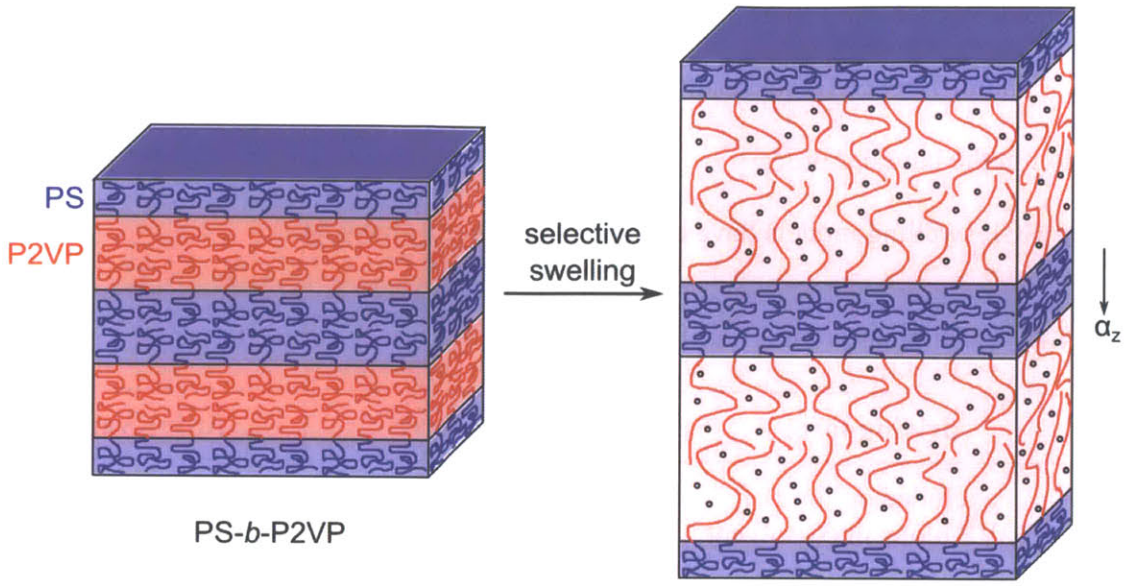

Figure 4.6. Schematic of the P2VP brush swelling model. P2VP chains are tethered on the interfaces with PS due to the diblock connectivity and can only expand along the lamellae normal with the confinement imposed by the glassy PS layers.

The free energy of brush swelling per P2VP chain is:

$$\Delta F_{brush} = kT\left(\frac{3h^2}{2Nb^2} + v_2 N^2 \frac{\sigma}{h}\right) \tag{4.8}$$

h is the brush height ($h = d_{P2VP}/2$ half the P2VP layer thickness), N the number of Kuhn segments, b the Kuhn length, v_2 the excluded volume, σ the grafting density (number of chains per unit area).

The excluded volume is related to the Flory-Huggins χ parameter by:[24]

$$v_2 = (1-2\chi)b^3 \tag{4.9}$$

The grafting density of P2VP in the lamellar PS-P2VP is:

$$\sigma = 1/\left(\frac{M_{n,P2VP}}{N_{Av}\rho_{P2VP}h_0}\right) = \frac{h_0 N_{Av}\rho_{P2VP}}{M_{n,P2VP}} \tag{4.10}$$

$M_{n,P2VP}$ is the number average molecular weight of the P2VP block, N_{Av} the Avgadro's number, ρ_{P2VP} the bulk density of P2VP, h_0 the dry brush height ($h_0 = d_0/2$).

P2VP has a similar molecular structure with PS, so we assume P2VP has the same Kuhn length as PS, $b = 9.2$ Å.[25] Therefore, the contour length of P2VP is given by:

$$L_C = Nb = 2\frac{M_{n,P2VP}}{M_{2VP}} l_{C-C} \sin\frac{109.5°}{2} = 232.4 \text{ nm} \tag{4.11}$$

So the free energy of swelling per P2VP chain or BCP molecule is:

$$\Delta F_{brush} = kT\left(\frac{3h^2}{2Nb^2} + \frac{(1-2\chi)b^3N^2}{h}\frac{h_0 N_{Av}\rho_{P2VP}}{M_{n,P2VP}}\right) = kT\left[\frac{3\alpha^2 d_0^2}{8L_C b} + (1-2\chi)\frac{N_{Av}\rho_{P2VP}L_C^2 b}{\alpha M_n}\right] \tag{4.12}$$

And the total free energy of brush swelling for n PS-P2VP molecules is:

$$\Delta F_{BCP\ swelling} = nkT\left[\frac{3\alpha^2 d_0^2}{8L_C b} + (1-2\chi)\frac{N_{Av}\rho_{P2VP}L_C^2 b}{\alpha M_{n,P2VP}}\right] \tag{4.13}$$

The swelling equilibrium can be obtained by minimizing $\Delta F_{BCP\ swelling}$ with respect to α:

$$\frac{\partial \Delta F_{BCP\ swelling}}{\partial \alpha} = nkT\left[\frac{3\alpha d_0^2}{4L_C b} - (1-2\chi)\frac{N_{Av}\rho_{P2VP}L_C^2 b}{\alpha^2 M_{n,P2VP}}\right] = 0 \tag{4.14}$$

The calculated P2VP swelling ratio is given by:

$$\alpha = \left[(1-2\chi)\frac{4N_{Av}\rho_{P2VP}L_C^3 b^2}{3M_{n,P2VP}d_0^2}\right]^{1/3} \sim 4.82(1-2\chi)^{1/3} \tag{4.15}$$

We assume that the effective interaction parameters χ_{eff} between P2VP and the co-solvent are the same in crosslinked homopolymer gels and in BCP gels, so that the χ_{eff} values measured from the crosslinked P2VP gels can be used in the model calculations. The P2VP block swelling ratios of a PS-P2VP in an alcohol-water co-solvent with the measured Flory-Huggins χ parameter can be calculated using Equation (4.15). The results are shown in Figure 4.7.

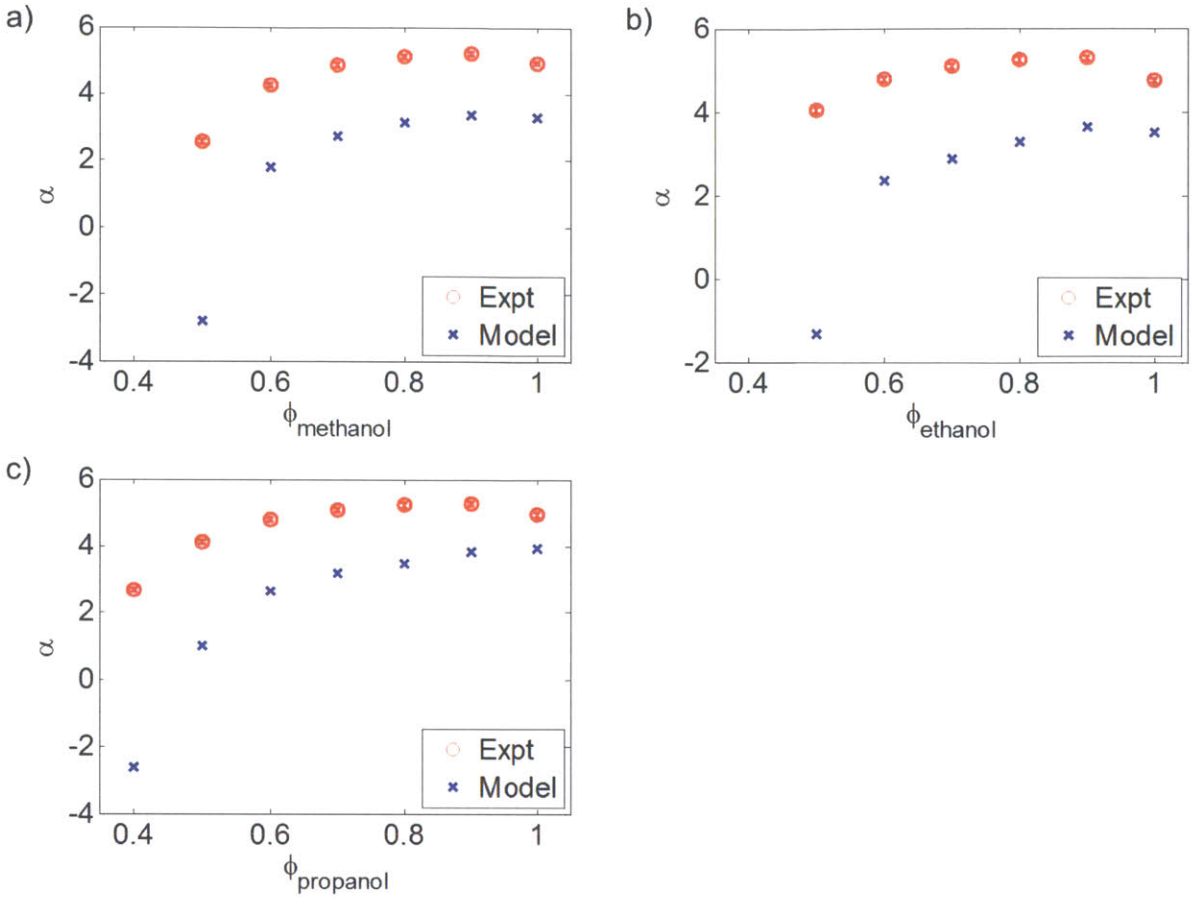

Figure 4.7. Results of the P2VP brush swelling model for a) methanol-, b) ethanol-, and c) 1-propanol-water co-solvents.

The modeling results suggest that the calculated equilibrium swelling ratios of the P2VP brushes are lower than the experimental data measured by reflection spectra and TMM. This counterintuitive result is likely due to the simplifications used in the calculation, e.g. the relationship between the excluded volume and χ, the value of the Kuhn length, etc. Both P2VP and the alcohol-water co-solvents are polar and their interaction may involve hydrogen bond formation, so it is not surprising that the brush swelling model using the excluded volume fails to capture the more complicated BCP swelling behaviors.

4.4.2. **Model 2: effective P2VP "network" swelling**

The swelling of the P2VP block is 1D (only along the layer normal) due to the lamellar confinement. In Model 2, we modify the Flory-Rehner theory for the isotropic 3D swelling of crosslinked polymer networks to model the BCP swelling. We assume that the P2VP block layers are entangled and have an effective crosslink density or molecular weight between crosslinks M_c that can be estimated from model fitting.

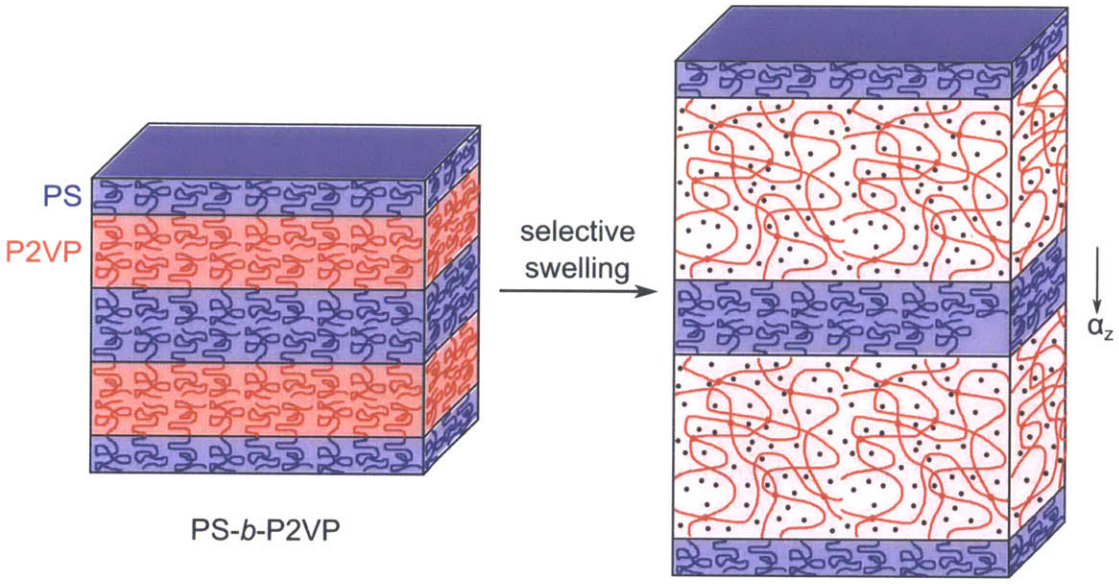

Figure 4.8. Schematic of the effective P2VP "network" swelling model. The P2VP block is treated as a crosslinked network that follows the Flory-Rehner theory modified for the 1D swelling.

The free energy of 1D swelling can be obtained by following S. Bruck's derivation of the extended Flory-Rehner theory for anisotropic polymer swelling.[26] The elasticity term of P2VP chain or "subchain network" stretching due to swelling for the system of n BCP molecules is given by:

$$\Delta F_{elasticity} = \frac{kT\nu_e}{2}\left(\alpha^2 - 1 - \ln\alpha\right) \tag{4.16}$$

α is the swelling ratio along the layer normal or z direction; ν_e is the number of subchains in the P2VP "network" and is related to the molecular weight between crosslinks by:

$$\nu_e = \frac{nM_{P2VP}}{M_c}\left(1-\frac{2M_c}{M_{P2VP}}\right) \sim \frac{nM_{P2VP}}{M_c} \tag{4.17}$$

M_{P2VP} is the molecular weight of the P2VP block and $M_{P2VP} >> M_c$ since we assume the crosslinks are dense enough.

For the favorable free energy of mixing term, we neglect the tethered brush configuration of the P2VP block and assume that the mixing is homogeneous within the P2VP gel layers. The free energy of mixing per n BCP molecules (and thus n P2VP molecules) is assumed to be given by the Flory-Huggins mean-field theory:[27]

$$\Delta F_{mix} = kT\left[n_s \ln\left(1-\frac{1}{\alpha}\right)+n\ln\frac{1}{\alpha}+\frac{\chi n_s}{\alpha}\right] \tag{4.18}$$

n_s is the number of co-solvent molecules swelling the n P2VP chains and can be obtained by $n_s = n\,(\alpha-1)\,M_{P2VP}\rho_s/\rho_{P2VP}M_s$, with M_{P2VP} and M_s the molecular weights of the P2VP block and the solvent respectively. M_{P2VP} is much larger than M_s, therefore n is much smaller than n_s and the second term in Equation (4.18) can be neglected.

The total free energy of BCP swelling is:

$$\Delta F_{BCP\ swelling} = \Delta F_{mix} + \Delta F_{elasticity} \tag{4.19}$$

The swelling equilibrium is reached when the free energy of BCP swelling is minimized with respect to α. The condition is given by:

$$\left[\ln\left(1-\frac{1}{\alpha}\right)+\frac{\chi}{\alpha^2}+\frac{1}{\alpha}\right]+\frac{V_1}{2\bar{v}M_c}\left(2\alpha-\frac{1}{\alpha}\right)=0 \tag{4.20}$$

V_1 is the molar volume of the solvent; $\bar{v}$ is the specific volume of the polymer in the dry state and can be calculated from the polymer's density by $\bar{v} = 1/\rho$.

M_c can be fitted using the $\alpha-\chi$ data at all compositions for the three alcohol-water co-solvents. The results are shown in Figure 4.9.

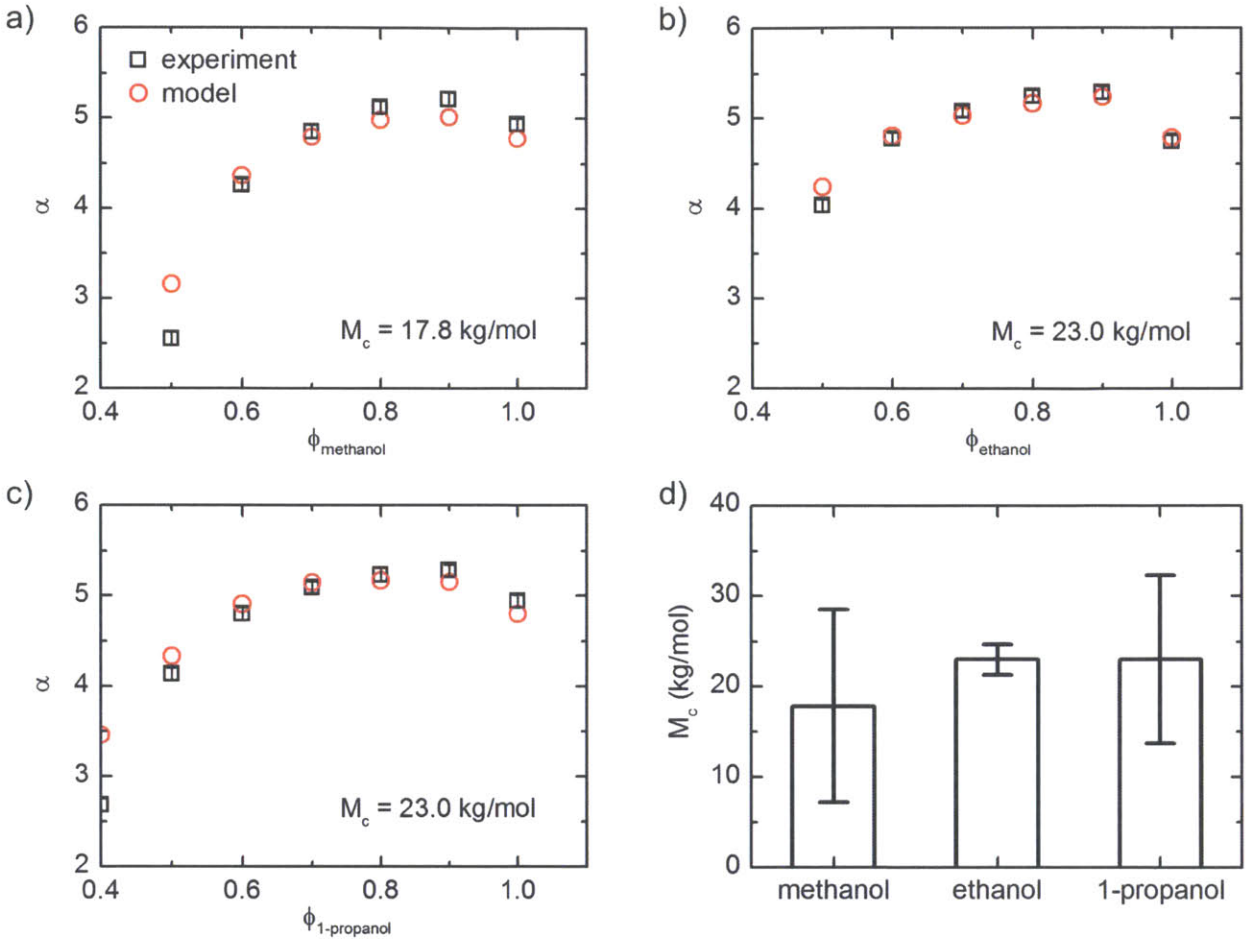

Figure 4.9. Fitting results of the P2VP "network" swelling model for a) methanol-, b) ethanol-, and c) 1-propanol-water co-solvents; and d) the effective molecular weights estimated from model fitting. The error bars show the overlapping 95% confidence intervals.

The quality of the data fitting is good; however, the fitting results for the variable M_c do not match the physical picture. The values of M_c (~ 20 kg/mol) is 1.5 times the entanglement molecular weight of polystyrene (13.3 kg/mol)[28] and 1/5 the P2VP block molecular weight (97 kg/mol). Moreover, entanglement between P2VP chains is very unlikely to exist in the ~ 5x

swollen state. Therefore, Model 2 does not describe the BCP swelling well albeit the good fitting quality.

4.4.3. **Model 3: PS defect core deformation**

Thin films of a lamellar BCP tend to organize with the layers parallel to the substrate. Both edge and screw types of dislocations are frequently observed in such films.[29, 30] Cross-sectional TEM (see Figure 4.10 and Figure 4.11) and 3D stimulated emission depletion (STED) microscopy[31] show both types of line defects in lamellar PS-P2VP samples. The defects form an interconnected network of glassy PS layers that retard the P2VP swelling. We find the swelling/deswelling behavior reproducible over multiple cycles, which suggests that the network of glassy PS layers does not undergo fracture or large plastic deformation during swelling which would irreversibly alter the BCP structure. Therefore, we use the elastic deformation strain energy of the PS network to model the BCP swelling.

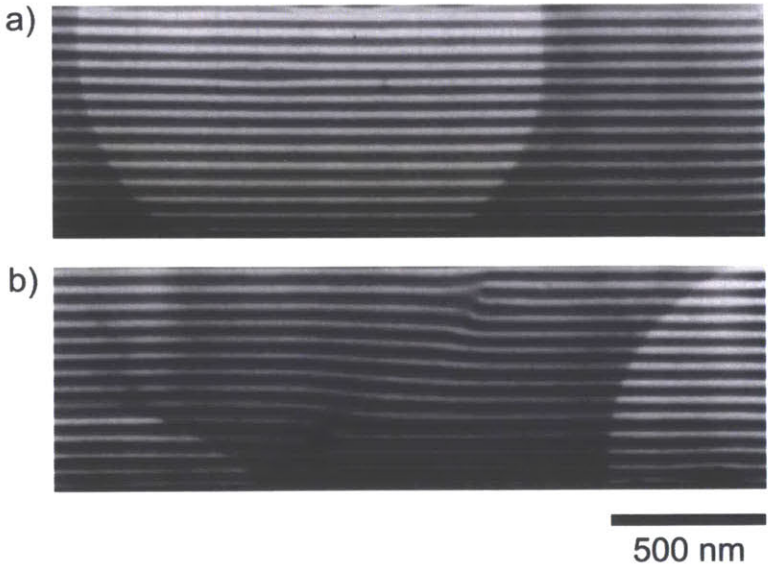

Figure 4.10. Bright-field cross-sectional TEM image of a) a defect free region and b) a region with a pair of edge dislocations (a dislocation dipole) in the PS-P2VP film (M_n 102/97 kg

mol^{-1}) used for the photonic gels. After iodine staining, the P2VP layers are dark and the PS layers light. The lamellar periodicity d_0 is calculated from the TEM as 56 nm. The light circular regions are holes in the amorphous specimen support film.

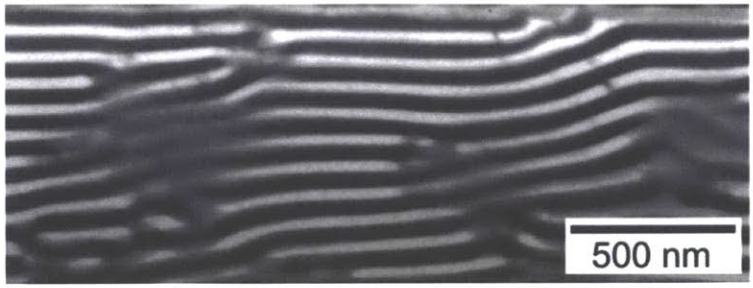

Figure 4.11. Bright-field cross-sectional TEM image of a lamellar PS-P2VP film (M_n 190/190 kg mol^{-1}). The P2VP domains have been stained by iodine vapor and appear dark. A set of screw dislocation lines and end-on views of several edge dislocations are evident.

In Model 3, the defect deformation is assumed to be localized at the defect core regions (see Figure 4.12). The distance between defects is constant.

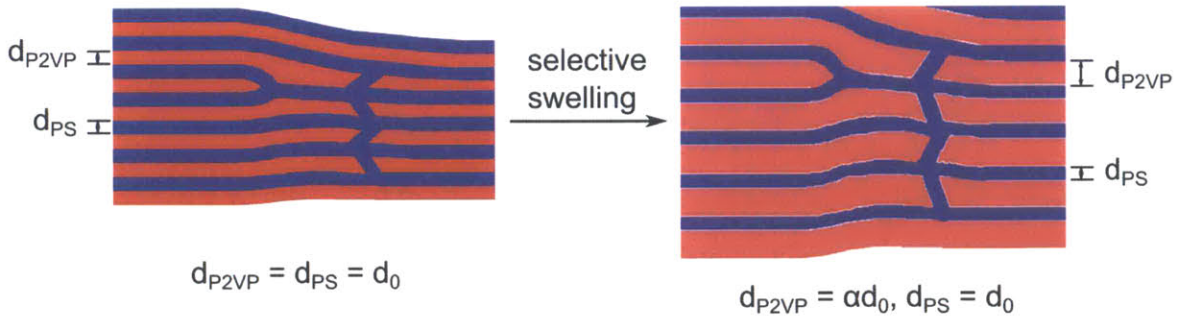

Figure 4.12. Schematic of the localized PS defect core deformation model. The width of the defect cores is assumed to be equal to the thickness of the PS or P2VP layers d_0.

We assume that the elastic deformation is confined to the defect region only and the defect size d_0 does not change during selective swelling. Assuming that the defects take a random 2D distribution in the plane parallel to the lamellae and the average distance between defects is L,

the fraction of PS in the defect region is roughly $(d_0/L)^2$. The swelling stretches the PS layers near the defect by an elongation ratio of $\sqrt{1+\alpha^2}$. The strain energy for the elastic deformation of PS due to a $d\alpha$ change in P2VP swelling ratio can be estimated as:

$$dF_{defects} = E_{PS}V_{PS}\left(\frac{d_0}{L}\right)^2 d\sqrt{1+\alpha^2} \tag{4.21}$$

E_{PS} is the Young's modulus of PS, 3 GPa at room temperature; V_{PS} is the total volume of PS in the BCP and can be calculated by $V_{PS} = n_{P2VP}V_{P2VP}$ assuming that PS and P2VP have equal molar volumes.

The total free energy of swelling for n_{P2VP} PS-P2VP is:

$$\begin{aligned}\Delta F &= \Delta F_{mix} + \Delta F_{defects} \\ &= n_{P2VP}kT(\alpha-1)\frac{V_{P2VP}}{V_s}\left[ln\left(1-\frac{1}{\alpha}\right)+\frac{\chi}{\alpha}\right]+E_{PS}n_{P2VP}V_{P2VP}\left(\frac{d_0}{L}\right)^2\int d\sqrt{1+\alpha^2}\end{aligned} \tag{4.22}$$

At swelling equilibrium, the total free energy of BCP swelling should be minimized. The condition of $\partial\Delta F/\partial\alpha = 0$ gives an equation for α and χ with L the defect spacing as a fitting variable:

$$\left[\ln\left(1-\frac{1}{\alpha}\right)+\frac{\chi}{\alpha^2}+\frac{1}{\alpha}\right]+\frac{E_{PS}V_s}{RT}\left(\frac{d_0}{L}\right)^2\frac{\alpha}{\sqrt{1+\alpha^2}} = 0 \tag{4.23}$$

In this equation, α are calculated by TMM from the reflection spectra of the photonic gels; χ are measured by homopolymer gel swelling and Flory-Rehner theory as mentioned earlier; L is an unknown constant because the same BCP sample was used in photonic gel measurements. L can be fitted from α and χ data at all co-solvent compositions. The P2VP swelling ratios from model fitting are shown in Figure 4.13 and compared to experimental data measured from the photonic properties. The fitting gives an estimated L, the distance between defects as ~ 2 μm. Fitting for three alcohols was done separately due to the difference in V_s, and the three L values

from the model fitting were within the 95% confidence intervals of each other. This estimation seems reasonable comparing to a sampling of cross-sectional TEM images on the as-annealed lamellar PS-P2VP samples.

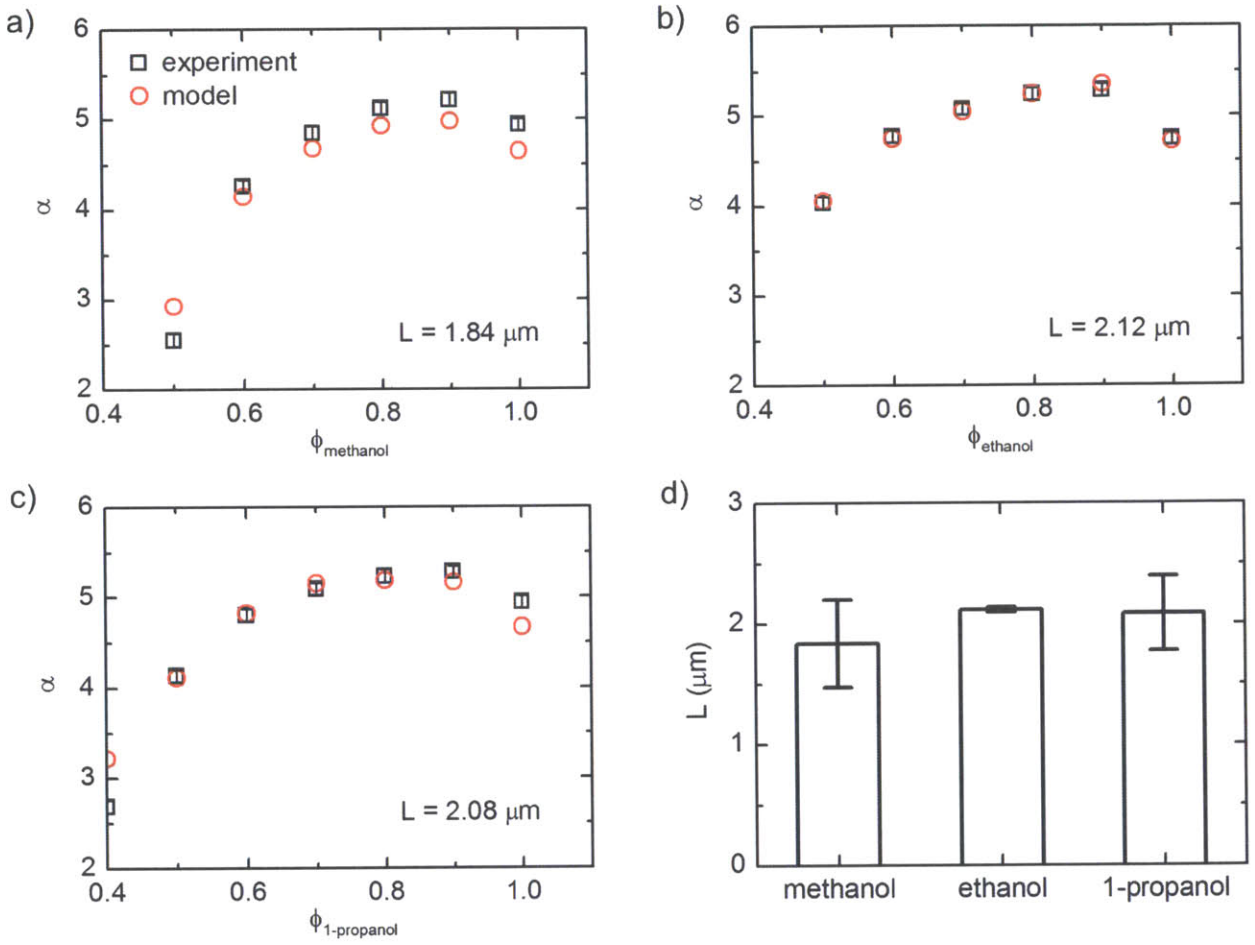

Figure 4.13. Fitting results of the PS defect core deformation model for a) methanol-, b) ethanol-, and c) 1-propanol-water co-solvents; and d) the average distance between defect cores estimated from model fitting. The error bars show the overlapping 95% confidence intervals.

The fitting results are reasonable. However, the model is limited because of the localized deformation assumption. The maximum swelling ratios of P2VP in these data sets are ~ 5. It is

unlikely that glassy PS remains in the elastic regime at 500% strain. Since linear mechanics is used for the deformation energy terms in the equations, the model is not practically valid.

4.4.4. **Model 4: dislocation network strain energy**

In Model 4, we continue the discussion of defect deformation strain energy as the retarding force for BCP swelling and use the dislocation network strain energy to substitute the localized defect core deformation.

Dislocations in 1D periodic layered media can only have their Burgers vector along the layer normal with magnitude equal to the period. For the in-plane ordered, periodic BCP bilayer film, the Burgers vector in the dry film is equal to the lamellar period. The edge dislocations have their line vectors in the plane of the film, whereas the screw dislocations have their line vectors along the normal to the film direction. Screw dislocations pin together multiple layers along the core region oriented normal to the layers whereas edge dislocations only pin two adjacent layers along a horizontally oriented core region. Dislocation lines in layered media must form continuous loops, end at external surfaces and/or form networks as first suggested by Y. Bouligand.[32]

The opposing force to swelling is the enthalpic strain energy due to the glassy PS layer network deformation driven by the P2VP swelling. We use the balance of the free energies of mixing and the change in the dislocation line energies (elastic strain fields) to determine the swelling equilibrium.

We assume the defects' contribution to the free energy of BCP swelling is equal to the difference of the strain energy of dislocations before and after swelling. The strain energy of dislocations depends on both the core energy and the surrounding strain field energy.

$$F_{defects} = \left(E_{core,s} + E_{field,s}\right)L_s + \left(E_{core,e} + E_{field,e}\right)L_e \tag{4.24}$$

Here E_i are the energies per unit dislocation line length, and L_i are the dislocation line lengths. The subscripts "core" and "field" stand for the core energy and the strain field energy, and "s" and "e" for the screw or edge dislocation types respectively. The dislocation lines tend to form networks as depicted in Figure 4.14.

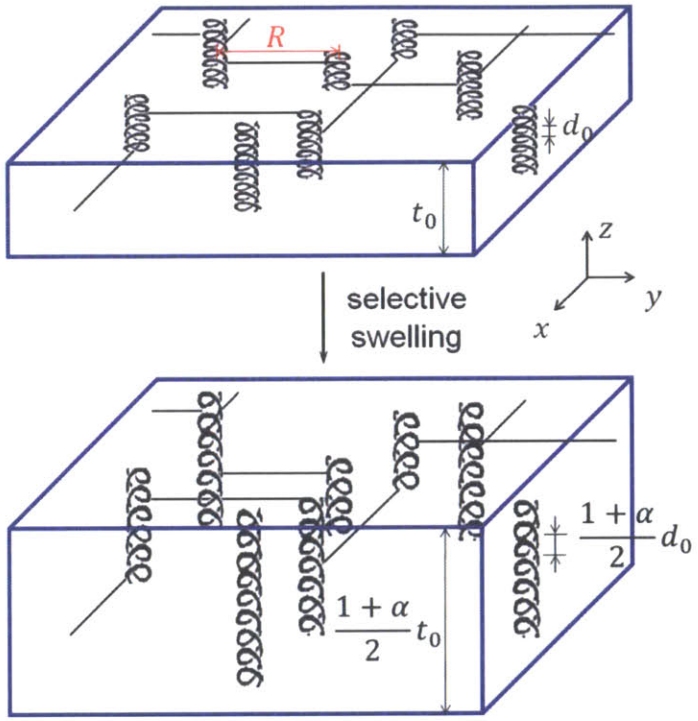

Figure 4.14. Schematics of a defect region in a lamellar PS-P2VP film with dislocation networks before and after selective swelling. Adapted from the work of Y. Bouligand.[32]

Swelling of the layers in the dislocation core region depends on the type of dislocation. For the left- and right-handed helicoidal screw dislocations, the core region connects alternating layers of PS to PS and P2VP to P2VP.[31, 33] Swelling expands the P2VP layers but is retarded by the helix-like springs formed by the connected glassy PS layers. Edge dislocations are comprised of either PS or P2VP terminating layers. A P2VP terminating layer results in joining of the two adjacent PS layers, locally inhibiting the terminating layer from swelling. A PS

terminating layer does not inhibit swelling as the adjacent P2VP layers are free to expand. Assuming that there are equal numbers of terminating PS and P2VP layers, half of the edge dislocations are ineffective at retarding swelling. Overall, the defects provide variations in the degree of P2VP layer swelling, consistent with the observed broad reflectivity peak profiles.

The complicated swelling behaviors of the dislocation cores also make it difficult to estimate the E_{core} terms in Equation (4.24). The screw dislocation cores are partially swollen due to the helical connectivity of PS and P2VP layers; the cores of the P2VP terminating edge dislocations are swollen, while the PS terminating ones are not swollen. In order to have a tractable analysis, we neglect the difference in the total defect core energies between the swollen and dry states. Therefore, the total strain energy of dislocations in Equation (4.24) can be simplified as:

$$F_{defects} = E_{field,s} L_s + \frac{1}{2} E_{field,e} L_e \tag{4.25}$$

The strain field energy per unit length of dislocation line is given by:[34]

$$E_{field,s} = \frac{Gb_s^2}{4\pi} \ln \frac{R}{R_0}, E_{field,e} = \frac{Gb_e^2}{4\pi(1-\nu)} \ln \frac{R}{R_0} \tag{4.26}$$

Here b is the Burgers vector, R the average distance between dislocations, and R_0 the size of the dislocation cores. G and ν are the shear modulus and the Poisson's ratio. In the dry state, PS and P2VP have equal moduli and Poisson's ratios, so we use the shear modulus G_0 and Poisson's ratio of amorphous PS for the BCP film, $G_{\text{dry}} = 1$ GPa and $\nu_{\text{dry}} = 1/3$.[35] In the swollen state, the modulus and the Poisson's ratio can be calculated by treating the lamellae as a composite of glassy PS and gel P2VP layers. The modulus and the Poisson's ratio of a lamellar composite is the average of the in-plane and normal components, which can be calculated by the parallel or in-series models:[36]

$$G_{swollen} = \frac{2}{3}G_{in-plane} + \frac{1}{3}G_{normal} = \frac{2}{3}\left(G_1\varphi_1 + G_2\varphi_2\right) + \frac{1}{3}\left(\frac{\varphi_1}{G_1} + \frac{\varphi_2}{G_2}\right)^{-1} = \frac{2}{3(\alpha+1)}G_0 \qquad (4.27)$$

$$\nu_{swollen} = \frac{2}{3}\nu_{in-plane} + \frac{1}{3}\nu_{normal} = \frac{2}{3}\left(\nu_1\varphi_1 + \nu_2\varphi_2\right) + \frac{1}{3}\frac{\frac{\varphi_1}{G_1}\nu_1 + \frac{\varphi_2}{G_2}\nu_2}{\frac{\varphi_1}{G_1} + \frac{\varphi_2}{G_2}} = \frac{9\alpha+7}{18(\alpha+1)} \qquad (4.28)$$

φ_1 and φ_2 are the volume fractions of the glassy PS or gel P2VP layers in the lamellae. The shear modulus of P2VP gels was measured as ~ 6 kPa in the compression tests of the crosslinked P2VP gels. The shear modulus of the homopolymer P2VP gels is a few kPa. As $G_{PS,\,dry} >> G_{P2VP,\,gel}$, Equations 6 and 7 can be simplified. The Possion's ratio of the gel layers $\nu_{P2VP,\,gel}$ is approximately 1/2.

To estimate the dislocation line lengths in the BCP film, we assume that the line vectors of edge dislocations lie along the x or y axis and the screw dislocations along z. We also assume that the average distances between dislocations are the same for both the screw and edge dislocations, $R_s = R_e = R$. For simplicity, the dislocation lines are assumed to decorate a cubic lattice. The average lengths of dislocations lines are taken to be R, the same as the average distance between dislocations. The dislocation line lengths per unit volume are $1/R^2$ for screw and and $2/R^2$ for edge dislocations respectively and the total dislocation line lengths in the film of n BCP molecules in the dry state are:

$$L_s = \frac{V}{R^2} = \frac{nM_{BCP}}{N_A\rho_{BCP}R^2}, L_e = \frac{2nM_{BCP}}{N_A\rho_{BCP}R^2} \qquad (4.29)$$

M_{BCP} and ρ_{BCP} are the molecular weight and density of the BCP, and N_A is Avgadro's number. Then the dislocation strain energy at the dry state can be calculated and is given by:

$$F_{defects}^{dry} = \frac{5nM_{BCP}G_0d_0^2}{8\pi N_A\rho_{BCP}R^2}\ln\frac{R}{d_0} \qquad (4.30)$$

The Burgers vectors for both screw and edge dislocations are equal to the lamellar periodicity, which is d_0 in the dry state and increases to $(1+\alpha)d_0/2$ when the P2VP layers swell. The lengths of screw dislocation lines also increase $(1+\alpha)/2$ times during swelling while the lengths of the edge dislocations stay constant. The dislocation strain energy in the swollen state is:

$$F_{defects}^{swollen} = \frac{nM_{BCP}G_0d_0^2}{\pi N_A \rho_{BCP} R^2} \frac{(1+\alpha)^2}{12}\left(\frac{1}{4}+\frac{9}{9\alpha+11}\right)\ln\frac{R}{d_0} \tag{4.31}$$

Therefore, the strain energy difference between the dry and the swollen states is:

$$\Delta F_{defects} = \frac{nM_{BCP}G_0d_0^2}{\pi N_A \rho_{BCP} R^2}\left[\frac{(1+\alpha)^2}{12}\left(\frac{1}{4}+\frac{9}{9\alpha+11}\right)-\frac{5}{8}\right]\ln\frac{R}{d_0} \tag{4.32}$$

The free energy of swelling for n PS-P2VP molecules is:

$$\begin{aligned}\Delta F &= \Delta F_{mix} + \Delta F_{defects} \\ &= nkT\frac{M_{P2VP}\rho_s}{M_s\rho_{P2VP}}(\alpha-1)\left[\ln\left(1-\frac{1}{\alpha}\right)+\frac{\chi}{\alpha}\right]+\frac{nM_{BCP}G_0d_0^2}{\pi N_A \rho_{BCP} R^2}\left[\frac{(1+\alpha)^2}{12}\left(\frac{1}{4}+\frac{9}{9\alpha+11}\right)-\frac{5}{8}\right]\ln\frac{R}{d_0}\end{aligned} \tag{4.33}$$

At swelling equilibrium, the total free energy of the BCP gel should be minimized. The condition of $\partial\Delta F/\partial\alpha = 0$ gives an equation for α and χ with the average distance between dislocations R as a fitting variable:

$$\frac{12\pi RT}{G_0V_s}\left[\ln\left(1-\frac{1}{\alpha}\right)+\frac{1}{\alpha}+\frac{\chi}{\alpha^2}\right]+\frac{(1+\alpha)(\alpha^2+4.44\alpha+4.38)}{(\alpha+1.22)^2}\frac{\ln(R/d_0)}{(R/d_0)^2}=0 \tag{4.34}$$

In Equation (4.34), α is the swelling ratio of P2VP layers and is calculated by TMM from the reflection spectra of the photonic gels; χ is measured by homopolymer gel swelling and Flory-Rehner theory; R is an unknown constant because the same BCP sample was used in measurements of photonic repsonses. R can be fitted using the α and χ data for all three co-solvents. Fitting for three co-solvents was done separately due to the difference in the molecular

volume V_s and the results are shown in Figure 4.15. The calculated swelling ratios using the fitted parameter and the model equation (red) agree with the experimental values (black). The average distance between dislocations R is estimated as ~ 3 μm. The estimation of R seems reasonable with respect to a sampling of cross-sectional TEM images of the as-annealed lamellar PS-P2VP samples. The overlapping 95% confidence intervals suggest that the model is effective in capturing the role of the dislocation networks in the BCP sample.

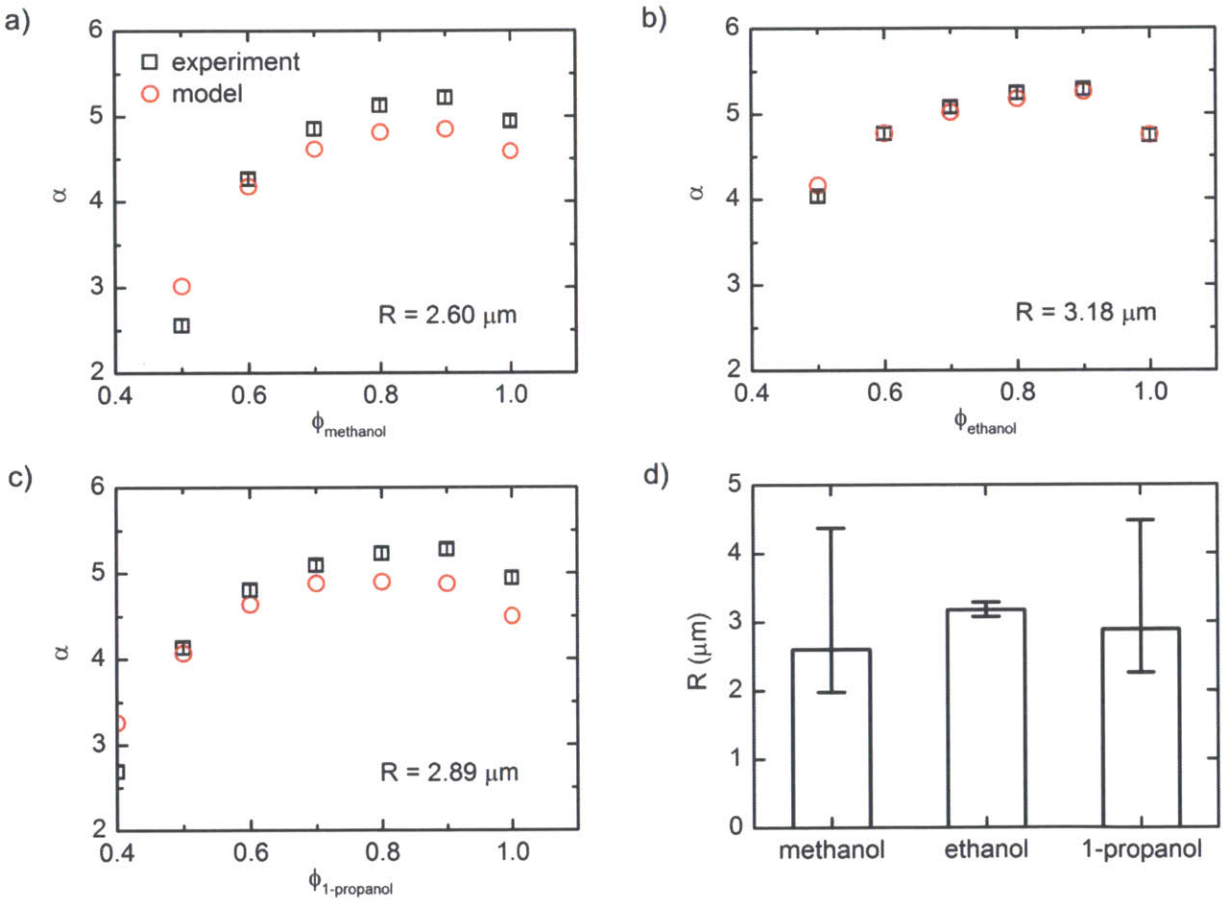

Figure 4.15. Fitting of swelling ratio α_{P2VP} versus co-solvent composition $\phi_{alcohol}$ for the swelling model. a) ~ c) P2VP swelling ratios in PS-P2VP gels in co-solvents of water and a) methanol, b) ethanol, and c) 1-propanol. Red circles are estimated by the model using the fitting parameter R ~ 3 μm and black squares are experimental data measured from the

photonic responses. d) Fitting parameter R (the average dislocation-dislocation distance) calculated independently for the three alcohol-water co-solvents. The error bars show the overlapping 95% confidence intervals.

Model 4 gives satisfactory fitting results for experimental data and the fitting variables have reasonable values. Therefore, the swelling behaviors of lamellar PS-P2VP gels in alcohol-water co-solvents are best described by the Model 4 that uses Flory-Huggins mean-field mixing and dislocation line network strain energy.

4.5. *Summary and future work*

In summary, this chapter demonstrates that the PS-P2VP photonic gels show responsive reflective color according to the composition of alcohol-water co-solvents. Quantitative models have been proposed to describe the BCP swelling and the model based on Flory-Huggins mean-field mixing and the line defect strain energy of the interconnected dislocation network comprised of glassy PS layers successfully fits the experimental data. The model quantitatively relates the photonic gel's reflectance and the P2VP swelling ratio to the effective Flory-Huggins χ parameter between P2VP and the co-solvent and the average defect density. The results indicate that the defects in BCP self-assembly impact selective swelling and suggest that the lamellar BCP photonic gels have a potential application as sensing materials for χ or defect density.

To better support the defect network picture depicted in Model 4, additional work on microstructure characterization is necessary. Statistical analysis of the defects (or more specifically, the screw and edge dislocations as line defects) is desired. Parameters to be

surveyed include the types, Burgers and line vectors, distribution and density of the defects in the lamellar BCP films used for the photonic gels.

So far the swelling ratios of the P2VP block in the BCP gels have only been calculated from the photonic properties using TMM. Direct imaging of the BCP gels can provide evidence about the swollen structure and thus support the TMM analysis and the swelling models. Possible tools include cryo-SEM or TEM, confocal microscopy. Quartz-crystal microbalance is another interesting tool that can measure the P2VP swelling ratios and compare to the TMM calculations.

References

1. Kang, Y.; Walish, J. J.; Gorishnyy, T.; Thomas, E. L. *Nat. Mater.* **2007**, *12*, 957-960.

2. Walish, J. J.; Kang, Y.; Mickiewicz, R. A.; Thomas, E. L. *Adv. Mater.* **2009**, *30*, 3078-3081.

3. Chan, E. P.; Walish, J. J.; Thomas, E. L.; Stafford, C. M. *Adv. Mater.* **2011**, *40*, 4702-4706.

4. Walish, J. J.; Fan, Y.; Centrone, A.; Thomas, E. L. *Macromol. Rapid Commun.* **2012**, *18*, 1504-1509.

5. Lim, H. S.; Lee, J.; Walish, J. J.; Thomas, E. L. *ACS Nano* **2012**, *10*, 8933-8939.

6. Blandame, M.; Fox, M.; Powell, E.; Stafford, J. *Makromol. Chem.* **1969**, *1*, 222-231.

7. Cowie, J. M. G.; Mohsin, M. A.; McEwen, I. J. *Polymer* **1987**, *9*, 1569-1572.

8. Winnik, F. M.; Ringsdorf, H.; Venzmer, J. *Macromolecules* **1990**, *8*, 2415-2416.

9. Young, T. H.; Cheng, L. P.; Hsieh, C. C.; Chen, L. W. *Macromolecules* **1998**, *4*, 1229-1235.

10. Grulke, E. A. Polymer Handbook (4th Edition) - VII. Solution Properties, Solubility Parameter Values. In John Wiley & Sons: 2005; Vol. 7, pp 675-714.

11. Shrader, D. Polymer Handbook (4th Edition) - V. Physical Constants of Poly(styrene). In John Wiley & Sons: 2005; Vol. 5, pp 91-96.

12. Wohlfarth, C. Polymer Solutions. In *Landolt-Börnstein: Numerical Data and Functional Relationships in Science and Technology;* Lechner, M. D., Arndt, K. F., Eds.; Springer: Berlin, 2010; Vol. 6D2.

13. Haynes, W. M. In *CRC Handbook of Chemistry and Physics, Section 5, Concentrative Properties of Aqueous Solutions: Density, Refractive Index, Freezing Point Depression, and Viscosity.* Taylor and Francis Group, LLC: 2013; Vol. 5, pp 123-148.

14. El-Kashef, H. *Physica B: Condensed Matter* **2000**, *4,* 295-301.

15. Rheims, J.; Köser, J.; Wriedt, T. *Measurement Science and Technology* **1997**, *6,* 601-605.

16. Hale, G. M.; Querry, M. R. *Appl. Opt.* **1973**, *3,* 555-563.

17. Born, M.; Wolf, E. *Principles of optics: electromagnetic theory of propagation, interference and diffraction of light;* ; New York ; Cambridge University Press: Cambridge, UK, 1997.

18. Yeh, P. *Optical waves in layered media;* Wiley: New York, 1988.

19. Ho, P.; Thomas, D.; Friend, R.; Tessler, N. *Science* **1999**, *5425,* 233-236.

20. Zha, W.; Han, C. D.; Lee, D. H.; Han, S. H.; Kim, J. K.; Kang, J. H.; Park, C. *Macromolecules* **2007**, *6,* 2109-2119.

21. Flory, P. J.; Rehner, J. *J. Chem. Phys.* **1943**, *11,* 521-526.

22. Alexander, S. *J. Phys.* **1977**, *8,* 977-981.

23. Milner, S. *Science* **1991**, *4996,* 905-914.

24. Rubinstein, M.; Colby, R. H. *Polymer physics;* Oxford University Press: Oxford ; New York, 2003.

25. Brulet, A.; Boue, F.; Cotton, J. *J. Phys. II* **1996**, *6,* 885-891.

26. Bruck, S. D. *J. Res. Natl. Bur. Stand.* **1961**, *6,* 485-487.

27. Flory, P. J. *Principles of polymer chemistry;* Cornell University Press: Ithaca, 1953.

28. Fetters, L. J.; Lohse, D. J.; Richter, D.; Witten, T. A.; Zirkel, A. *Macromolecules* **1994**, *17,* 4639-4647.

29. Urbas, A.; Sharp, R.; Fink, Y.; Thomas, E. L.; Xenidou, M.; Fetters, L. J. *Adv. Mater.* **2000**, *11,* 812-814.

30. Lee, W.; Yoon, J.; Lee, H.; Thomas, E. L. *Macromolecules* **2007**, *17,* 6021-6024.

31. Ullal, C. K.; Schmidt, R.; Hell, S. W.; Egner, A. *Nano Letters* **2009**, *6,* 2497-2500.

32. Bouligand, Y. *Journal De Physique* **1972**, *5-6,* 525-547.

33. Gido, S.; Gunther, J.; Thomas, E.; Hoffman, D. *Macromolecules* **1993**, *17,* 4506-4520.

34. Hull, D.; Bacon, D. J. Chapter 4 - Elastic Properties of Dislocations. In *Introduction to Dislocations (Fifth Edition);* Butterworth-Heinemann: Oxford, 2011; pp 63-83.

35. Schrader, D. Polymer Handbook (4th Edition) - V. Physical Constants of Some Important Polymers, Physical Constants of Poly(styrene). In John Wiley & Sons: 2005; Vol. 5, pp 91-96.

36. Ward, I. M.; Sweeney, J. Polymer Composites: Macroscale and Microscale. In *Mechanical Properties of Solid Polymers;* John Wiley & Sons, Ltd: 2012; pp 227-259.

5. Protein Responsive PS-QP2VP Photonic Gels

This chapter studies the dynamic photonic responses of BCP gels in contact with protein solutions. The P2VP block in the lamellar PS-P2VP is first converted into a polycation QP2VP by quaternization reactions. PS-QP2VP swells in water and displays structural color. Proteins have surface charges in aqueous solutions and undergo ionic interactions with polyelectrolytes. The ionic interaction triggers the swelling/deswelling of the QP2VP gel block, which changes the structural color of the lamellar PS-QP2VP photonic gels. Real-time photonic responses of the PS-QP2VP gels are characterized by the reflective spectra recorded as a function of time and are related to the dynamic swelling behaviors of the QP2VP gel layers in protein solutions. Parameters such as charge density, hydrophobicity, and crosslink density of the QP2VP gel layers as well as the charge and size of the proteins play significant roles and are studied in this chapter. The results suggest that the BCP gels and their associated structural colors provide a fast and visually interpretable method to differentiate proteins due to differences in size and charge.

5.1. *Motivation and design*

It has been shown both in literature[1-6] and in previous chapters of this thesis that lamellar BCP gels show structural colors in selective solvents and the reflected color from the gel is responsive to a variety of stimuli via the swelling/deswelling of the gel block. Next we explore proteins as a new stimulus to trigger photonic responses by the ionic interactions with the polyelectrolyte block in the photonic gels.

Proteins and polyelectrolyte form coacervates due to ionic complexation in solution (Figure 5.1).[7] A change in swelling ratios of the polyelectrolyte is expected during coacervation. The structural colors of the BCP gels are quantitatively related to the swelling ratios of the gel layers and can thus be used to measure the effect of the ionic interactions between the protein and the polyelectrolyte block. The fast and sensitive responses of the BCP gels should be able to provide a quick and visually interpretable method to differentiate proteins by their interactions with polyelectrolytes.

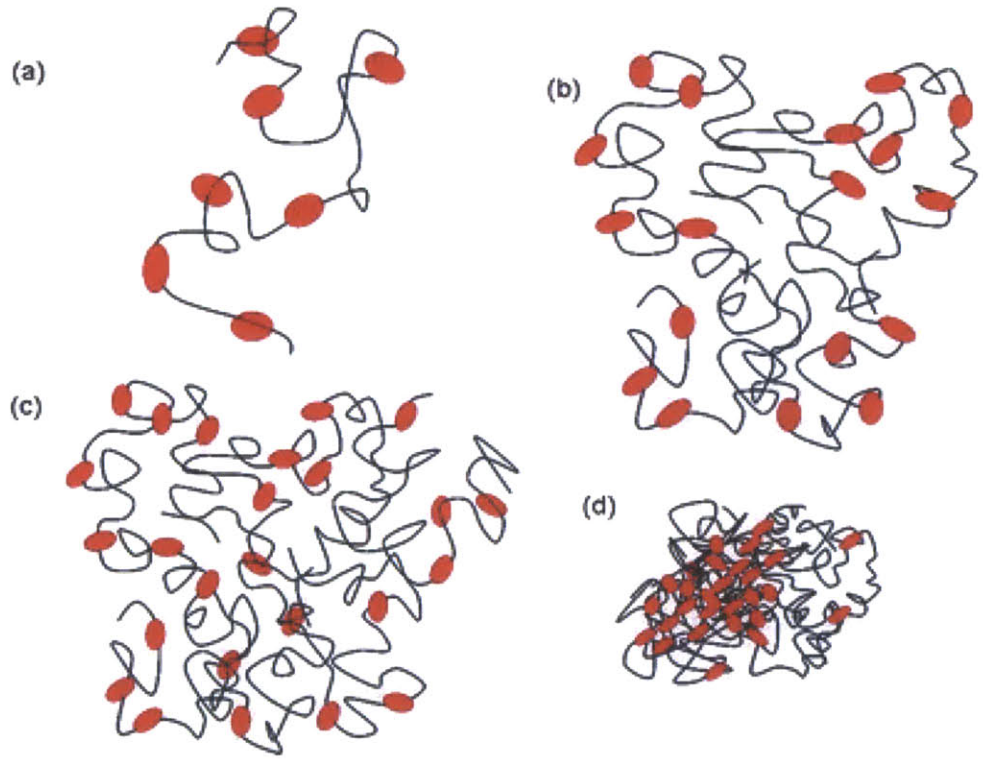

Figure 5.1. Protein-polyelectrolyte coacervate formation.[8] The black lines represent the polyelectrolyte and the red ovals represent the proteins. (a) Intrapolymer complex, (b) soluble aggregate of (four) intrapolymer complexes, (c) hypothetical intermediate interpolymer complex, and (d) coacervate with dense and dilute domains.

In addition to the steady-state photonic responses, the real-time spectra collected using a high-speed spectrometer can help understand the transport of the proteins within the lamellar BCP gels, which is interesting not only for the biomolecule-synthetic macromolecule interactions but also for the lamellar BCP microstructure studies. The mass transport is related to the diffusion of proteins and other ionic species (the Br^- and Cl^- counterion, tris and protonated tris, H_2O H^+ and OH^-) into the gel layers driven by the osmotic pressure and the charge equilibrium, and diffusion of water in or out of the gel layers due to the thermodynamic equilibrium concentration of the proteins in the QP2VP gel. The transport of the proteins and the associated small molecule solvent in the BCP gels is expected to be much slower compared to small molecule solvents because of the bigger sizes of proteins. In the cases that the BCP gels deswell in protein solutions, the diffusion of proteins in the shrunken gel layers would be expected to be even slower. Slower transport makes the swelling/deswelling kinetics easier to be captured in spectral characterizations and therefore provides an excellent model system to study the effect of defects and microstructure on the mass transport in lamellar BCP films (see Chapter 4 for a detailed discussion about the role of defects in the lamellar BCP photonic gels).

The P2VP block in the annealed lamellar PS-P2VP films is first converted into a polycation by a quaternization reaction to convert the pyridines to form pyridinium (see Figure 5.2). The properties of the quaternized P2VP (QP2VP) can be tuned by adjusting the reaction conditions. This chapter looks into three molecular level QP2VP parameters imparted by the quaternization reaction in particular: (1) the charge density, (2) the hydrophobicity and (3) the crosslink density of the QP2VP block. The charge density on the QP2VP chains can be controlled by the reaction time for the conversion of the pyridines and can be quantitatively assessed by Fourier transform infra-red spectroscopy (FTIR). The hydrophobicity of the QP2VP gel layers can be controlled

by the choice of the quaternization reagent, as longer alkyl substituents on the pyridinium make the gel more hydrophobic. The QP2VP can be crosslinked by using difunctional quaternization reagents and the crosslink density can be adjusted by the molar ratios of the difunctional additives to the major monofunctional component as well as the extent of reaction and reactant concentration.

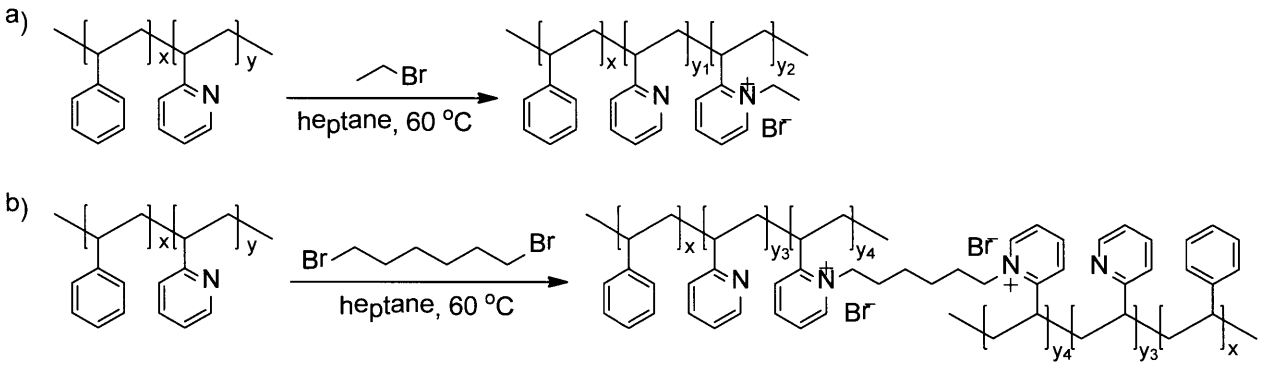

Figure 5.2. Quaternization reactions on the pyridine groups in annealed lamellar PS-P2VP films with a) bromoethane and b) dibromohexane. Bromoethane (EtBr) converts the P2VP into a polycation block that swells in water; dibromohexane (DBH) quaternizes and crosslinks the P2VP into a less swellable network. Crosslinking can be both inter-block and intra-block.

The lamellar PS-QP2VP films swell in water or buffer solutions and show structural colors. The BCP gels are then exposed to protein solutions and the transmission spectra are subsequently recorded as a function of time. The sizes and charges of the proteins are key parameters to the photonic responses. The driving force for the proteins to enter the QP2VP gel layers is the protein concentration gradient across the BCP film and in the solution reservoir. The QP2VP gel block is positively charged, therefore, proteins with negative surface charges bind to the QP2VP and result in blue-shifts, and proteins with positive charges lead to higher swelling ratios in the

gel block and red-shifts due to electrostatic repulsion (see Figure 5.3). The charge of a protein can be tuned by adjusting the pH of the buffer solution. Proteins of different isoelectric points (pI) have different charges in the same buffer solution. The protein charges can be estimated by theoretical calculation (see the electrostatic potential map for bovine serum albumin (BSA) in Figure 5.4a) or by measuring the ζ potential which is the electrostatic potential difference between the solution medium and the stationary layer of fluid attached to the protein. The diffusion rate of the proteins in the BCP gels depends on the protein size. Globular proteins of higher molecular weights are bigger in size and will diffuse more slowly into the photonic gels and can be captured in the real-time photonic spectra.

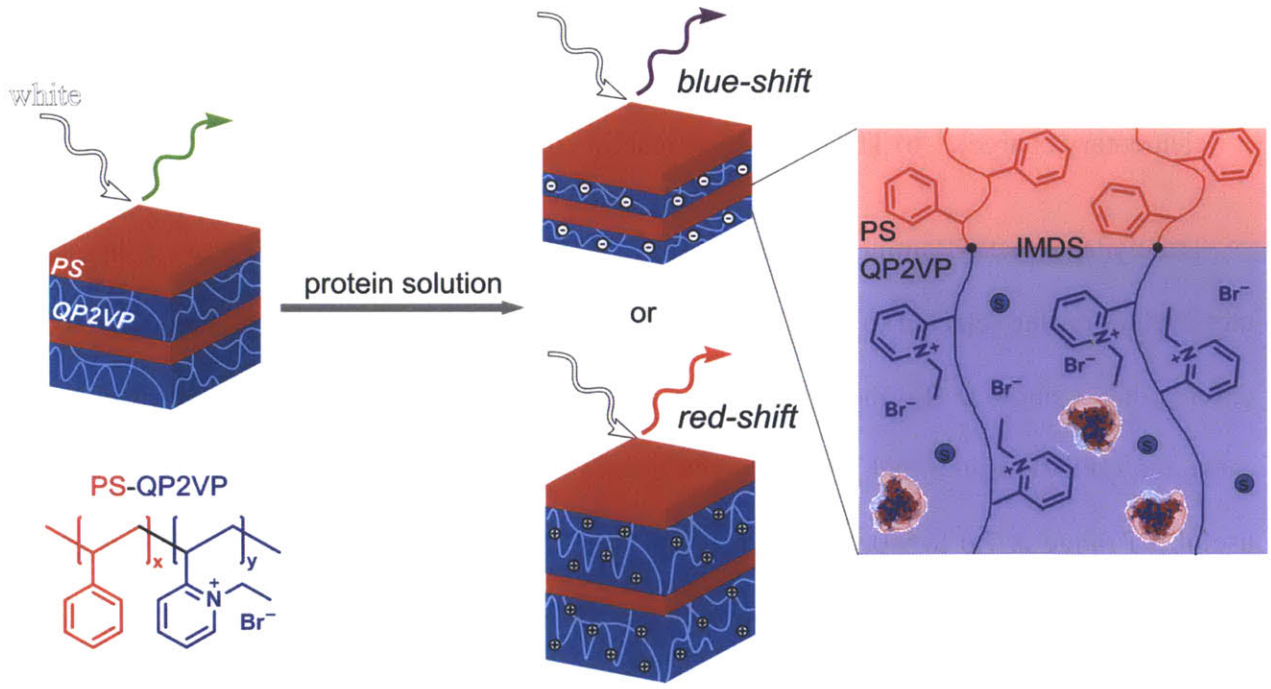

Figure 5.3. Schematic of the lamellar PS-QP2VP photonic gel and its two possible behaviors in protein solutions, and a zoom-in view of the species present near the inter-material dividing surface (IMDS). The PS block is glassy and the QP2VP block is swollen in an aqueous solution. The red and blue particles represent the proteins. The blue circles labeled

with "s" represent the solvent molecules (water). Buffer molecules and ions are omitted in the schematic. The sizes of the symbols do not reflect the actual sizes of the present species.

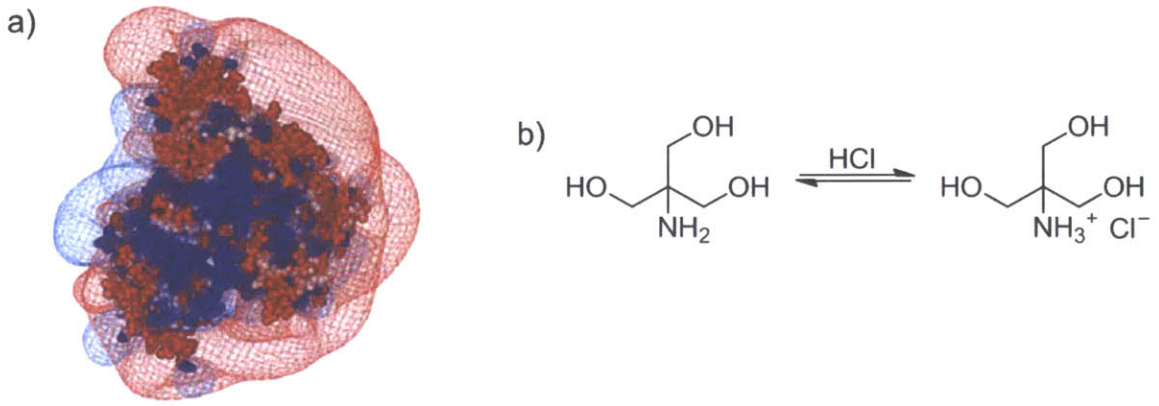

Figure 5.4. a) The electrostatic potential map of BSA at pH 7 (red and blue represent -/+ 0.1 kT/e respectively, where k is the Boltzmann constant, T the temperature, and e the elementary charge).[9] b) The association reaction of the tris buffer in HCl.

Tris(hydroxymethyl)aminomethane ($(HOCH_2)_3CNH_2$, "tris", see Figure 5.4b) is a monovalent buffer selected to control the pH of the protein solutions. The monovalency of tris ensures that a single buffer molecule does not bind to multiple sites in the QP2VP or protein to cause the QP2VP/protein gel layer's swelling ratio to decrease. The pK_a of tris is 8.06 and its useful pH range is 7.0 to 9.0, and therefore the pH of the protein solutions used in this chapter are 7, 8, and 9. The 10 mM buffer concentration is low enough so that the ionic strength of the buffer does not overshadow the ionic interactions between the protein and the QP2VP gel block.

The five proteins examined are listed in Table 5.1. The proteins were selected because they are commercially available in the lyophilized powder form at prices lower than $ 100/mg. The proteins also have to be colorless so that the solutions have negligible absorption in the visible light regime. The five proteins in Table 5.1 were selected so that contrast in both size and charge

is accessible in the pH range studied with the tris buffer solutions. Low concentrations are preferred for cost efficiency, and 1 weight % used in this chapter is sufficient for detectable photonic responses.

Table 5.1. Proteins and their molar weights and isoelectric points from the suppliers.

protein	acronym	MW (kDa)	pI
Albumin from bovine serum	BSA	66	5.3
α-Amylase from Aspergillus oryzae	Amy	51	
Ribonuclease A (Bovine Pancrease)	Rib	13.7	9.63
Trypsin from porcine pancreas	Try	23.8	10
Lysozyme from chicken egg white	Lys	14.3	11.35

The effect of six parameters on the PS-QP2VP gels' photonic responses to proteins is studied: the swelling kinetics, the charge density, hydrophobicity, and crosslink density of the QP2VP gel block, as well as the buffer pH and protein species.

The dynamic photonic responses captured by the high-speed acquisition spectrometer provide evidence for the transport of the proteins in the lamellar BCP gels and the kinetics of the consequent gel swelling or contraction. As discussed in Chapter 4, the self-assembled BCP lamellae have defects such as vertical holes, screw and edge type dislocations. The defects play an essential role in the mass transport in the BCP films. Proteins are considerably larger than the small molecule solvents or ions used in the past studies, and thus the kinetics of protein transport in the PS-QP2VP gels is slower and easier to be captured in experiments.

The hydrophobicity of the QP2VP gel block is related to the substituents on the pyridinium which come from the reactants used in the quaternization reaction. In this chapter, we compare the ethyl and propyl groups by using mixtures of bromoethane and 1-bromopropane (PrBr) as the quaternization reagents.

The pore size of the molecular network in the gel layers affects the diffusion rate of the proteins into the QP2VP gel layers and thus the dynamic photonic responses. The pore size can be tuned via the crosslink densities of the QP2VP block. By using a *difunctional* bromide DBH as an additive to the quaternization reagent EtBr, the P2VP block can be quaternized and crosslinked in one step. The reactivity of the bromides is assumed to be constant in the different EtBr/DBH mixtures because of the low amounts of DBH. Thus, PS-QP2VP films quaternized with EtBr/DBH mixtures of higher DBH fraction have higher crosslink densities.

Proteins can display various charge states in solutions due to the dissociation and association of the amino acids in aqueous environments. Thus, the charge of a protein can be simply varied by changing the pH of the buffer solution. The sign of the charge depends on the protein's isoelectric point (pI) and the solution pH. The protein does not have any net charge when the solution pH equals its pI. In solutions of higher pH than the pI, the protein is negatively charged as the dissociation of carboxyl groups dominates, and in solutions of lower pH, the protein is positively charged as the protonation of amine groups dominates. If a change in pH does not induce any change in protein folding or degradation, the size of the protein does not change within a certain range of pH. Therefore, by changing the pH of the buffer solutions, the correlation between the PS-QP2VP gels' photonic responses and the charges of the proteins at constant size in solution can be explored.

The sizes of the proteins cannot be altered independently of the pI or charges due to the limited choices of commercially available and affordable proteins. Therefore, we select five proteins (see Table 5.1) and study the effect of charge and size as a combined parameter on the photonic responses of the BCP gels.

5.2. *Dynamic swelling*

The real-time transmission spectra of the PS-QP2VP photonic gels during the swelling in protein solutions are recorded by an Ocean Optics optical fiber spectrometer with high-speed acquisition and converted to reflectance by assuming zero absorbance and scattering (which is valid given that the protein solutions appear clear and colorless).

The time scale of the photonic gel's dynamic swelling in protein solutions is very different compared to that in buffer solutions. Figure 5.5 present two dynamic swelling spectra of the first minute of the same PS-QP2VP film in buffer and in protein solutions, respectively. The dry PS-QP2VP film swells quickly in the first 10 seconds in the buffer solution and reaches a steady state in which the reflection spectra and hence the swelling ratio of the QP2VP block do not change much. The red-shift that the PS-QP2VP gel shows in the trypsin solution is much slower and the QP2VP layer is still undergoing significant expansion even after 10 min as evident in Figure 5.7c. Similar time scale responses are observed in other proteins solutions. Figure 5.5 clearly suggests that the photonic responses of the BCP gels in protein solutions are slower than that for small molecule solutions by a factor of 10 ~ 100. Variability of the defect content and microstructure of the BCP films can be ruled out here because the same BCP films are used for the swelling in buffer and in protein solutions. The difference in dynamic photonic responses is

likely caused by the larger sizes of the proteins and their slower transport in the lamellar BCP gels compared to the buffer or water molecules.

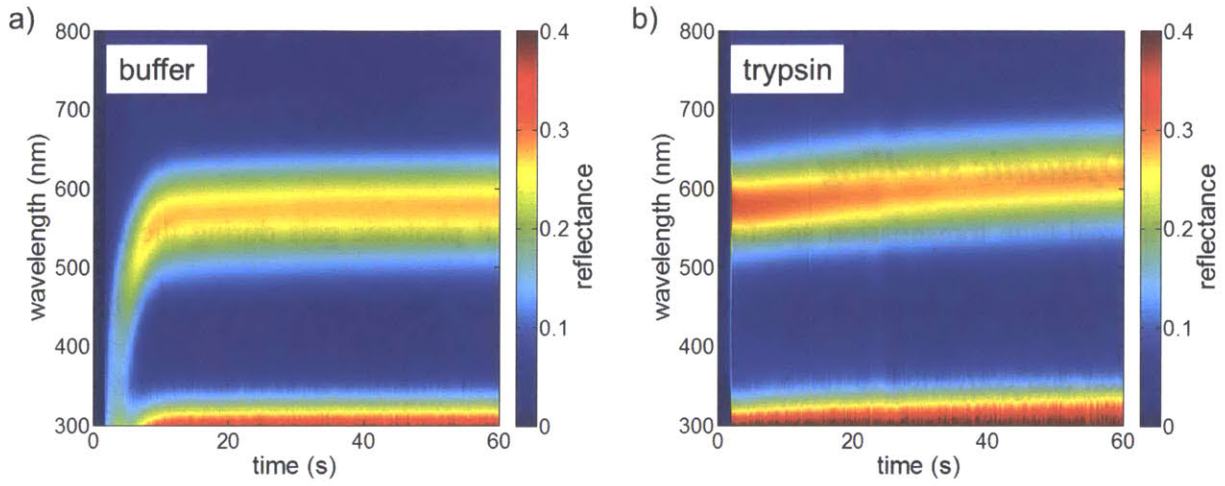

Figure 5.5. Real-time dynamic swelling spectra of an initially dry PS-QP2VP photonic gel in a) 10 mM pH 7 tris buffer from the dry state and b) 1 % trypsin solution in the same buffer after soaking in the tris buffer for 10 min. Both color maps are on the same time scale (from t = 0 to t = 60 sec).

As expected and depicted in Figure 5.3a, protein solutions can lead to both blue-shifts and red-shifts of the reflectivity of the PS-QP2VP photonic gels. Figure 5.6 and Figure 5.7 are examples of blue-shift and red-shift respectively. The PS-QP2VP films were initially soaked in tris buffer solutions for 10 min before being transferred into the protein solutions, so the dynamic swelling spectra collected are not related to the swelling process and solvent transport into dry BCP films.

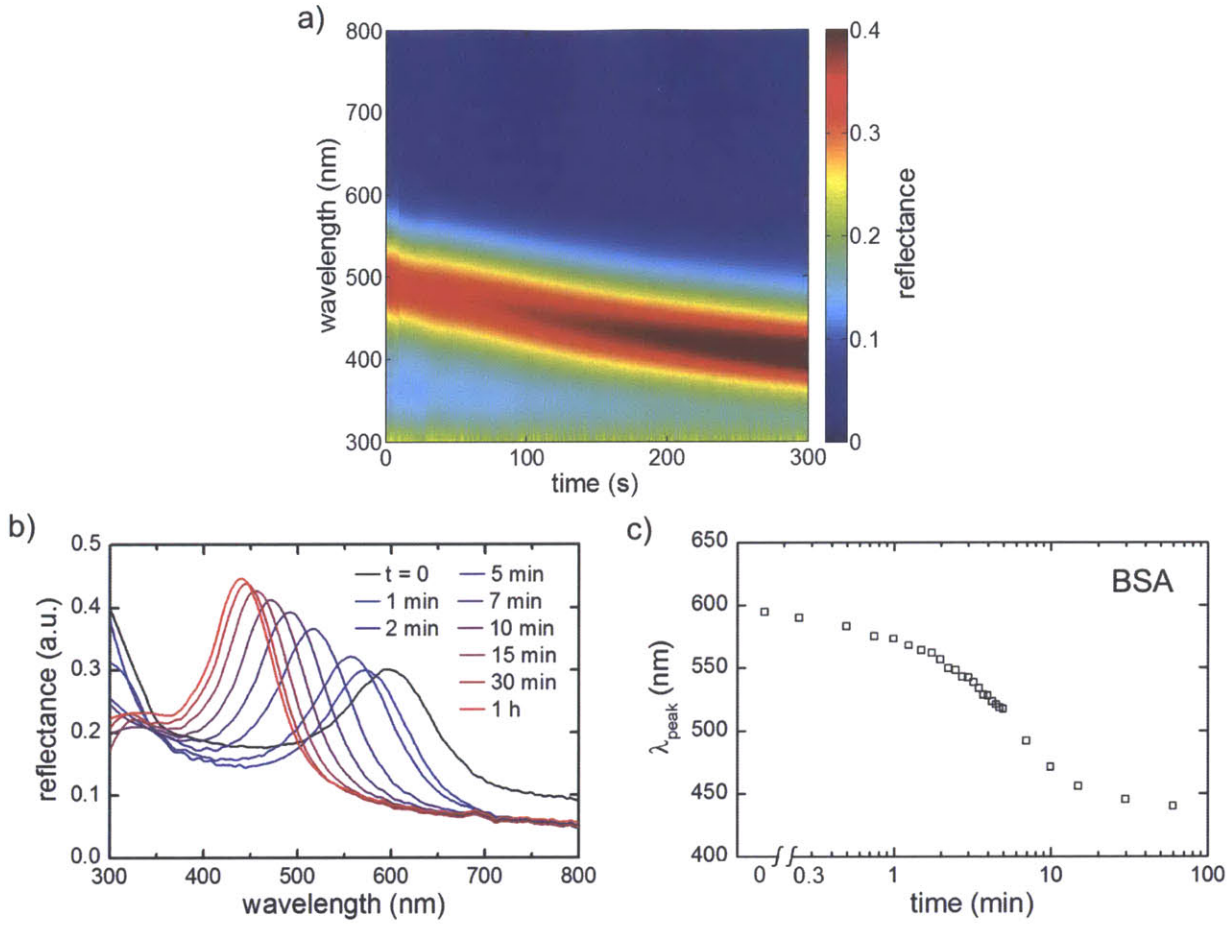

Figure 5.6. Real-time dynamic swelling spectra showing the blue-shift in reflectivity of a PS-QP2VP photonic gel in 1 % BSA solution in 10 mM tris buffer at pH 9 after soaking in the same buffer solution for 10 min. a) Color map of the reflectance over the first 5 min; b) reflection spectra from t = 0 (equilibrium swelling in the buffer solution) to t = 1 hour in protein solution; c) the reflectivity peak wavelengths as a function of the soaking time in the BSA solution.

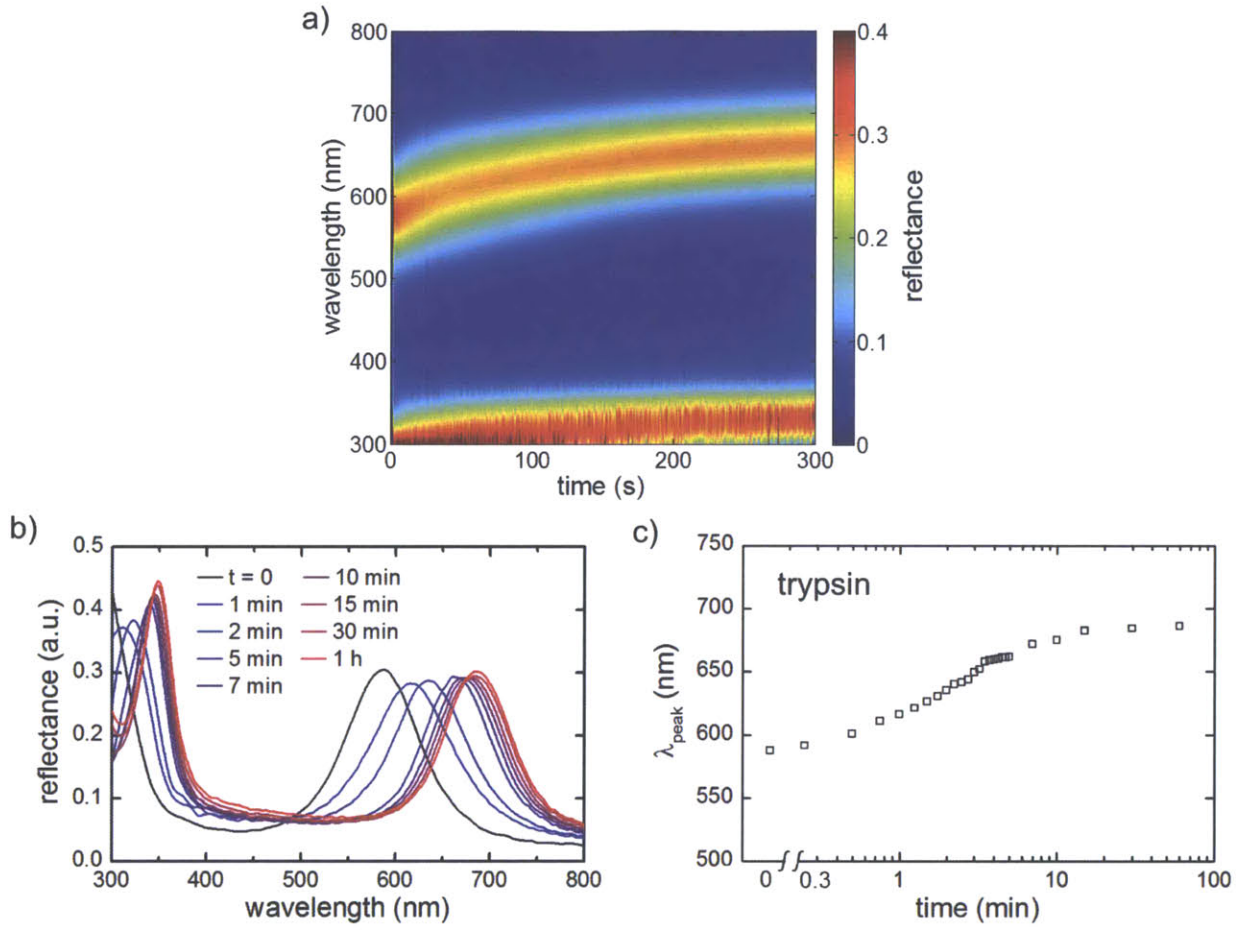

Figure 5.7. Real-time dynamic swelling spectra showing the red-shift in reflectivity of a PS-QP2VP photonic gel in 1 % trypsin solution in 10 mM tris buffer at pH 7 after soaking in the same buffer solution for 10 min. a) Color map of the reflectance over the first 5 min; b) reflection spectra from t = 0 (equilibrium swelling in the buffer solution) to t = 1 hour in protein solution; c) the reflectivity peak wavelengths as a function of the soaking time in the trypsin solution.

The sign of the peak shifts is related to the sign of charges of the particular protein. The actual charges of the proteins in the solutions need be determined by ζ potential measurements, but a rough estimation can be made by comparing the protein's pI with the solution pH. The pI

of BSA is 5.3 and thus BSA likely has negative charges in solutions at pH 7, 8, or 9. Trypsin has a pI of 10 and may be positively charged in pH 7 tris buffer. The dynamic swelling spectra in Figure 5.6 and Figure 5.7 suggest that solutions of positively charged proteins lead to red-shifts of the reflectivity of lamellar PS-QP2VP photonic gels while solutions containing negatively charged proteins result in blue-shifts. This observation is consistent with our hypothesis that oppositely charged proteins form coacervates with QP2VP, shrink the polyelectrolyte gel block and result in blue-shifts, while like-charged proteins increase the swelling ratio of the polyelectrolyte gel block due to electrostatic repulsion and lead to red-shifts in the structural color.

5.3. *Photonic gel parameters*

5.3.1. **Charge density**

Next we use EtBr as the quaternization reagent to make the PS-QP2VP films from the as-annealed lamellar PS-P2VP and vary the reaction time to make photonic gel samples of different QP2VP charge densities.

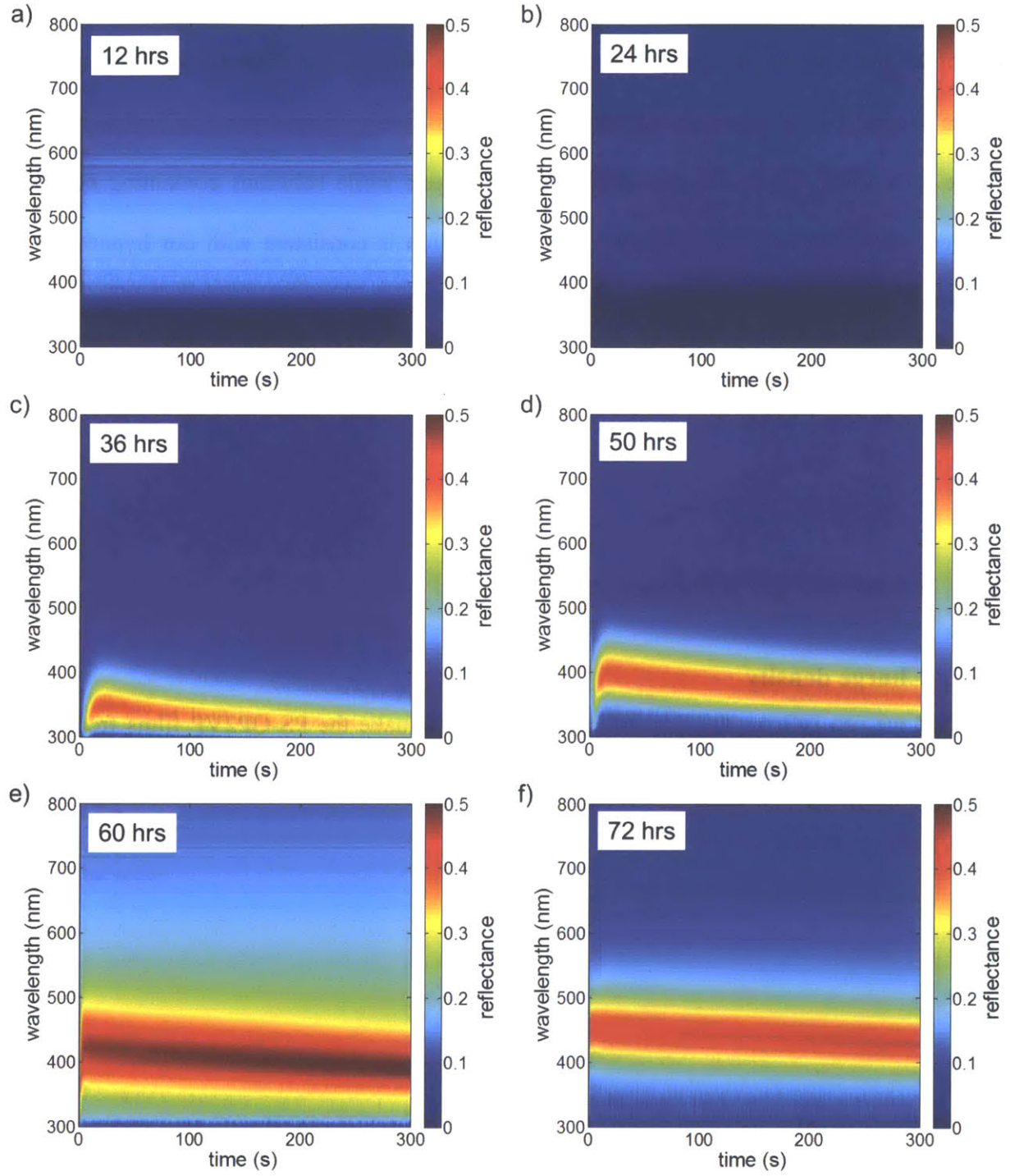

Figure 5.8. Real-time dynamic swelling spectra of PS-QP2VP films quaternized with EtBr for different reaction times swelling in 1 % BSA solutions in 10 mM pH 9 tris buffer after soaking in the same buffer solution for 10 min. a) to f) are collected with films quaternized

for 12, 24, 36, 50, 60, and 72 hours, respectively. The red-shifts in the first 5 seconds of c) to e) are due to the recovery of swelling after dehydration during the transfer process between the solutions.

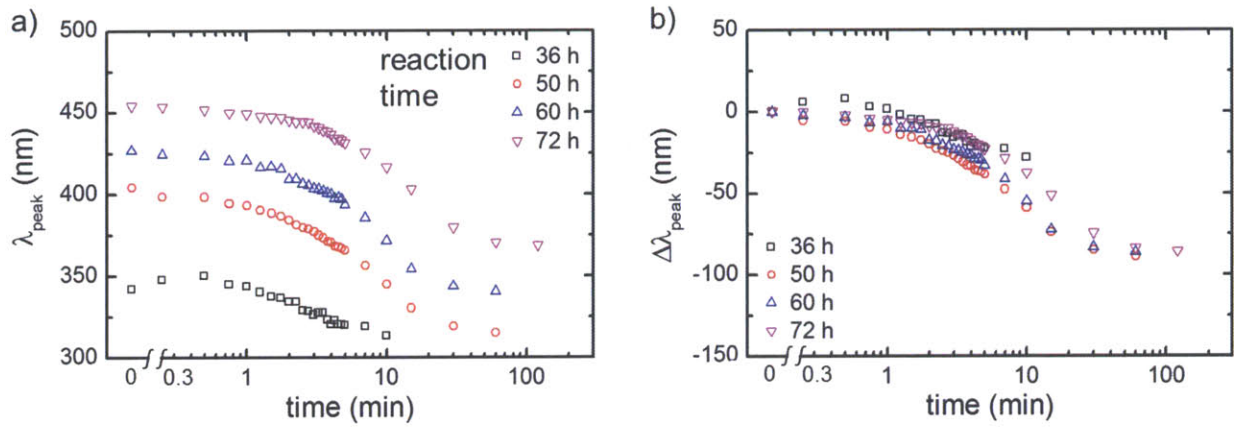

Figure 5.9. Reflectivity peak wavelengths and peak shifts of PS-QP2VP photonic gels vs. swelling time when samples with various EtBr quaternization times ranging from 36 to 72 hours were swollen with 1 % BSA solution in 10 mM pH 9 tris buffer after soaking in the same buffer solution for 10 min.

Figure 5.8 shows the dynamic swelling spectra of the photonic gels quaternized for different reaction times. The surfaces of as-annealed or weakly quaternized PS-P2VP films are hydrophobic, so the films may dehydrate during the transfer process between solutions. The red-shifts in the first ~ 5 seconds in c), d), e) are due to the recovery of swelling after the transfer. The two samples quaternized for 12 and 24 hours do not show a reflectivity peak in the 300 to 800 nm wavelength range. Samples quaternized for longer times have reflectivity peaks between 300 and 800 nm and the peaks are plotted in Figure 5.9a as a function of swelling time. The four samples quaternized for 36 to 72 hours show time-dependent blue-shifts in reflectivity in the BSA solution.

The reflectivity peaks of the films that are quaternized for longer times are higher at any swelling time. The start points at t = 0 are the steady-state swelling in the 10 mM pH 9 tris buffer solution. Since the QP2VP blocks in the six samples have different charge densities, their swelling ratios in the buffer solution are different. Therefore, the blue-shifts of the four PS-QP2VP gels are different. More pyridines are converted to pyridinium in quaternization reactions of longer times, so the charge densities of the QP2VP block increase with the reaction time. The swelling ratios of the QP2VP block layers increase with their charge densities and so do the reflectivity peak wavelengths, which explains the trends of the four $\lambda_{peak} \sim t$ curves in Figure 5.9a.

To eliminate the effect of the different start points, the reflectivity peak shifts rather than the absolute peak wavelengths should be used while comparing the series of films. The reflectivity peak shifts are defined as the difference between the current reflectivity peak wavelength and the start point when the film was at equilibrium swelling in the buffer solution. The peak shifts ($\Delta\lambda_{peak}$) for the quaternization time series are plotted in Figure 5.9b. All four curves overlap and the differences are within the variations from the measurements or the films themselves. This result indicates that in the photonic gels that have reflectivity peaks between 300 and 800 nm, the charge density of the QP2VP block affect the photonic response by changing the solubility or swelling ratio of QP2VP in the tris buffer but does not affect the peak shifts when the photonic gel is transferred into the BSA solution. The observation suggests that the interaction between the QP2VP gel layers and BSA in the 10 mM pH 9 tris buffer is independent of the charge density of the QP2VP block. It is of note that due to the limited numbers of experiments so far, the conclusion here is limited to the range of quaternization reaction times, the pH and

concentration of the buffer solution, and the protein species, and therefore may not apply to other systems.

5.3.2. **Hydrophobicity**

To study the effect of QP2VP gel hydrophobicity, we next compare the ethyl and propyl groups by using mixtures of bromoethane and 1-bromopropane (PrBr) as the quaternization reagents.

The propyl group has one more CH_2 than ethyl and is thus more hydrophobic. PS-QP2VP films quaternized solely with PrBr are too hydrophobic and do not swell sufficiently to show structural color in water. Therefore, we used PrBr as an additive with EtBr to tune the hydrophobicity. To identify the PrBr fraction range that hydrophobicity is effective on the PS-QP2VP gels' photonic responses, three sets of reactions were designed. The first set uses 0, 10 %, 20 %, and 40 % (mole fractions) PrBr in EtBr. As shown in a) and b) of Figure 5.10, the reflectivity peaks of the three samples quaternized with reagents containing PrBr are very close to each other but different from the ones of the EtBr quaternized sample, which suggests that the high sensitivity regime of PrBr fraction is below 10 %. The second set uses 0, 1 %, 2 %, and 5 % PrBr in EtBr. The overlapping $\lambda_{peak} \sim t$ curves in c) and d) of Figure 5.10 suggest that the high sensitivity regime is probably above 5 %.

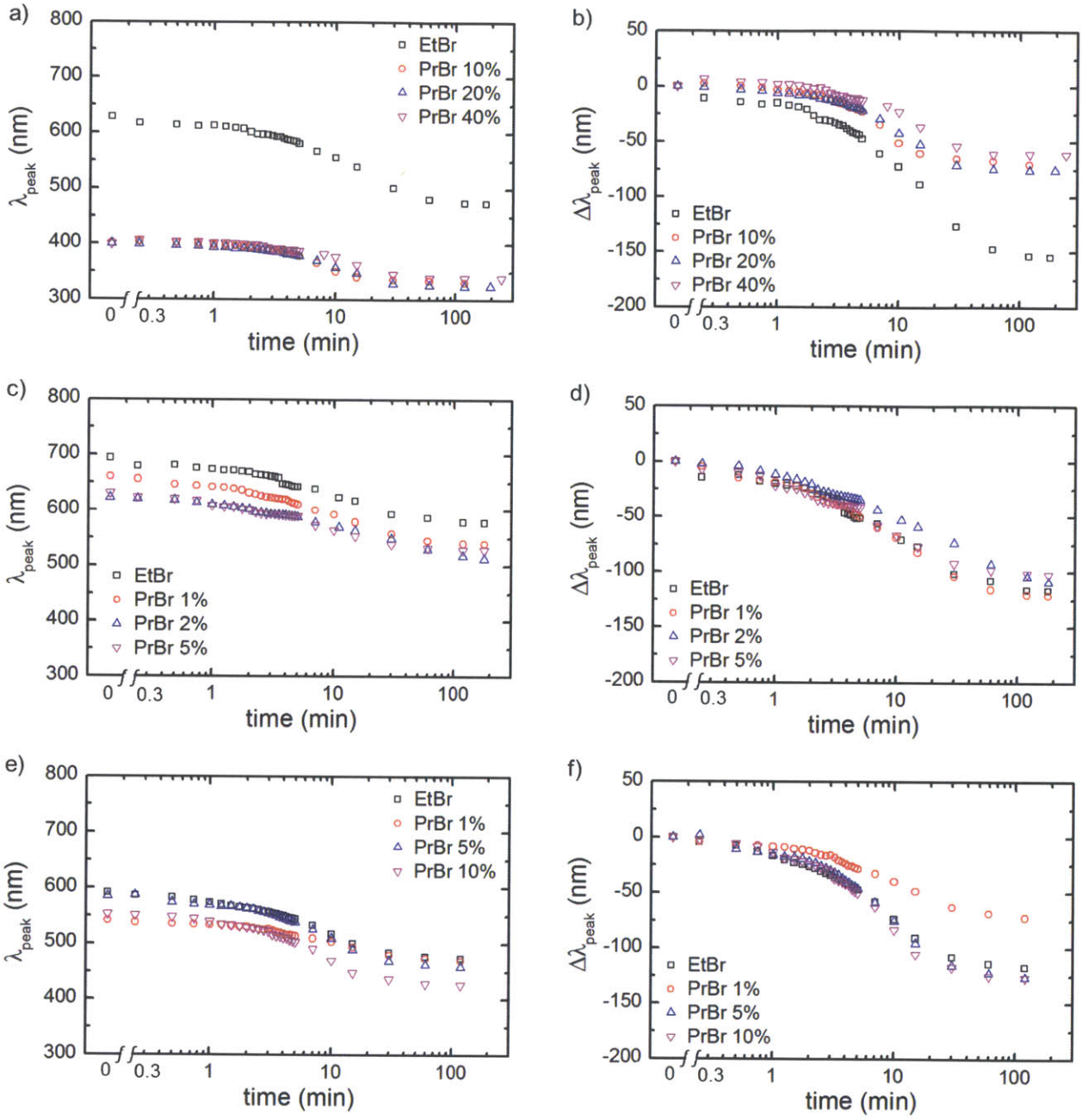

Figure 5.10. Reflectivity peak wavelengths and peak shifts of PS-QP2VP photonic gels quaternized with EtBr/PrBr mixtures swelling in 1 % BSA solutions in 10 mM pH 9 tris buffer after soaking in the same buffer solution for 10 min. The percentages in the legends are the mole fractions of PrBr in the reagents and all reaction mixtures contain 10 volume %

the reagents and 90 % heptane solvent. The reactions are carried out in three sets: a) and b); c) and d); and e) and f).

The mole fraction range of PrBr in EtBr in which the photonic responses are sensitive to the addition of PrBr is therefore likely between 5 % and 10 %. The third set uses 0, 1 %, 5 %, and 10 % PrBr in EtBr and covers the 5 % to 10 % range. The 1 % sample appears to be an outlier while the other three overlap. The 10 % sample of this set is not consistent with the one in the first set. The result from this set also contradicts the hypothesis in the last paragraph that the high sensitivity regime is between 5 % and 10 %. This variability is probably due to the poor reproducibility of the quaternization reactions and the non-uniformity of the quaternized BCP films. The quaternization reaction in the annealed PS-P2VP films occurs in the P2VP layers only, which are swollen in the bromide/heptane solution. At the beginning of the reaction (zero conversion), the distribution of the bromide in the BCP film may be non-uniform due to the presence of defects. As the reaction proceeds, the P2VP turns into a polycation that has a lower solubility in the reaction mixture due to the polymer's increased polarity. The partition of the bromide inside or outside the BCP film depends on the local conversion of the film, and therefore the initial non-uniformity may be amplified during the process of the reaction. It is normal for the conversion of an organic chemistry reaction to vary by 10 %, so the variation can be even larger for the reaction conversion in the lamellar BCP films. The observations suggest that the QP2VP hydrophobicity tuned via replacing ethyl with propyl only has a weak impact on the photonic responses of the PS-QP2VP gels so that the variability in the quaternization reactions and BCP films governs the comparison between the samples.

5.3.3. **Crosslink density**

The photonic responses of the PS-QP2VP gels in protein solutions are related to the diffusion of the proteins into the gel layers, which depends on the size of the protein and the pore size of the gel layers. The latter can be tuned via the crosslink densities of the QP2VP block. We add a *difunctional* bromide DBH as an additive to the quaternization reagent EtBr to quaternize and crosslink the P2VP block. Besides changing the average pore size, crosslinking also decreases the swelling ratios of the QP2VP gel layers, which can be observed from the systematic blue-shift of the photonic gel's structural color with increasing DBH additive content. Only a relatively small amount of DBH needs to be added before the photonic gel's reflectivity peak drops below 300 nm and becomes undetectable. Here we use 0, 0.5 %, 1 %, and 2 % DBH by mole fraction in the reagents and 10 volume % of EtBr/DBH mixture reagents in heptane to quaternize and crosslink the P2VP block in the cast and solvent annealed lamellar PS-P2VP films. The reactivity of the bromides is assumed to be constant in the different EtBr/DBH mixtures because of the low amounts of DBH. Thus, PS-QP2VP films quaternized with EtBr/DBH mixtures of higher DBH fraction have higher crosslink densities.

As expected, the equilibrium swelling ratios of the QP2VP gel layers in the buffer solution decrease with increasing DBH fraction and QP2VP crosslink density, thus the $\lambda_{peak} \sim t$ curves in Figure 5.11a start at lower wavelengths as the DBH fraction increases. The peak shifts plotted in Figure 5.11b show that the uncrosslinked sample quaternized just by EtBr shifts the most while the three crosslinked samples have almost overlapping $\Delta\lambda_{peak} \sim t$ curves. Increased DBH fractions result in slight decreases of the magnitudes of the reflectivity peak shifts, suggesting a consistent trend that crosslinking restricts the photonic gel's responses to protein solutions. The gap between the EtBr and 0.5 % DBH samples in Figure 5.11b indicates a regime of DBH

fraction below 0.5 % when the photonic responses are the most sensitive to QP2VP crosslink density.

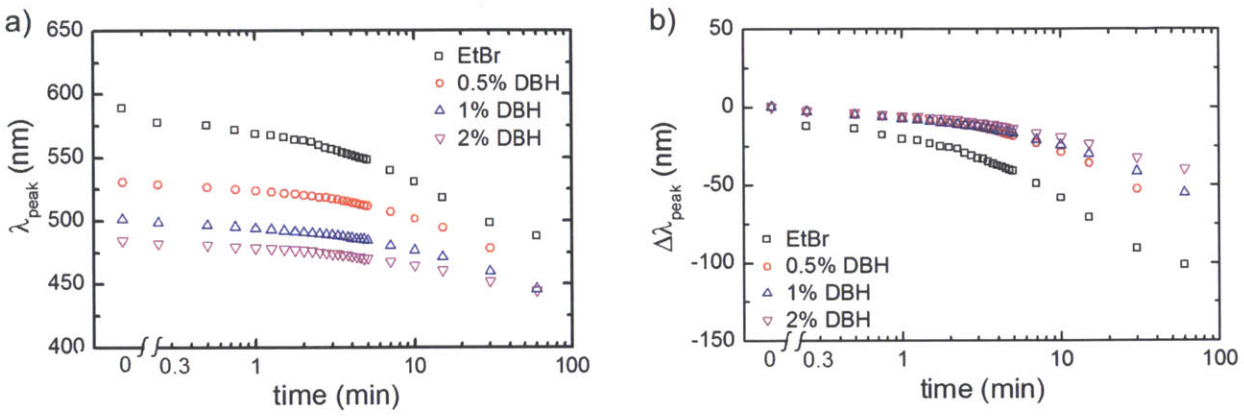

Figure 5.11. Reflectivity peak wavelengths and peak shifts of PS-QP2VP photonic gels quaternized with EtBr/DBH mixtures swelling in the 1 % BSA solution in 10 mM pH 8 tris buffer after soaking in the same buffer solution for 10 min.

5.4. *Protein solution parameters*

5.4.1. **Charge**

Two model proteins are used to study the effects of protein charges via varying the solution pH. The pIs of BSA and trypsin are 5.3 and 10, respectively. In aqueous solutions of pH 7, 8, and 9, BSA has negative charges while trypsin has positive charges. The photonic responses represented by the reflectivity peak wavelengths and peak shifts as a function of swelling time in the BSA and in the trypsin solutions are shown in Figure 5.12 and Figure 5.13.

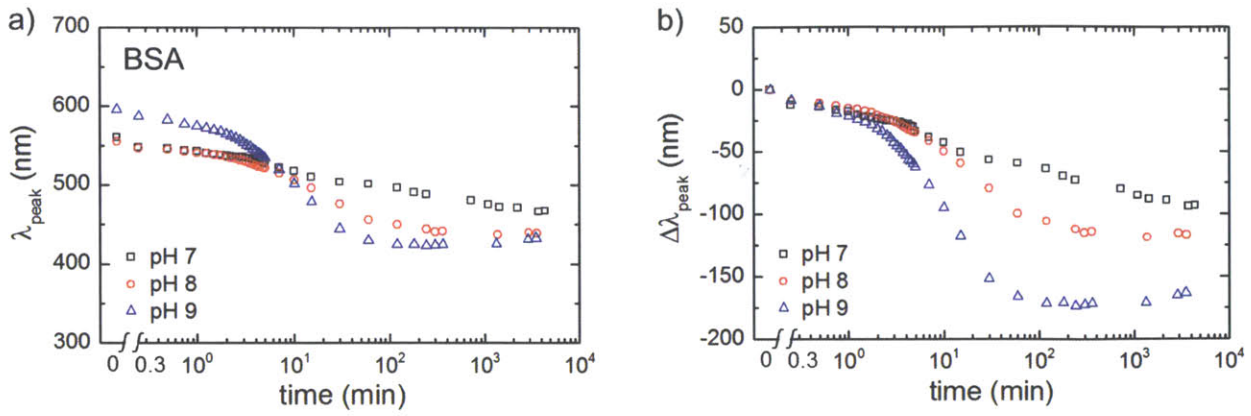

Figure 5.12. Reflectivity peak wavelengths and peak shifts of PS-QP2VP photonic gels swollen in 1 % BSA solutions in 10 mM tris buffer of pH 7, 8, and 9 after soaking in the corresponding buffer solutions for 10 min. All the BCP films are from the same batch of quaternization reaction with EtBr for 3 days.

BSA is negatively charged at all the three pHs and when the tris buffer swollen films are exposed to BSA with pH 7 to 9, the photonic gels' reflectivity blue-shifts. The blue-shifts are probably caused by the formation of coacervates between BSA and the QP2VP polycation. Increased pH results in more negative charges on the BSA and blue-shifts that are faster and higher in magnitude (see Figure 5.12b), which may suggest a stronger tendency of coacervate formation. The difference in the start points in Figure 5.12a is probably due to the variability of defect content and quaternization conversion in the BCP films, and the slight red-shifts at $t > 10^3$ min for pH 8 and 9 may result from BSA degradation after the long testing time at room temperature.

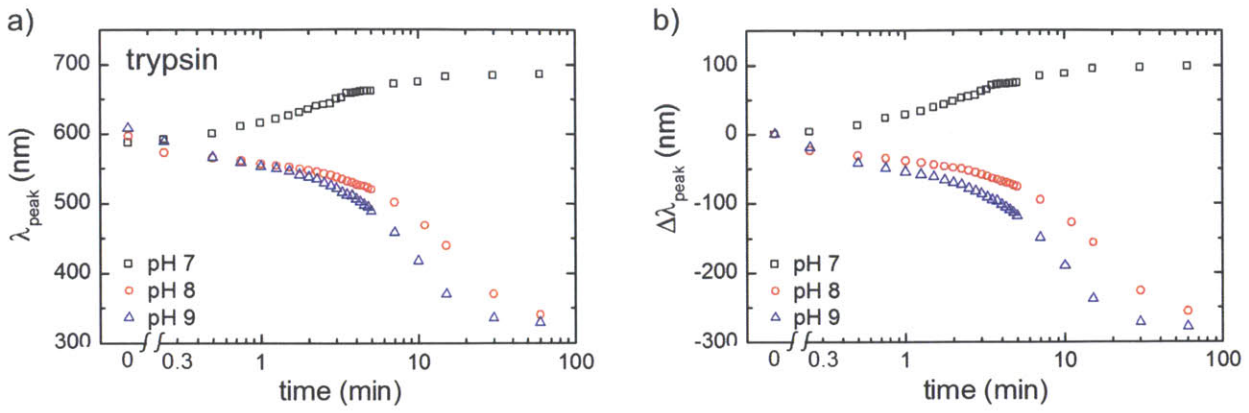

Figure 5.13. Reflectivity peak wavelengths and peak shifts of PS-QP2VP photonic gels swelling in 1 % trypsin solutions in 10 mM tris buffer of pH 7, 8, and 9 after soaking in the corresponding buffer solutions for 10 min. The BCP films are from the same batch of quaternization reaction with EtBr for 3 days.

According to its pI, trypsin should be positively charged at all the three pHs. Interestingly, the photonic gel's reflectivity red-shifts in the pH 7 solution and blue-shifts in the pH 8 and 9 solutions. The start points of the three curves in Figure 5.13 are close so the variability of BCP films can be neglected. The results indicate that the positively charged proteins may result in red-shifts of the photonic gel's reflectivity by electrostatic repulsion with the the QP2VP polycation and can also form coacervates and lead to blue-shifts. Figure 5.13b shows that the reflectivity peak shifts of the photonic gels in different pH solutions at the same swelling time have decreased numerical values as the solution pH increases, which is consistent with the results of the BSA solutions (Figure 5.12b). This observation suggests that there may be a general form for the correlation between the BCP gel's photonic responses and the protein's charges varied by the solution pH. We attempt to address this hypothesis in Section 5.4.2 by comparing more proteins.

5.4.2. **Charge and size**

The sizes of the proteins cannot be altered independently of the pI or charges due to the limited choices of commercially available and affordable proteins. Therefore, we select five proteins (see Table 5.1) and study the effect of charge and size as a combined parameter on the photonic responses of the BCP gels.

Figure 5.14 and Figure 5.15 show the photonic responses of the PS-QP2VP films quaternized with EtBr for 3 days swelling in the tris buffer solutions of the five proteins. Figure 5.14 groups the results by the solution pH to compare the proteins and Figure 5.15 groups the results by the protein species to compare the solution pH. The proteins are ordered by the peak shifts they result in in pH 7 tris buffer solutions (Figure 5.14b), which is roughly the same with the order of their pIs except for lysozyme and trypsin.

The photonic responses of the PS-QP2VP gels in the different protein solutions are different. The gels show different structural colors in the various protein solutions. Photos of the gel samples and the applications of the color difference will be discussed in Section 5.5.

Of the five proteins explored, trypsin has the most sensitive dependence on pH, and amylase is almost pH insensitive within the 1 hour swelling time. RNAse solutions in pH 8 and 9 show very fast responses within 15 seconds, which may result from the small size of the RNAse (molar weight 13.7 kDa). The pH dependence of each protein is consistent with the hypothesis in Section 5.4.1 that the photonic gels reflectivity peak wavelengths in protein solutions decrease with increase in the solution pH. The pH 8 curves in c), d), and e) of Figure 5.15 are lower than the pH 9 curves probably due to the variability in the quaternization degrees of the BCP films.

The slight variations in the peak wavelengths of the gels in the buffer solutions are likely caused by counterion exchange or experimental errors.

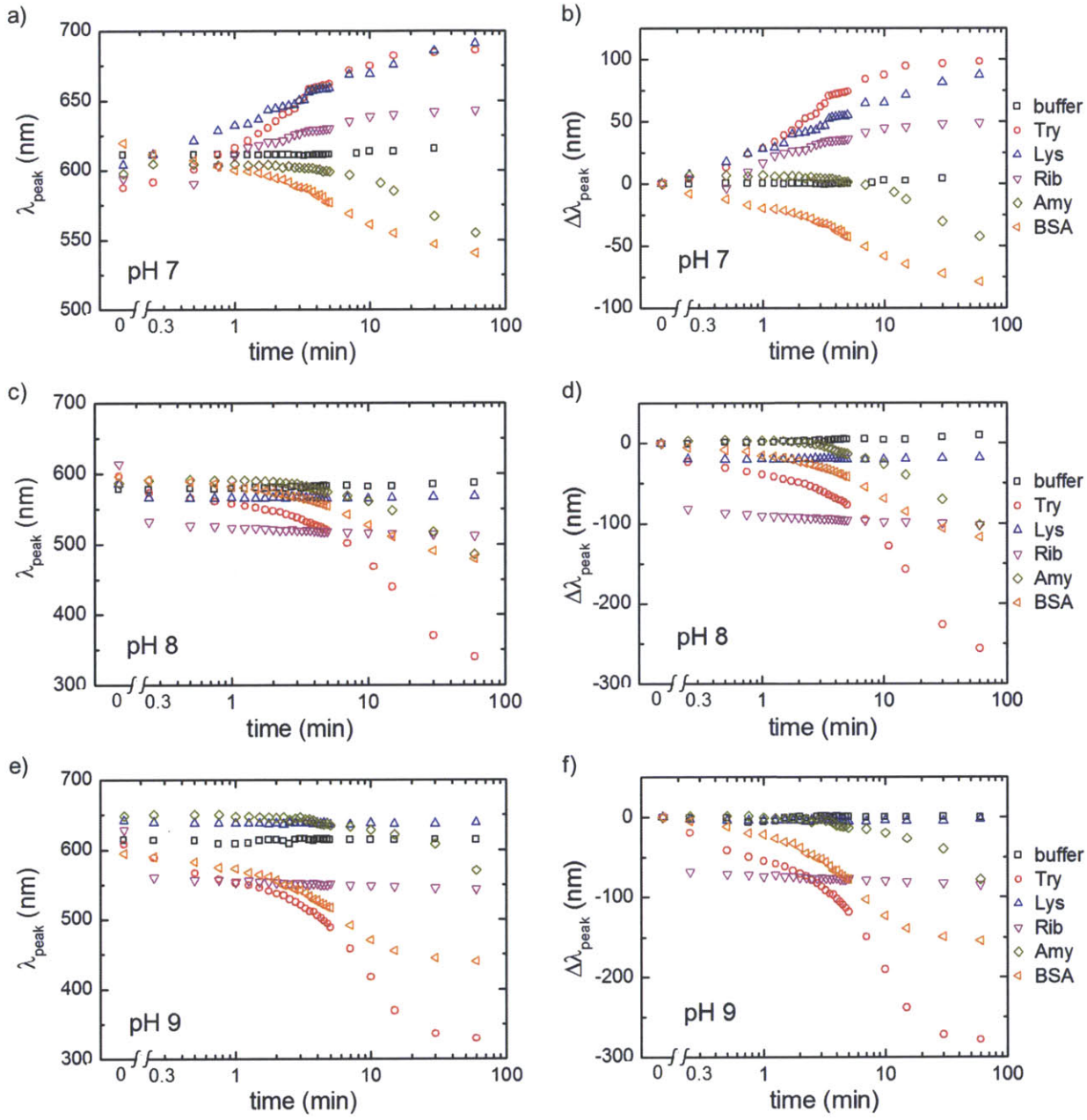

Figure 5.14. Reflectivity peak wavelengths (a, c, e) and peak shifts (b, d, f) of PS-QP2VP photonic gels swelling in 1 % protein solutions in 10 mM tris buffers at pH 7, 8, and 9 after

soaking in the corresponding buffer solutions for 10 min. The proteins are ordered by the positions of the curves in b) and represented by the same set of symbols throughout.

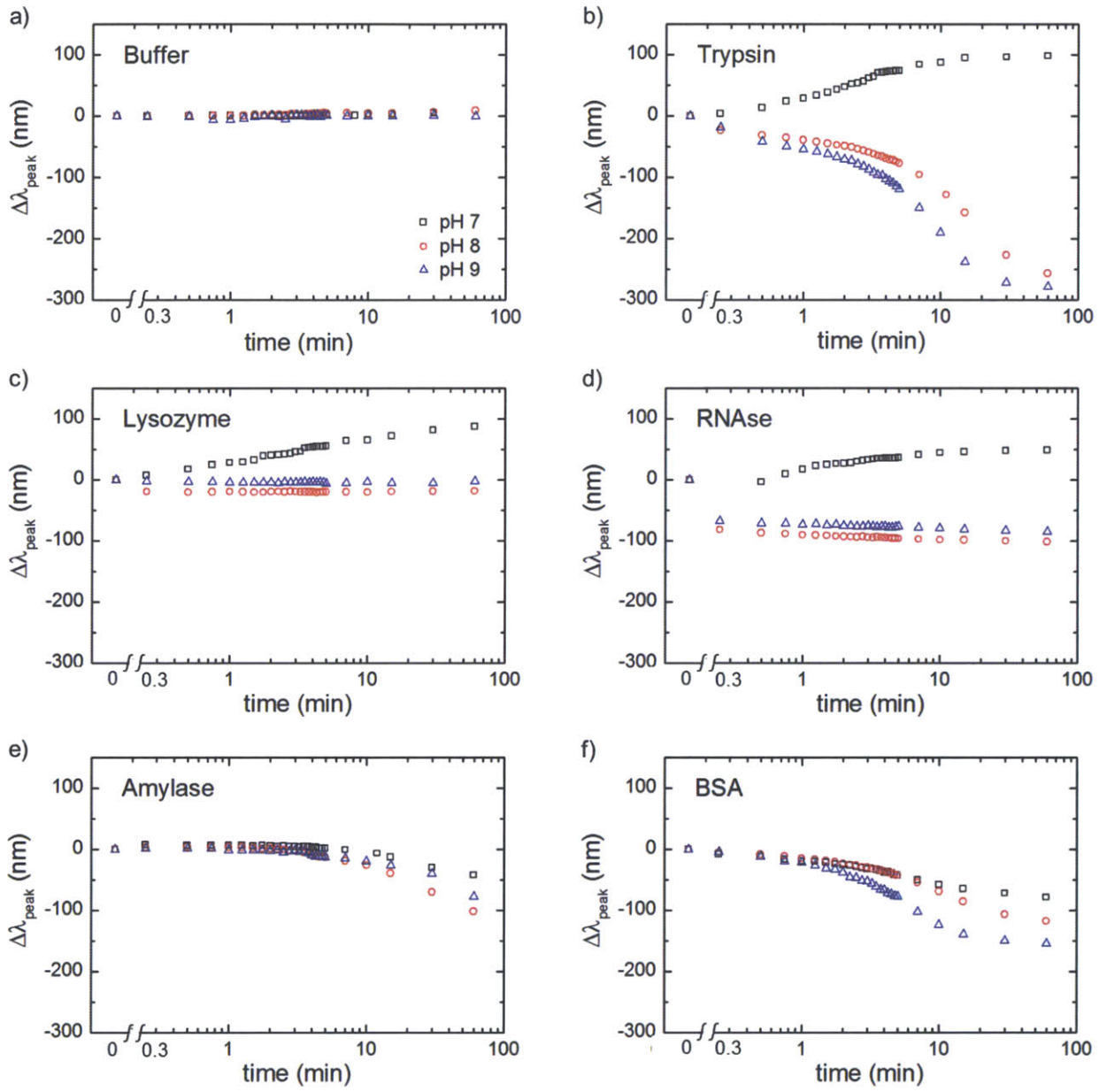

Figure 5.15. Reflectivity peak shifts of PS-QP2VP photonic gels swelling in 10 mM tris buffers or 1 % trypsin, lysozyme, RNAse, amylase, and BSA solutions at pH 7 (black), 8 (red), and 9 (blue) after soaking in the corresponding buffer solutions for 10 min.

The charge and size of the proteins need be quantified for further studies into the correlation between the photonic responses and protein solution properties. The protein sizes can be given in the form of hydrodynamic radii by dynamic light scattering (DLS) and the charges by ζ potentials of the protein solutions. Satisfactory ζ potential measurements have not been achieved so far, so the theoretically calculated charges are presented here.

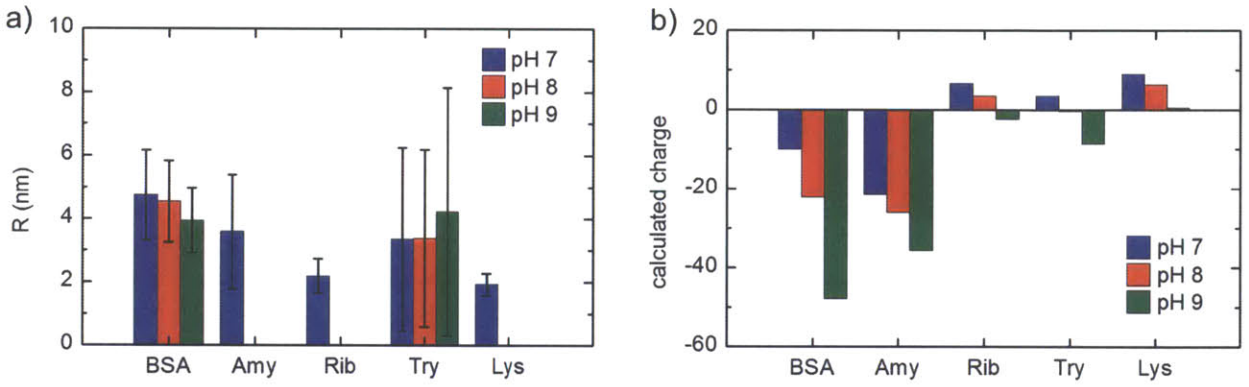

Figure 5.16. Sizes and charges of BSA, amylase, RNAse, trypsin, and lysozyme in 10 mM tris buffers at pH 7, 8, and 9. a) Hydrodynamic radii measured by DLS; b) charges calculated using the amino acid sequence of the proteins and the calculator at http://www.scripps.edu/~cdputnam/protcalc.html.

In general, the photonic responses are expected to be slower in solutions of proteins that are bigger in size due to the diffusion mechanism. However, it is not fair to compare the rate of peak shifts without considering the charges of the proteins, as Section 5.4.1 has shown that the rates of photonic responses to the solutions of a single protein depend on the pH. In addition, the reflectivity peaks data in Figure 5.14 and Figure 5.15 are not sufficient for the comparison between the different protein solutions because not all cases have reached steady state by the end of the tests. Longer tests and solutions of pH around the proteins' pIs are needed in the future.

5.5. *Multiplex protein assay*

The photonic responses of PS-QP2VP films in protein solutions can be used to differentiate proteins. The differentiation effect can be optimized for a group of proteins based on their sizes and pIs by tuning the protein solution's pH and the BCP film's charge density, hydrophobicity, and crosslink density. The photos in Figure 5.17 show the different colors of the PS-QP2VP gels in the five protein solutions of pH 7, 8, or 9. The BCP films are quaternized with EtBr for 3 days. The photos are taken after overnight exposure to 1 % protein solutions in 10 mM tris buffer, and therefore the colors are characteristic of the protein charges. Short-time responses can give more information about the size contrast of the proteins.

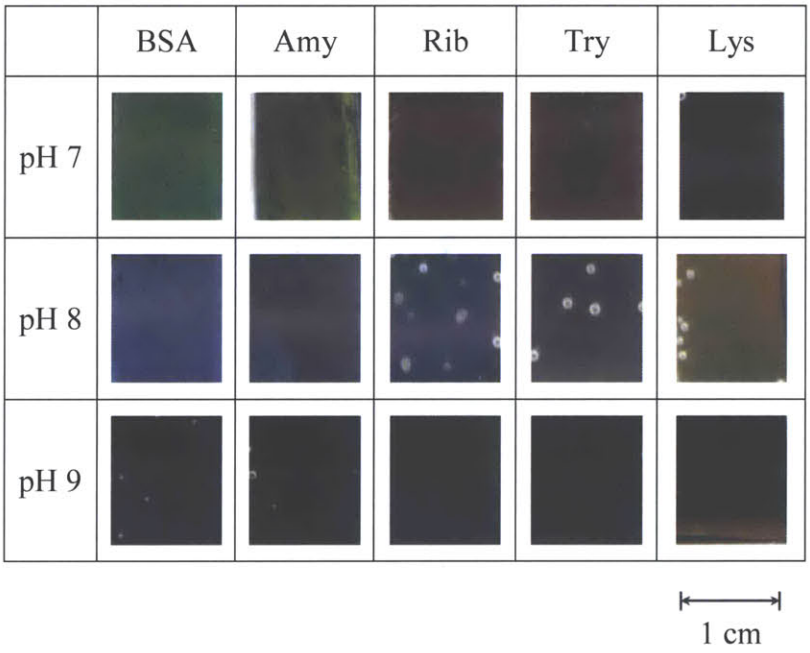

Figure 5.17. Photos of PS-QP2VP photonic gels after soaking in 1 % protein solutions in 10 mM tris buffer overnight. The BCP films were quaternized with EtBr solution (10 % in heptane) at 50 ˚C for 3 days. White spots are bubbles in the protein solutions.

5.6. *Summary and future work*

Lamellar BCP photonic gels that are responsive to protein solutions can be made by quaternizing the P2VP block in annealed PS-P2VP films with mono- and di-bromides. The structural colors of the PS-QP2VP gels are triggered by the swelling/deswelling of the QP2VP polycation gel block in solutions of positively or negatively charged proteins. Both blue-shifts and red-shifts of the photonic gels' reflectivity in protein solutions compared to the equilibrium swelling states in buffer solutions have been observed. The direction and degree of the peak shifts depend on the charge density, hydrophobicity, and crosslink density of the QP2VP gel block in the BCP films. The charge and size of the protein and the solution pH also affect the photonic responses.

The results presented in this chapter suggest that the BCP photonic gels with a polyelectrolyte block can be used for visual detection and differentiation of proteins or other charged biomolecules. This method has a broad range of tunabilities including the material parameters of the lamellar BCP films and the solution parameters of the proteins, which can be adjusted for optimized differentiation of specific proteins.

This topic has many interesting directions to be further explored. The quaternization reaction setup and conditions of the PS-P2VP films need be optimized so that the conversions of all films in the same batch are uniform. Additional quaternization reagents and their effects on the photonic responses can be examined, e.g. benzyl bromide for its bulky phenyl group and 2-bromoethanol for the additional hydrophilicity from the hydroxyl group. For ideal comparisons of quaternization reagents or crosslink densities, the quantitative conversions of the pyridines should be constant, which requires kinetics studies on the quaternization reactions with the various reagents or reagent mixtures and the quantitative conversion of P2VP. FT-IR on the

scrapped-off films can be used to quantify the P2VP conversion (ATR on the films does not work well due to surface roughness). So far all reagent series are compared on the basis of equal reaction times. It is also interesting to fabricate films with gradient quaternization degree or crosslink density that can display colors that vary with the position in the film.

If the choice of the BCP is not limited, lamellar BCP gels with a polyanion gel block are also interesting systems that may interact with the proteins in a different (or opposite) way, thus providing additional tunability or differentiation ability of the BCP photonic gels to proteins. The challenge is to cast and anneal the BCP film to achieve the lamellar ordering that is sufficient for the photonic effects. A common solvent is necessary for the film casting and annealing steps. Since it is difficult to find a common solvent for PS and a polyelectrolyte (especially when the charge density is high), converting a neutral block into a polyelectrolyte after solvent vapor annealing is preferred. Therefore, innovative chemistry that converts a neutral polymer into a polyanion is needed for the oppositely charged BCP photonic gel – protein solution interaction studies.

Homopolymer QP2VP gels are good reference systems for the protein-QP2VP interactions. Chemically crosslinked QP2VP gels can be made by crosslinking linear P2VP with dibromides such as DBH. The homopolymer gels will be soaked in buffer solutions and then transferred into protein solutions. Similarly to Chapter 4, the swelling ratios of the homopolymer gels can be measured and compared to the BCP gels.

Additional characterizations of the proteins are needed as well. Test conditions of DLS or ζ potential need be optimized to fit the size and charge range of the proteins. The error bars in Figure 5.16a are quite wide and the size ratios of the proteins measured by DLS are not

consistent with their molar weights (see BSA and trypsin). Figure 5.18 shows the current or ζ potential results that are clearly problematic because some data at pH 9 are higher than those at pH 7. The difficulty may result from the low charge densities on the proteins especially near the transition between positive and negative electrostatic potentials. It is also important to make sure that no air bubbles are present in the test solution for both DLS and ζ potential experiments.

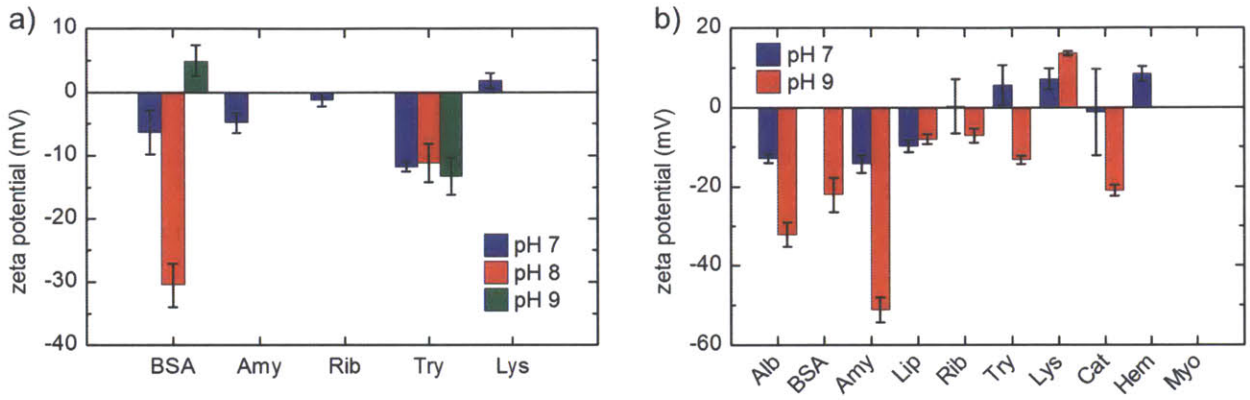

Figure 5.18. ζ potentials of the protein solutions in 10 mM tris buffers. a) Measurements with 0.1 % protein solutions filtered with 0.2 μm cellulose filters; b) measurements with 1 % protein solutions. Additional proteins shown in b) are chicken egg white albumin (Alb), lipase from *Rhizopus niveus* (Lip), catalase from bovine liver (Cat), hemoglobin from bovine blood (Hem), and myoglobin from equine skeletal muscle (Myo), all purchased from Sigma.

Protein stability is a concern in long-time photonic measurements and should be checked with tests before and after the photonic measurements with methods specifically designed for the protein in accordance to its degradation mechanism. For example, BSA forms dimers in solution so its degradation can be monitored by size data from DLS. To prevent protein degradation or structural change, refrigerated experimental conditions (e.g. 4 ˚C) are desired. The optical constants and diffusion coefficients at the test temperature need be used for calculations.

More systematic studies on the effect of protein charge and size can be conducted by modifying a model protein rather than by using different proteins in the current approach. Synthetic macromolecules can be covalently bonded to protein surfaces to alter the size without changing the pI or charge in certain buffer solution. The pI and charge of a protein can be varied independently of the size by genetic engineering to substitute certain amino acids in the protein sequence.

The coacervation effect has been previously used for enzyme immobilization and protein delivery, separation, and purification.[7] If the activity of an enzyme can be retained after binding to the polyelectrolyte block, the enzyme-BCP photonic gel may change its structural color during the reaction that the enzyme catalyzes due to a change of the structure or charge of the enzyme or the solution pH etc. Thus, the enzyme-lamellar BCP hybrid gels can be used as photonic indicators for enzymatic reactions. The first step is to test if the enzyme's activity is retained after its binding into the PS-QP2VP gels. The testing method depends on the function of the protein. Enzymes can be tested by the detecting the products of the reactions they catalyze when the PS-QP2VP/enzyme gel films are soaked into the reactant mixtures. If the enzyme's activity is related to its structure, the activity may be tested by the absorption peak in UV-Vis.

In addition to proteins, other charged biomolecules such as polysaccharides and DNAs may have ionic interactions with the QP2VP block and result in photonic responses. The solution properties of these molecules are different from proteins which may add variables to the responsive biomolecule/BCP photonic gel topic. The challenge is that in the experiment setup so far, a minimum of 20 mg biomolecule (2 mL 1 weight % solution is needed to fill the 1 cm path-length cuvette to 2 cm height as required by the spectrometer setup) is needed to test the

photonic responses, which may be an amount difficult to obtain or too costly for certain biomolecules.

Diffusion models are needed to explain the photonic responses of the PS-QP2VP gels in protein solutions. The time-dependent swelling ratios of the QP2VP/protein gel layers can be calculated using TMM (see Chapter 2 for details). Transport of the solvent in or out of the gel layers can be calculated based on the swelling ratio data. The diffusion of protein into the BCP is the cause of the gel swelling or deswelling but also depends on the gel layer's swelling ratio. The mass transport model should consider the diffusion of proteins and other ionic species (the Br^- and Cl^- counterion, tris and protonated tris, H_2O H^+ and OH^-) into the gel layers driven by the osmotic pressure and the charge equilibrium, and diffusion of water in or out of the gel layers due to the thermodynamic equilibrium concentration of the proteins in the QP2VP gel.

References

1. Kang, Y.; Walish, J. J.; Gorishnyy, T.; Thomas, E. L. *Nat. Mater.* **2007**, *12*, 957-960.

2. Walish, J. J.; Kang, Y.; Mickiewicz, R. A.; Thomas, E. L. *Adv. Mater.* **2009**, *30*, 3078-3081.

3. Chan, E. P.; Walish, J. J.; Thomas, E. L.; Stafford, C. M. *Adv. Mater.* **2011**, *40*, 4702-4706.

4. Walish, J. J.; Fan, Y.; Centrone, A.; Thomas, E. L. *Macromol. Rapid Commun.* **2012**, *18*, 1504-1509.

5. Lim, H. S.; Lee, J.; Walish, J. J.; Thomas, E. L. *ACS Nano* **2012**, *10*, 8933-8939.

6. Fan, Y.; Walish, J. J.; Tang, S.; Olsen, B. D.; Thomas, E. L. *Macromolecules*, Article ASAP.

7. Cooper, C. L.; Dubin, P. L.; Kayitmazer, A. B.; Turksen, S. *Current Opinion in Colloid & Interface Science* **2005**, *1–2,* 52-78.

8. Kayitmazer, A. B.; Bohidar, H. B.; Mattison, K. W.; Bose, A.; Sarkar, J.; Hashidzume, A.; Russo, P. S.; Jaeger, W.; Dubin, P. L. *Soft Matter* **2007**, *8,* 1064-1076.

9. Seyrek, E.; Dubin, P. L.; Tribet, C.; Gamble, E. A. *Biomacromolecules* **2003**, *2,* 273-282.

6. Summary and Future Work

This chapter summarizes the research work in this thesis and points out some future directions. The future works listed build on the summary sections of Chapters 3, 4, and 5.

6.1. *Summary*

This thesis studies the photonic responses of lamellar block copolymers gels. The gels are made by selectively swelling one block in the lamellar PS-P2VP films and the photonic responses are driven by the swelling/deswelling of the gel block in response to various types of stimuli. The stimuli explored in this thesis are temperature, co-solvent quality, and protein solutions.

The photonic gels can display two types of temperature responses. The PS-P2VP/acetic acid photonic gels show blue-shifts in reflection color at increased temperatures that can be tuned by the acid concentration (see Figure 6.1).[1] The PS-P2VP/cyclohexane photonic gels show red-shifts with increased temperature and the temperature responses can be tuned by choice of the BCP molecular weight. The temperature responsive photonic gels can be applied as sensing, smart display, and coating materials.

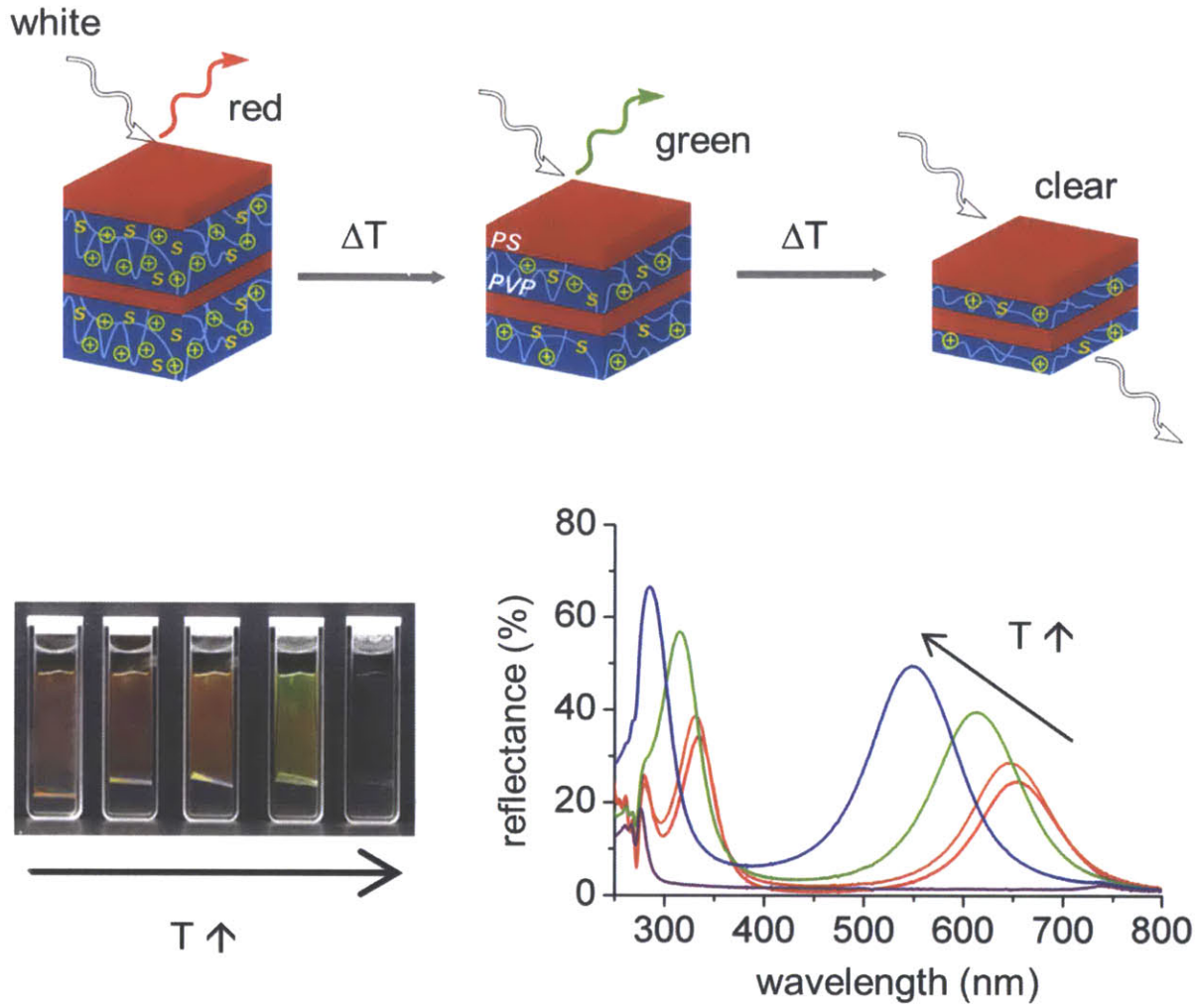

Figure 6.1. Schematic, photos and reflective spectra of the temperature-responsive PS-P2VP/acetic acid photonic gels.

The photonic gels are also responsive to the composition of alcohol-water co-solvents (see Figure 6.2).[2] A model based on Flory-Huggins mixing and line defect network strain energy quantitatively relates the photonic gel's reflectivity to the Flory-Huggins interaction parameter χ between P2VP and the co-solvent and the average defect density. The results indicate that the edge and screw dislocation line defects in lamellar self-assembly serve to create an interconnected network of glassy PS layers that limit the selective swelling and hence the

photonic response. The co-solvent quality responsive photonic gels provide a method to measure the Flory-Huggins χ parameter and the defect density in the lamellar BCP film.

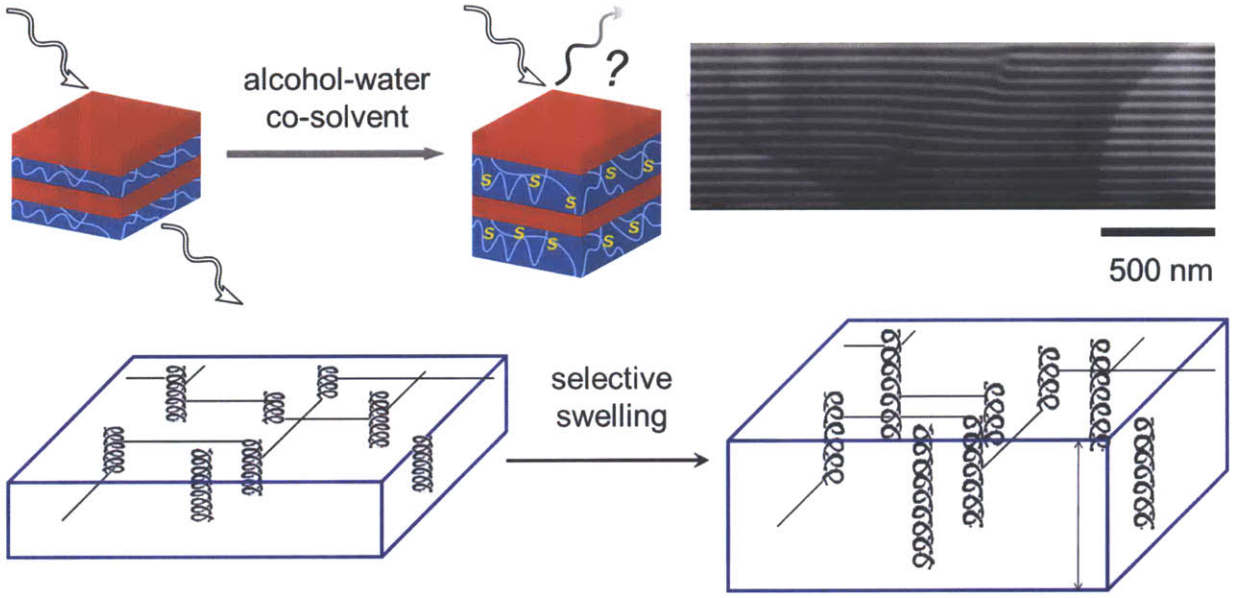

Figure 6.2. Schematics of the two designs for temperature-responsive photonic gels that show a) blue-shift and b) red-shift in reflectivity at increased temperatures. "S" indicates the solvents.

The photonic gels are responsive to protein solutions (see Figure 6.3). The reflectivity peak shifts depend on the charge density, hydrophobicity, and crosslink density of the quaternized P2VP gel block as well as the charge and size of the protein and the solution pH. The results suggest that the photonic gels can be used for visual detection and differentiation of proteins or other charged biomolecules.

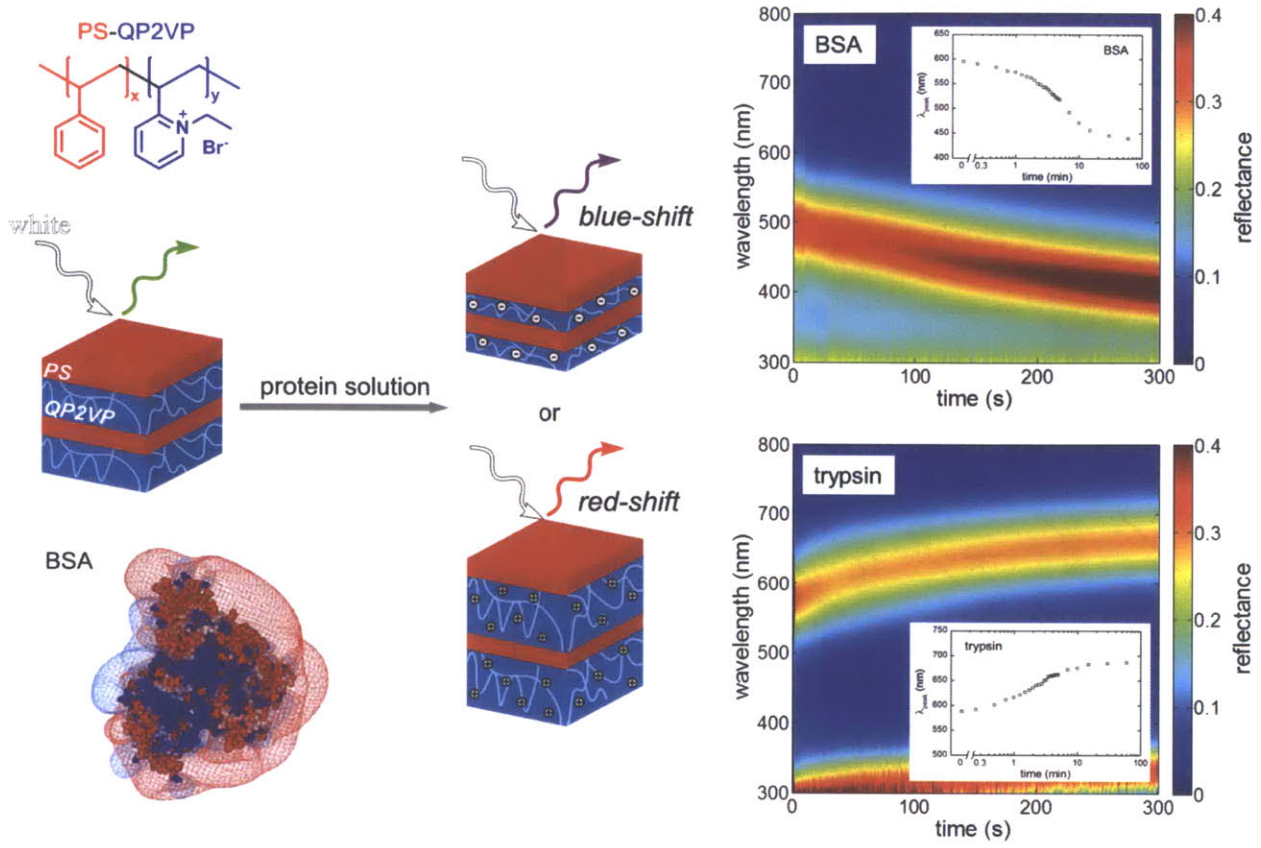

Figure 6.3. Schematics of the two designs for temperature-responsive photonic gels that show a) blue-shift and b) red-shift in reflectivity at increased temperatures.

In summary, the key contributions of this thesis on the stimuli-responsive PS-P2VP photonic gels include the development of two types of temperature-responsive photonic gels, quantitative modeling of the steady-state swelling, and preliminary experiments on the dynamic swelling of the BCP gels in protein solutions. The thesis work suggests many interesting topics to study in the future, such as processing conditions and microstructure of the lamellar BCP films, binding and release of biomolecules in the photonic gels, etc. The major challenge in the lamellar BCP photonic gel studies is film processing and reproducibility. Suggestions for future work are listed in Sections 6.2 to 6.5.

6.2. *Microstructure characterization*

As shown in Chapter 4, defects in the lamellar BCP films have significant impacts on the reflection colors of the photonic gels. More detailed structural characterization of the films is necessary for further studies on the photonic gels.

Tools that can be used to characterize the microstructures of the dry lamellar BCP films include TEM and FIB-SEM. The latter is more efficient because successive cross-sectioning can be performed at the same time along with the secondary electron imaging. A large number of sequential cross-sections from the same film can yield a detailed 3D picture of the dislocation network. Many such 3D reconstructions should be done for the statistical analysis of the defect networks. Parameters to be surveyed include the types, geometry, density, and distribution of the screw and edge dislocations in the lamellar BCP films as a function of film processing condition, BCP molecular weight, and film thickness. Fluorescent dyes may be added and laser scanning confocal microscope may be a good method to image the defect structure.[3]

Thus far the swelling ratios of the P2VP block in the BCP gels have only been calculated from the photonic properties using TMM. We assume that the thickness and refractive index of PS are constant during swelling and calculate the thickness and refractive index of the P2VP gel layers by the P2VP swelling ratios in the TMM model. *Direct imaging* of the layers in the BCP gels can provide evidence about the swollen structure and thus directly assess the TMM analysis and the swelling models. Possible tools include cryo-SEM/TEM, confocal STED microscopy, and ionic liquid swelling.[3, 4] A quartz-crystal microbalance can be used to measure the weight increase caused by swelling that can be used to calculate the P2VP layer swelling ratios.

6.3. *Thin film preparation*

Effective control over the defect structure of the PS-P2VP films is desired for reproducible photonic responses.

During film preparation, film thickness is determined in the film casting step. The free surface (film-air interface) is shaped at the same time but may change during annealing. The annealing step is essential for defect control. Vapor of a common solvent of the blocks is used to swell the film and increase the chain mobility. The solvent vapor pressure needs be high enough so that the BCP has enough mobility to self-assemble into the lamellar morphology parallel to the substrate surface, but not be too high otherwise solvent condensation may occur and the film may be locally dissolved. Vertical pores often form due to solvent condensation. By adjusting the temperatures of the film and the annealing chamber (separately if possible), solvent vapor condensation and the vertical pore defects can hopefully be eliminated. The formations of screw and edge types of dislocations are likely functions of kinetic factors such as annealing temperature and time.

Another approach to study the role of defects is to introduce designed defects that dominate the kinetics and equilibrium of the swelling/deswelling of the photonic gels. Chemically or physically patterned substrates can be used to induce defects during film casting and annealing. Holes can also be introduced to the annealed films by mechanical forces (e.g. to punch the film with needles) or laser burning (e.g. two-photon direct-write lithography). One defect every 1 ~ 10 μm^2 or a square lattice of 1x1 ~ 3x3 μm is a promising regime for the density of the induced defects since the distance between dislocations is estimated as ~ 2 μm in Chapter 4.

6.4. *Temperature responsive photonic gels*

Other acids can be used to make photonic gels with the lamellar PS-P2VP. Counterion species plays an important role to the photonic gel's properties.[5] Strong acids such as hydrochloric acid can be used to compare the effect of acidity and counterions. Sulfuric acid and phosphoric acid or other multivalent acids are good solvents to study the effect of counterion valency.

More experiments on the PS-P2VP/cyclohexane photonic gels are needed. The quaternization or crosslinking reactions need be optimized so that the P2VP swelling is suppressed while the PS swelling is not restricted. High molecular weight BCPs are preferred in order to achieve reflections in the NIR regime.

Ionic liquids may be used to make temperature responsive photonic gels by selectively swelling lamellar PS-P2VP films. The phase behaviors of PS-P2VP diblock copolymers in ionic liquids have been studied.[6-10] Several ionic liquids show UCST type behavior for P2VP and low solubility for PS. Such ionic liquids are good solvent candidates to make photonic gels with red-shifts in reflectivity. BCP photonic gels have been made from PS-P2VP and ionic liquids[4] and the temperature responses are worth exploring.

BCPs such as poly(styrene-*b*-*N*-isopropylacrylamide) (PS-PNIPAM) and poly(styrene-*b*-methyl methacrylate) (PS-PMMA) may be interesting to explore as well. The gels of PS-PNIPAM swollen in water may show dramatic blue-shifts at increased temperatures because of the sharp LCST transitions of PNIPAM in water.[11] PMMA also has a UCST in methanol[12] so PS-PMMA/methanol gels may show red-shifts in reflectivity at increased temperatures.

6.5. *Protein/biomolecule responsive photonic gels*

Additional quaternization reagents and their effects on the photonic responses of the quaternized PS-P2VP films can be explored. For example, benzyl bromide can be used as a bulkier substituent and 2-bromoethanol may increase the hydrophilicity with its hydroxyl group. For ideal comparisons of quaternization reagents or crosslink densities, the quantitative conversions of the pyridines should be constant, which requires kinetics studies on the quaternization reactions with the various reagents or reagent mixtures and the quantitative conversion of P2VP. FT-IR on the scrapped-off films can be used to quantify the P2VP conversion (ATR on the films does not work well due to surface roughness). So far all reagent series are compared on the basis of equal reaction times. It is also interesting to fabricate films with gradient quaternization degree or crosslink density that can display colors that vary with the position in the film.

If the choice of the BCP is not limited, lamellar BCP gels with a polyanion gel block are also interesting systems that may interact with the proteins in a different (or opposite) way, thus providing additional tunability or differentiation ability of the BCP photonic gels to proteins. The challenge is to cast and anneal the BCP film to achieve the lamellar ordering that is sufficient for the photonic effects. The film samples can either be made by casting and annealing a BCP with a polyanion block, or by converting a neutral block in an annealed lamellar BCP film into a polyanion.

Homopolymer QP2VP gels are good reference systems for the protein-QP2VP interactions. Chemically crosslinked QP2VP gels can be made by crosslinking linear P2VP with dibromides such as DBH. The homopolymer gels will be soaked in buffer solutions and then transferred into

protein solutions. Similarly to Chapter 4, the swelling ratios of the homopolymer gels can be measured and compared to the BCP gels.

Additional characterizations of the proteins are needed as well. Test conditions of DLS or ζ potential need be optimized to fit the size and charge range of the proteins. The proteins' sizes are close to the lower limit of the DLS instrument and therefore difficult to measure. The difficulty in ζ potential measurements may result from the low charge densities on the proteins especially near the transition between positive and negative electrostatic potentials. It is also important to make sure that no air bubbles are present in the test solution for both DLS and ζ potential experiments. Protein stability is a concern in long-time photonic measurements and should be checked with tests before and after the photonic measurements with methods specifically designed for the protein in accordance to its degradation mechanism. To prevent protein degradation or structural change, refrigerated experimental conditions (e.g. 4 °C) are desired. The optical constants and diffusion coefficients at the test temperature need be used for TMM calculations.

More systematic studies on the effect of protein charge and size can be conducted by modifying a model protein comparing to by using different proteins in the current approach. Synthetic macromolecules can be covalently bonded to protein surfaces to alter the size without changing the pI. The pI and charge of a protein may be varied independently of the size by genetic engineering to substitute certain amino acids in the protein sequence.

The coacervation effect has been previously used for enzyme immobilization and protein delivery, separation, and purification.[13] If the activity of an enzyme can be retained after binding to the polyelectrolyte block, the enzyme-BCP photonic gel may change its structural color during

the reaction that the enzyme catalyzes due to a change of the structure or charge of the enzyme or the solution pH etc. Thus, the enzyme-lamellar BCP hybrid gels can be used as photonic indicators for enzymatic reactions. The first step is to test if the enzyme's activity is retained after its binding into the PS-QP2VP gels. The testing method depends on the function of the protein. Enzymes can be tested by the detecting the products of the reactions they catalyze when the PS-QP2VP/enzyme gel films are soaked into the reactant mixtures. If the enzyme's activity is related to its structure, the activity may be tested by the absorption peak in UV-Vis.

In addition to proteins, other charged biomolecules such as polysaccharides and DNAs may have ionic interactions with the QP2VP block and result in photonic responses. The solution properties of these molecules are different from proteins which may add variables to the responsive biomolecule/BCP photonic gel topic. The challenge is that in the experiment setup so far, a minimum of 20 mg biomolecule (2 mL 1 weight % solution is needed to fill the 1 cm path-length cuvette to 2 cm height as required by the spectrometer setup) is needed to test the photonic responses, which may be an amount difficult to obtain or too costly for certain biomolecules.

Diffusion models are needed to explain the photonic responses of the PS-QP2VP gels in protein solutions. The time-dependent swelling ratios of the QP2VP/protein gel layers can be calculated using TMM. Transport of the solvent in or out of the gel layers can be calculated based on the swelling ratio data. The diffusion of protein into the BCP is the cause of the gel swelling or deswelling but also depends on the gel layer's swelling ratio. The mass transport model should consider the diffusion of proteins and other ionic species (the Br^- and Cl^- counterion, tris and protonated tris, H_2O H^+ and OH^-) into the gel layers driven by the osmotic

pressure and the charge equilibrium, and diffusion of water in or out of the gel layers due to the thermodynamic equilibrium concentration of the proteins in the QP2VP gel.

References

1. Walish, J. J.; Fan, Y.; Centrone, A.; Thomas, E. L. *Macromol. Rapid Commun.* **2012**, *18,* 1504-1509.

2. Fan, Y.; Walish, J. J.; Tang, S.; Olsen, B. D.; Thomas, E. L. *Macromolecules*, Article ASAP.

3. Ullal, C. K.; Schmidt, R.; Hell, S. W.; Egner, A. *Nano Letters* **2009**, *6,* 2497-2500.

4. Noro, A.; Tomita, Y.; Shinohara, Y.; Sageshima, Y.; Walish, J. J.; Matsushita, Y.; Thomas, E. L. *ACS Nano* , Submitted.

5. Lim, H. S.; Lee, J.; Walish, J. J.; Thomas, E. L. *ACS Nano* **2012**, *10,* 8933-8939.

6. He, Y.; Li, Z.; Simone, P.; Lodge, T. P. *J. Am. Chem. Soc.* **2006**, *8,* 2745-2750.

7. Lu, H.; Chen, W.; Russell, T. P. *Macromolecules* **2009**, *22,* 9111-9117.

8. Lu, H.; Lee, D. H.; Russell, T. P. *Langmuir* **2010**, *22,* 17126-17132.

9. Virgili, J. M.; Hexemer, A.; Pople, J. A.; Balsara, N. P.; Segalman, R. A. *Macromolecules* **2009**, *13,* 4604-4613.

10. Virgili, J. M.; Nedoma, A. J.; Segalman, R. A.; Balsara, N. P. *Macromolecules* **2010**, *8,* 3750-3756.

11. Tanaka, T. *Sci. Am.* **1981**, *1,* 124-138.

12. Cowie, J. M. G.; McEwen, I. J.; Garay, M. T. *Polym. Commun.* **1986**, *5,* 122-124.

13. Cooper, C. L.; Dubin, P. L.; Kayitmazer, A. B.; Turksen, S. *Current Opinion in Colloid & Interface Science* **2005**, *1–2,* 52-78.

Appendix: Transfer Matrix Method (TMM) code

The TMM code was written for MATLAB by following the method described by Yeh.[1] The effective refractive index of the P2VP gel layers was calculated using the equation in the Ho paper.[2] Details of the calculation can be found in Section 2.4.

```
% function to compute the effective refractive index of a binary mixture
% based on a quadratic equation, by Yin Fan 02/28/2011
% Ho, P. K. H.; Thomas, D. S.; Friend, R. H.; Tessler, N. Science 1999, 285,
233- 236
% f1*[(n1^2 - ne^2)/(n1^2 + 2ne^2)] + f2*[(n2^2 - ne^2)/(n2^2 + 2ne^2)] = 0
% INPUT
%   n1, n2: refractive indices of the two components
%   f2: volume fraction of component 2
% OUTPUT
%   ne: effective refractive index of the binary mixture

function ne = nMix(n1,n2,f2)

a = 2;
b = (1-3*f2)*n2^2+(3*f2-2)*n1^2;
c = -n1^2*n2^2;

ne = sqrt((-b+sqrt(b^2-4*a*c))/2/a);


% function to compute the effective refractive indices and thickness of a
% selectively swollen 1D stack, by Yin Fan 02/28/2011
% Solvent distribution profile: zero in odd layers; uniform in even layers
% Numbering top to bottom, top layer glassy, bottom layer gel
% Calls for nMix, function to compute the refractive index of a binary
mixture
% INPUT
%   N: total number of bilayers
%   n1,n2,nsol: refractive indices of [glassy gel solvent]
%   d0 (nm): initial thickness of a dry layer (single block)
%   phi0: volume fraction of solvent in gel layers
% OUTPUT (matches function TMM input)
%   n: N-d vector of refractive indices
%   d: N-d vector of layer thickness

function [n d] = uniform(N,n1,n2,nsol,d0,phi0)

for i = 1:N
    n(2*i-1) = n1;
    n(2*i) = nMix(n2,nsol,phi0);
    d(2*i-1) = d0;
    d(2*i) = d0/(1-phi0);
```

```
end


% Function using TMM to compute the reflectivity spectrum in a 1D photonic
% crystal, by Yin Fan 02/28/2011
% Incidence from air; silica substrate
% INPUT
%   n: vector of refractive indices, from top to bottom
%   d (nm): vector of layer thickness, from top to bottom
%   theta0 (deg): incidence angle to the first layer
%   lambda (nm): vector of output wavelength
% OUTPUT
%   R: reflectivity at each wavelength in lambda

function R = TMM(n,d,theta0,lambda)

n0 = 1; % incidence from air
n_s=1.5; % silica substrate

N = length(n);

theta(1) = theta0*pi/180; % theta(1,1): angle of incidence onto 1st layer
[radian]

% theta(2,1): angle of incidence of light onto 2nd layer
theta(2)=asin(n0/n(1)*sin(theta(1)));

% theta(i) : angle of incidence onto ith layer

for i=2:1:N
    theta(i+1)=asin(n(i-1)/n(i)*sin(theta(i)));
end

%theta_s: angle of transmission of light onto substrate
theta_s=asin(n(N)/n_s*sin(theta(N+1)));

for m = 1:length(lambda)
    k0=2*pi/lambda(m);

    %Y: characteristic coefficients
    Y_0=n0*cos(theta(1)); % air
    Y_s=n_s*cos(theta_s); % substrate

    M = eye(2,2);

    for i=1:1:N
        % h(i): optical path length difference of ith layer
        h(i)=n(i)*d(i)*cos(theta(i+1));

        % Y(i): characteristic coefficient of ith layer for TE polarization
        Y(i)=n(i)*cos(theta(i+1));

        % MM: transfer matrix for the current layer
        MM(1,1)=cos(k0*h(i));
```

```
        MM(1,2)=j*sin(k0*h(i))/Y(i); % j: imaginary unit e.g. 1+2j
        MM(2,1)=j*Y(i)*sin(k0*h(i));
        MM(2,2)=cos(k0*h(i));

        M = M*MM;
    end

    %r: amplitude coefficient of reflection
    r=(Y_0*M(1,1)+Y_0*Y_s*M(1,2)-M(2,1)-
Y_s*M(2,2))/(Y_0*M(1,1)+Y_0*Y_s*M(1,2)+M(2,1)+Y_s*M(2,2));

    R(m)=r*conj(r);
end


% Function to calculate the solvent volume fraction in P2VP from spectra
% peaks, assuming gel layers have uniform swelling profile
% by Yin Fan 02/28/2011
% based on TMM, nMix, uniform
% INPUT
%   pk_exp (nm): peak position from experimental spectrum
%   phi0: initial guess for the solvent volume fraction
%   ep: peak search reflectivity threshold
% OUTPUT (DISPLAY)
%   volume fraction of solvent in gel layers
%   plot of spectrum using calculated phi

function f = peak2phi(ep,phi0,pk_exp)

N = 20; % total number of bilayers
d0 = 28; % dry state single layer thickness

n1 = 1.6
n2 = 1.6;
nsol = 1.33;

theta0 = 0;
lambda = [200:800];

f = fzero(@(phi) peak_error(phi,
N,n1,n2,nsol,d0,theta0,lambda,ep,pk_exp),phi0);
phi = fzero(@(phi) peak_error(phi,
N,n1,n2,nsol,d0,theta0,lambda,ep,pk_exp),phi0);

[n,d] = uniform(N,n1,n2,nsol,d0,phi);
R = TMM(n,d,theta0,lambda);

plot(lambda,R), xlabel('Wavelength (nm)'), ylabel('Reflectivity')

function err = peak_error(phi, N,n1,n2,nsol,d0,theta0,lambda,ep,pk_exp)
% function under peak2phi to compute the error in peak position between exp
input and TMM estimate
[n,d] = uniform(N,n1,n2,nsol,d0,phi);
R = TMM(n,d,theta0,lambda);
```

```
ind = -ones(length(lambda),1);
ind(find(R>ep)) = 1;
left = find(diff(ind)==2);
right = find(diff(ind)==-2);
pkwid = right - left;
[maxe maxind] = max(pkwid);

[Ymax, Yind]=max(R(left(maxind):right(maxind)));
peak  = lambda(Yind+left(maxind)-1);
err = peak - pk_exp;
return
```

References

1. Yeh, P. *Optical waves in layered media;* Wiley: New York, 1988.

2. Ho, P.; Thomas, D.; Friend, R.; Tessler, N. *Science* **1999**, *5425,* 233-236.